Factors Influencing Biotite Weathering

by

Ryan Ronald Reed

Thesis submitted to the Faculty of the
Virginia Polytechnic Institute and State University
in partial fulfillment of the requirements for the degree of
MASTER OF SCIENCE
in
Crop and Soil Environmental Sciences

APPROVED:

Dr. Lucian Zelazny (Committee Chair)	Dr. James Baker
Dr. Matthew Eick	Dr. Jack Hall (Department Head)

December, 2000
Blacksburg, Virginia

Factors Influencing Biotite Weathering

by

Ryan Reed

Lucian W. Zelazny, Chairman

Crop and Soil Environmental Sciences

(ABSTRACT)

Weathering products of primary minerals such as biotite can greatly influence soil properties and characteristics. Weathering of biotite supplies nutrients such as K^+ and weathers into vermiculite/montmorillonite or kaolinite, which have varying influences on soil properties and characteristics. Various laboratory studies and field investigations have suggested that biotite weathers predominantly to kaolinite in the Piedmont of Virginia, and to vermiculite/montmorillonite in the Blue Ridge. This study was conducted to determine if the weathering mechanisms of biotite are controlled by temperature, or if other factors, such as vegetation or leaching intensity dominantly influence the weathering process. A column study investigation was conducted to assess the influence of different acids, simulated rainfall rates, surface horizons, and temperature on the weathering and cation release of biotite. A field investigation was also conducted on the clay mineral fraction of soils in Grayson County, VA formed above biotite granite. The soils were sampled at two elevational extremes to assess clay mineral weathering at the maximum climatic difference in the region. Leaching of columns packed with biotite with selected treatments of acids, surface horizons, leaching rates, and temperatures produced no detectable secondary weathering-products of biotite by x-ray diffraction (XRD). Selected acid leachates did show a greater Al^{+3}, Fe^{+2}, and Si^{+4} release with organic acids (ascorbic, citric, and fulvic) than that with hydrochloric acid treatment at high leachate rates. Loss of K^+ is greater with ascorbic acid than all other acids at high leachate rates. Temperature studies showed the greatest release of cations at the lowest temperature (4^oC) when compared to 25^o and 38^oC; and spruce-fir surface horizons release significantly greater amounts than hardwood and sand horizons. Leachate rate interaction with low temperature was an influencing factor in cation release. Field investigations revealed a greater weathering intensity at high elevations evidenced by; (i)

higher clay content, (ii) a dominance of 2:1 minerals, (iii) greater surface area in the upper horizons, (iv) minerals indicative of later stages in the biotite weathering mechanism, and (v) precipitation of halloysite in the C horizon at the high elevation site where temperature is lower and a suspected higher leaching intensity occur. Initial biotite weathering appears to experience dissolution / reprecipitation reactions more intensely at low temperatures and high leaching rates. No mechanistic differences were observed in the data.

Acknowledgements

I would like to express my appreciation to the members of my graduate committee, who have been a tremendous help in my pursuit of knowledge and experience: Dr. Lucian Zelazny, for providing me with wisdom, guidance and attempting to teach me patience, he will be able to get a lot of other things done now that I won't be constantly knocking on his door; Dr. James Baker, for agreeing to put up with me for an additional two years after serving as my advisor for the first 4½ years of my college career and for always having a good fishing story; Dr. Matthew Eick, for sparking my interest in soil chemistry, after I signed up for his 1st course on a whim and for his ability to relate information in layman's terms.

Many thanks are extended to Hubert Walker for his knowledge and experience in the laboratory and willingness to offer his assistance at anytime. To Dr. Pam Thomas, for her infinite wisdom and understanding of soils and our department, Athena VanLear, W.T. Price, Jarrod Miller, Brian Jones, and Jim Jerden for the assistance and expertise in the field. I would like to offer appreciation to the companionship of Lori Stanley, who has been my lab partner and officemate as we mutually pursued our degrees.

I would like to thank all of my friends, at Virginia Tech and beyond, I would not have been able to do this without them. I am grateful for the occasional visits from my dog Zach, and I would like to thank, above all, my parents and God for the continued and unwaivering love and support along my path.

Table of Contents

List of Figures

List of Tables

Chapter 1

Introduction

Weathering of primary minerals within soil systems is well documented, and their study perpetuates an understanding of many phenomenona in soil systems. Mineral weathering in soils is dependent upon many variables, commonly accepted to be within one of five pedogenic factors; climate, relief, biotic factors, time and parent material (Jenny, 1941). Jenny (1941) believed that the effect of each soil forming factor or soil properties could be quantified if all other soil forming factors were held constant. The idea is simplistic and general, it does not account for interactions between factors or more complex processes, but these five soil-forming factors do give a basis which to work from when studying and understanding soils and their reactions. The degree to which each of these factors influence weathering of minerals inherently determines the characteristics of secondary mineral formation. The contribution of each factor and the interaction between factors is complex; therefore, the understanding of rates, mechanisms, and products of weathering remains incomplete. Controlled systems in laboratory conditions have allowed scientists to predict the behavior and weathering of minerals; however, this often fails when applied to natural systems. Furthermore, other studies, which have incorporated field data, have had difficulty isolating variables in the system, such as the five soil forming factors identified above, because of the complexity of the environment.

This complexity of soil variables creates a challenge when attempting to develop prediction models. The simplest model would be a linear regression, where there is only one variable and all other factors are held constant, however due to interactions and the complexity of soils mentioned above, this model is rarely applicable. Discovering which soil forming factor or interacting factors is the most influential in the weathering of a mineral would allow a simple prediction model for future weathering. As environmental conditions change over time, soils will often weather differently, with varying magnitudes. Depending on the change and the duration of the climatic event, some soil characteristics and morphologies from past events may be preserved within the soil, therefore allowing researchers to discover what paleoclimates were like and how they

effected the soil (Feldman and Zelazny, 1998). For example, any variation in climate would be expected to initiate changes in weathering process, the magnitude dependent on the influence of temperature and moisture availability on mineral weathering. Potential effects, resulting from an increase in temperature and moisture availability, on soil properties would include a reduction of CEC, an increase in anion retention, an increase in K^+ and NH_4^+ selectivity, and changes in flocculation/dispersion phenomena therefore effecting soil structure (L.W. Zelazny, personal communication, 2000).

Biotite is a trioctahedral primary mineral particularly susceptible to weathering. It weathers readily in the soil environment. By identifying the specific factors of weathering that influence biotite's degradation, scientists could characterize past geologic events and possibly predict the ramifications of future climatic and geologic changes. Studying the weathering of biotite can be useful for explaining past geologic events but also is useful for predicting future weathering. Weathering of existing biotite can play an essential role in the soil fertility for agricultural and agroforestery areas (Ulen and Snall, 1998). Biotite is an important mineral for nutrient availability in soils, most often contributing K^+ and Fe^{2+} to the soil system during its transformation (Pozzuoli et al., 1992; Velbel, 1985; Peters and Hofmann, 1984), along with several minor elements. Even a small amount of biotite (5 wt. %) can produce a significant mineralogical contribution through its weathering process (Jeong, 2000). Because biotite weathering releases substantial amounts of K^+ and other cations, it is an important factor in long term productivity, nutrient sustainability in soils, stream chemistry and groundwater quality.

To evaluate the influences of various factors on the weathering of biotite, a field study and column study were conducted. The field study was conducted in the Elk Creek quadrangle of Grayson County, Virginia (Fig. 1.1) overtop a biotite rich granite pluton. The extent of this uniform pluton limited the elevation range that could be sampled. The column study included several treatments of different weathering agents in order to simulate weathering environments acting upon the biotite mineral. This study was limited in time to 6 months. Limitations also included biotite quantity and clay percentage of the biotite samples. This thesis reports the results of field investigations

concerning general description and mineralogical analysis, and lab investigations of the columns with regard to statistical analysis of column leachates and column mineralogy.

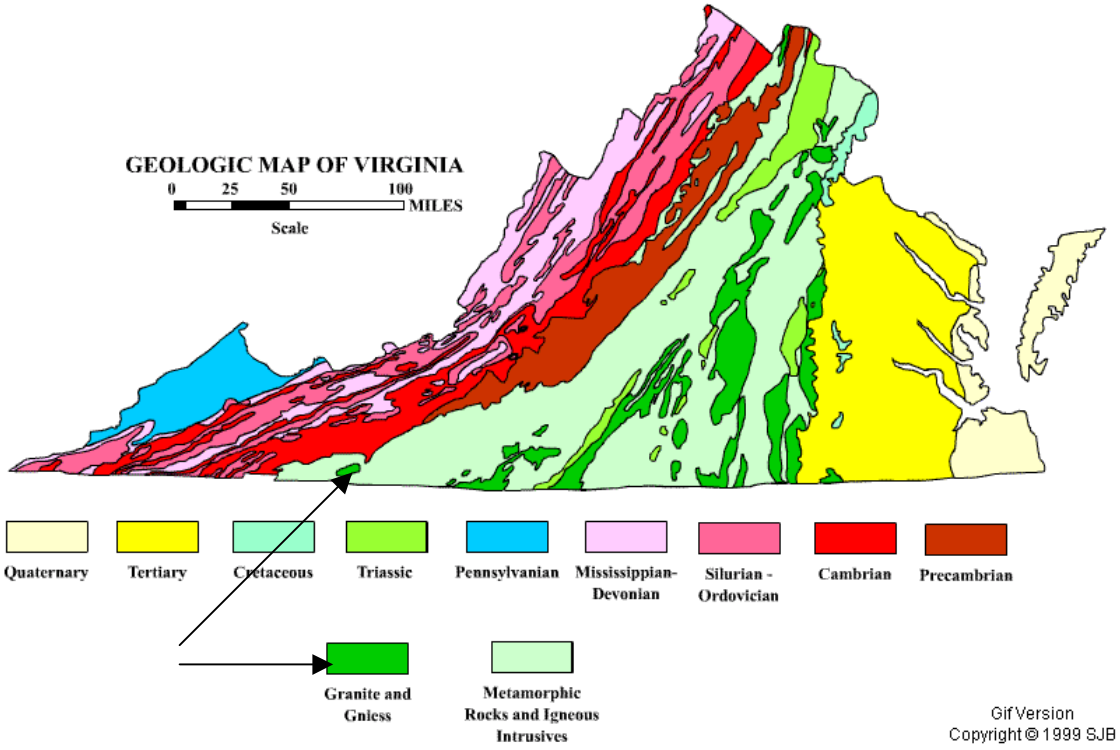

Figure 1.1 Geology of Virginia. Sampling area and rock type designated by arrows.

Toward that end, this research has been conducted in an attempt to accomplish the following objectives:

1) To describe and classify soil features and characterize the mineralogy of the soils derived from the biotite rich parent material in the study area,

2) To explain the differences observed in the soil mineralogy caused by genesis and weathering processes,

3) Through repeated measures of the pH and cation contents of leachates from the columns, an attempt will be made to explain any observed differences in the treatments,

4) To characterize the mineralogical nature observed between the various column treatments and explain any observed differences in the results.

Mechanisms of Weathering

Biotite is a primary mineral common in parent materials in the Southeastern United States. Biotite is a 2:1 trioctahedral mineral with a high degree of isomorphic substitution, but generally Si substituted by Al in the tetrahedral layer, Fe^{2+} and Mg^{2+} in the octahedral layers and K^{+} in the interlayer region (Grim, 1953). It is unstable in the soil environment because of the Mg^{2+} substitution in the octahedral layer, resulting both in a shared electrostatic bond strength of ⅓ to each surrounding oxygen instead of ½, as found when Al^{3+} is present in the octahedral layer and a larger size of Mg^{2+} in comparison to Al^{3+}. The generic mineral formula, $K_2(Mg, Fe^{2+})_6(Al_2Si_6)O_{20}(OH)_4$, exemplifies the level of substitution in both tetrahedral and octahedral layers and the presence of K in the interlayer, satisfying the excess negative charge. Though it is prevalent in the parent material, biotite is rarely found in the soil matrix due to its relative instability in soil environments. It weathers quickly to secondary minerals. Biotite weathering occurs both by solid-state alteration and dissolution/reprecipitation mechanisms. The products of these weathering reactions are minerals such as vermiculite, smectite, pedogenic chlorite, hydroxy-interlayered vermiculite (HIV), gibbsite or kaolinite, dependent on various factors (Kogure and Banfield, 2000; Feldman, unpublished data, 1995; Banfield and Eggleton, 1988). Many researchers suggest that biotite weathering leading to end products (i.e. kaolinite, gibbsite) is the result of weathering through intermediates such as vermiculite (Fordham, 1990; Rebertus, et al., 1986; Coen and Arnold, 1972; Reynolds, 1971; McCracken, et al., 1962; Cady, 1950). Others, however, introduce the idea that minerals like kaolinite or halloysite may be formed from a direct transformation from the biotite (Furman et al., 1998; Murphy, et al., 1998; White, et al., 1998; Fordham, 1990; Harris, et al., 1985a&b; Stoch and Sikora, 1976).

The generally accepted mechanism of biotite weathering through an assortment of intermediates is: biotite > hydrobiotite > randomly interstratified mica / vermiculite

(RMV) > vermiculite > montmorillonite or hydroxy-interlayered vermiculite (HIV) > kaolinite (Feldman, et al., 1991b). Many variations of this idea exist with different mineral intermediates, fewer intermediates, and different end products. Several studies have observed the transformation of biotite to vermiculite, often with HIV or RMV as the intermediate step (Jeong, 2000; White et al., 1999; White, et. al., 1998; Pozzuoli et al., 1992; Sverup & Warfvinge, 1990; Ghabru et al., 1989; Lietzke and McGuire, 1987; April et al., 1986; Rebertus, et al., 1986; Velbel, 1985; Calvert et al., 1980; Stoch and Sikora, 1976; Kittrick, 1973; Coen and Arnold, 1972; Reynolds, 1971; McCracken et al., 1962). Theoretically, clay minerals form or transform only under conditions where it is the least soluble of the clay minerals competing for that group of elements or where it is the most stable structure under the given weathering environment. The transformation of a mineral to another without dissolution or loss of the entire mineral structure is termed alteration. The formation of new minerals precipitating from the constituents of dissolved minerals is referred to as neoformation. The rate of mineral reaction in the process of neoformation is controlled by the rate-limiting step. The rate limiting step is either: 1) dissolution of reactant phases; 2) diffusion of chemical components from dissolved areas to those where the new minerals precipitate; 3) nucleation and growth of products; and 4) changes in temperature and pressure that produce the free-energy driving force (Sanchez-Navas, 1999). The degradation of micas are thought to occur by 3 possible pathways; complete dissolution, K^+ replacement, critical K^+ levels and the K^+ content of natural waters (Kittrick, 1973). The basic reaction for complete dissolution is:

$$K_2(Mg_x, Fe_y^{2+})_6(Al_2Si_6)O_{20}(OH)_4 + 20H^+ \Rightarrow 2K^+ + (6\text{-}Y)Mg^{2+} + (6\text{-}X)Fe^{2+} + 2Al^{3+} + 6H_4SiO_4 \quad (1)$$

however, this dissolution reaction most often takes place in a series of steps (Kittrick, 1973; Huang, et al., 1968; Newman and Brown, 1966). The steps usually occur as; oxidation of Fe^{+2} in the mica structure (Farmer and Wilson, 1970), octahedral ions initially going into solution (Sawhney and Voigt, 1969) and neutralization of OH^- groups by H^+ (Newman and Brown, 1966). Replacement of K^+ simply occurs when the level of K^+, or other ions of low hydration energies, is low in solution.

A simple replacement can be illustrated as:

$$K\text{ - mica} + M^x = M\text{ - vermiculite} + xK^+. \quad (2)$$

where M^x is any metal cation with valency "x."

Structural K^+ is exchanged by ions with higher hydration energy. This replacement most often occurs as a concurrent process with the dissolution reactions that can either encourage or resist the replacement of K^+ (Raman and Jackson, 1966; Newman, 1970; Gilkes et al., 1973, Kittrick, 1973). Upon replacement of K^+, internal alterations within the crystal lattice prevent reversibility. The critical K^+ level is the amount of K^+ required in solution to prohibit the release of K^+ from the mineral structure. It is the equilibrium point of the above equation. The critical level of K^+ is temperature dependent when Al has formed hydroxy-Al groups in the interlayers because as the temperature increases, the amount of K^+ selectivity decreases, hence increasing K^+ in solution (Zelazny, 1970).

The mechanisms resulting in biotite weathering to intermediate minerals via alteration has often been observed at the single crystal level of sand size particles. Pozzuoli et al. (1992) observed biotite weathering to vermiculite in a localized, heterogeneous way, even in small samples normally characterized by different spatial concentrations of biotite, vermiculite and an intermediate interstratified phase. Pozzuoli et al. (1992) also quantitatively characterized the nonstiochmetric mass balance during the weathering of biotite to vermiculite. This incongruent loss is characteristic of phyllosilicate clay weathering selectively. The percentage losses of elements in biotite weathering to vermiculite followed the sequence: $K^+ > Fe^{2+} > F^- > Mn^{2+} > Si^{4+} > Mg^{2+} > Al^{3+} > Ti^{4+}$ with a gain in protons primarily in the form of water (Jolicoeur, et al., 2000). Biotite weathering to illite indicated that this process increased the mineral Si and Al content and decreased mineral content of Fe, Mg, Ti, Mn, and Na, with a slight decrease in K (Peters and Hofmann, 1984). Eggelton and Banfield (1985) and Kogure and Banfield (2000) however, observed a different mechanism as biotite weathered to chlorite. As the K^+ was replaced, the H^+ attached to the tetrahedral layer initiated dissolution of this layer. Eventually, two biotites became one chlorite therefore decreasing the volume, as seen

optically in the Kogure and Banfield (2000) study. Further weathering via this mechanism with Ca^{2+} inputs resulted in the formation of sphene and epidote. At elevated temperatures, measured K^{+} adsorption onto mineral surface decreases and Ca^{2+} adsorption increases (Zelazny, 1970) thereby possibly driving this reaction. At the same time, Eggelton and Banfield (1985) observed a simultaneous mechanism of neoformation of dissolved anions between tetrahedral layers creating a brucite like sheet and an increase in volume. Their overall conclusion was that while both mechanisms take place, the second is dominant, hence justifying the total increase in volume they observed with biotite weathering. White, et al., (1999) found a close correlation between Ca, Mg and Sr concentrations in effluents from a column study examining weathering of granitoid rocks. They suggest this correlation implies a control by ion exchange in the weathering reaction, attributing it to the initial stages of biotite vermiculitization. The tendency of trioctahedral biotite to transform into dioctahedral vermiculite is evidenced in oxidation and loss of structural Fe and other small cations like Mn^{2+} and Mg^{2+} (Ghabru, et al.; 1989). Shidhar and Jackson (1974) also observed the oxidation of Fe^{2+} to Fe^{3+} but cited the protonation of structural oxygen as the cause of the loss of layer charge in the weathering process to form vermiculite. A proposed transformation involving 1 unit cell of biotite forming 1.5 unit cells of kaolinite by Rebertus, et al., (1986) results from a pathway including vermiculite and HIV as the intermediates. Rebertus, et al., (1986) models the transformation by suggesting that the Al released from the weathering initially begins forming nonexchangeable hydroxy-Al in the interlayers. This mechanism thereby provides the hydroxyl necessary for kaolinite formation. To precipitate kaolinite in this manner, a large amount of Al must be imported because of the low Al content of biotite (Jeong, 2000). After the initial K^{+} loss and expansion to tri-octahedral vermiculite, Al is imported into the system and the hydroxy-Al replaces interlayer cations. Then, Mg is lost in the octahedral layer and any Al that was in the tetrahedra is converted to form part of the octahedral layer along with the hydroxy-Al. This creates a loss of one out of four tetrahedra. The complete transformation from biotite to kaolinite results in a slight increase in volume. Rebertus, et al., (1986) explains the apparent absence of HIV in field observations by suggesting a rapid transformation of HIV to kaolinite, perhaps at the rate that the hydroxy-Al interlayers are being formed. Stoch and Sikora (1976) also subscribe

to the belief that if biotite is weathering to kaolinite via intermediates, that it is necessary to have high concentrations of Al^{3+}. White, et al., (1998) observe biotite weathering in a soil in Puerto Rico, where the chemical weathering rates are extremely fast. The biotite from this region mostly weathers directly to kaolinite by epitaxial growth similar to what Harris, et al., (1985b) found, however, a small portion appears to weather to HIV as an intermediate alteration product of biotite. Also observed was the complete incorporation of all Al^{3+} from biotite weathering, into the kaolinite structure.

The observation by White, et al., (1998) of biotite mica weathering directly to kaolinite with no intermediate steps via growth on a single crystal or phase is not uncommon. This phenomenon has been observed, or suggested by various researchers as an explanation for biotite weathering to kaolinite in some areas (Jeong, 2000; Jolicoeur, et al., 2000; Furman, et al., 1998; Murphy, et al., 1998; Fordham, 1990; Norfleet and Smith, 1989; Rebertus, et al., 1986; Harris, et al., 1985a&b; Stoch and Sikora, 1976; Cady, 1950). The observation of large, micaceous-appearing books of kaolinite in piedmont samples from North Carolina led Cady (1950) to suggest that kaolinite might form directly from silicate minerals such as biotite in the A-horizon of soils. In samples from the Blue Ridge in Northern Virginia, metasediments of the Chilhowee formation were observed weathering in the solum with no intermediate stages of the biotite -> kaolinite weathering process evident (Furman, et al., 1998), therefore the direct weathering of biotite to kaolinite may be very likely. Jeong (2000) cites epitactic biotite kaolinization with no intermediate step as an explanation for a large increase in volume observed. This is concurrent with the theory that one biotite cell with two tetrahedral layers, with the import of Al will produce two kaolinite unit cells. Rebertus, et al. (1986), also studying biotite weathering in some North Carolina soils, points out the trend of decreasing biotite kaolinization with increasing depth, with the majority of this reaction occurring in the surface horizon. While Rebertus, et al., (1986) commonly observe an intermediate step in their samples, they cite those samples in which the HIV is not evident as possible products via direct weathering of biotite to kaolinite. The direct weathering of biotite to kaolinite is obviously dependent on the conditions of the soil environment. As discussed above, Stoch and Sikora (1976) suggested specific conditions for the weathering through

intermediates. The direct weathering is then predicted to occur in conditions that have relatively low concentration of Al^{3+} and a small value for the ratio of $[K^+]/[H^+]$. They attribute the direct formation of kaolinite to either incongruent dissolution or the result of transformation of the mica structure, where the transformation must occur with the participation of Al^{3+} ions from the soil solution. Harris et al. (1985a) observed biotite kaolinization with no intermediates in soils of the southeastern United States. Further investigations by Harris et al. (1985b) resulted in the discovery of topotaxial growth of kaolinite on biotite sand-sized grains. Optical properties influenced by the biotite parent, such as brown-green pleochroism, masked the presence of kaolinite as it grew from the edges inward on each grain. Kaolinite was evidenced by the 7.2Å x-ray diffraction spacing and by visual observation after oil immersion, which removed the pleochroism. A high Fe content and a high ratio of Si to octahedral cations characterized the grains. The divalent cations of the octahedral layer were concluded to be lost simultaneously with interlayer K^+ therefore resulting in the direct transformation. A study in the Luquillo mountains of Puerto Rico by Murphy, et al., (1997) supports the Harris, et al. (1985b) conclusion with additional optical work illustrating the direct weathering of biotite to kaolinite, however epitaxial, not topotaxial growth was observed by these researchers. Norfleet and Smith (1989) supports Harris, et al. (1985a) biotite kaolinization as an alternate process to explain the direct weathering of biotite to kaolinite in more siliceous environments of their South Carolina study. In central Virginia, the biotite observed weathering directly to kaolinite was suggested to be the only precursor to gibbsite formation in soils (Jolicoeur, et al., 2000). The direct weathering of biotite to kaolinite occurred in the saprolite of the Piedmont sediments.

Weathering Products versus Physiographic Provinces

In the Southeast, soils originating from a biotite rich parent material tend to exhibit one of two secondary mineral phases; a stable HIV intermediate, or kaolinite. This difference is most commonly observed between high altitude forested areas in the Blue Ridge and the lower elevation, arable Piedmont province. The ecological differences between the Southern Blue Ridge and the Piedmont has long been evident, however, until recently,

the soils of the two areas were not well compared due to the relatively general classification of mountain soils (Daniels, et al., 1987a). Nutrient cycling within these two provinces is a major factor in the long-term productivity of the areas. A balance between weathering, (Taylor and Velbel, 1991) atmospheric deposition, (Rennie, 1990) harvesting and leaching (Likens, et al., 1977) control the sustainability of nutrients in soils (Zelazny, unpublished data, 2000). Fertilizer is often added in agricultural areas such as the Piedmont to maintain a higher nutrient balance, however, in most forested areas, fertility of the soil is reliant upon mineral weathering and organic matter decomposition (Ulen and Snall, 1998). Biotite is an important source of K^+ and various other nutrients for plants in soils (Ulen and Snall, 1998; Zabowski, 1990; Fanning, et al., 1989) in both the Piedmont and the Blue Ridge.

The Piedmont soils, historically, have been recognized for their use in agriculture and hence, extensively mapped. The Piedmont of Virginia is dominated by Hapludults, occurring in a Udic moisture regime and either a mesic or thermic temperature regime (Soil Survey Staff, 1975). The soils of the Piedmont are underlain by Precambrian and lower Paleozoic igneous and metamorphic rocks (Fisher, 1970). The biotite schist found within these formations has been determined to be the source of the primary mineral biotite. Biotite kaolinization has been suggested to be the most important source of kaolinite in the Piedmont (Jolicoeur, et al., 2000; Furman, et al., 1998; Norfleet and Smith, 1989; Harris, et al., 1985a; Cady, 1950) and in many other well-drained, leached soils in several regions of the world (Jeong, 2000; Murphy, et al., 1998; White, et al., 1998; Novikoff et al., 1972).

The southern Appalachian soils have not received as much detailed study outside of the populated low elevation (<600 m) valleys because of the non-agricultural use of the land (Daniels et al., 1987a). Isolated studies however, discovered well-defined podzols (spodosols) in the high-elevation regions of West Virginia, Virginia, North Carolina and Tennessee (Wang and McKeague, 1984; Springer and Elder, 1980; Hole, 1975; McCracken et al., 1962; Coile, 1938). These areas of the Southeast have developed consistent soil morphology resulting from the dominance of climate in pedogenesis

(Clark and Ciolkosz, 1988; Connors, 1986; Richter, 1973; Clark, 1968; Smith, 1949). Similar discoveries of podzolic features were found in the Mount Rodgers, Whitetop Mountain, Mountain Lake and Poor Mountain areas of southwestern Virginia, with soils forming specifically under native spruce-fir stands (Baker, unpublished data, 2000; Feldman et al., 1991a).

Vermiculite is commonly reported as a semi-stable secondary phase in high elevation, boreal forest soils with frigid temperature regimes of the southeastern US (>1600m) (Lietzke and McGuire, 1987) and in cold environment soils in such regions as Saskatchewan, Canada (Ghabru, et al., 1989), the Adirondacks and Whiteface Mountain, New York (April, et al., 1986; Coen and Arnold, 1972), the Cascades, Washington State (Reynolds, 1971) and Sodermanland, Sweden (Ulen and Snall, 1998). The vermiculite, resulting from a random interstratified mica/vermiculite intermediate, occurs as a semi-stable 2:1 secondary mineral with high surface area and cation exchange capacity (CEC) (White and Zelazny, 1986).

Kaolinite, however, is the dominant product of biotite weathering in humid-temperate soils, under acidic, well-drained conditions in the southeastern US (Harris, et al., 1985a; Eswaran and Bin, 1978; Eswaran and Heng, 1976; Stoch and Sikora, 1976; Ojanuga, 1973; Novikoff, 1972) and in the tropics (Murphy, et al., 1998; White, et al., 1998; Kalpage, 1974). Kaolinite occurs in these soils as a stable 1:1 secondary mineral with low surface area and nominal CEC.

These studies suggest a temperature dependence of the specific weathering products of biotite. The biotite rich bedrock is of course the most necessary factor to discovering biotite and by products of biotite weathering in the soil. It is generally assumed that temperature is the next most influential factor to determining what the secondary phases of biotite will be, however no study to date has isolated the weathering reaction so that temperature effects may be quantified. Factors such as vegetation and precipitation rates may be commonly overlooked, though, there is quite a difference in these factors as well between the Piedmont and the Blue Ridge. Wolfe (1967) suggested that vegetation was

responsible for differences in soil chemistry such as exchangeable acidity and base saturation in the Great Smokey Mountains National Park in North Carolina. Lietzke and McGuire (1987) found no correlation between specific species of trees and the resulting morphology of the frigid areas of North Carolina but this could be a result of relatively recent anthropogenic factors and the inability of isolated areas to re-seed themselves. A correlation between base cations released into a watershed via a mass balance approach and the defoliation of the vegetation of the watershed was observed by Furman, et al. (1998) during a primary mineral weathering study in the Blue Ridge of central Virginia. Biotite alteration products, varying from kaolinite to vermiculite within the same soil series, have been found significant between samples with the same vegetation and very similar parent materials of the same age in South Carolina (Norfleet and Smith, 1989). These differences in the mineralogy as well as differences in drainage class, runoff, bulk density, exchangeable Al and organic carbon were attributed to some combination of slope, aspect, elevation and precipitation. McCracken et al. (1962) also notes the differences in lateral seepage as a possible factor influencing the differences in podzol morphology in the Great Smokies National Park. In addition, they cite the qualitative and quantitative differences between the complexing and chelating agents in the humus layers of spruce-fir forests and heath vegetation as influential factors controlling the movement of iron and therefore perpetuating the differences observed. The strong influence of continuous vegetation is evidenced in the Daniels, et al., (1987b) study in the Joyce Kilmer Memorial Forest in North Carolina. They site the unique fact that this area was never logged and exhibits a relatively constant parent material as factors developing a "steady-state weathering" in these particular soils. For such reason, the strong effects of aspect and slope position on the chemistry and mineralogy of the soils was not evidenced in their data in contrast with the results from Losche, et al., (1970) from an adjacent area. White, et al. (1990) also note dependency of mineral weathering in forested systems to microclimate (slope aspect and position) and vegetative cover but mention the increased influence due to increased soil temperature fluctuations after intensive harvesting of a forest.

Jolicoeur, et al. (2000) suggests that the intense leaching of freely drained soils is an important factor in biotite alteration to kaolinite. Contemporary and ancient pedoclimatic conditions, however, were not included, as Jolicoeur, et al (2000) mention. The relation of these factors to the process was not addressed. The correlation, however, of biotite kaolinization on well drained acidic soil conditions is agreed upon by many researchers (White, et al., 1999; Murphy, et al., 1998; White, et al., 1998; Norfleet and Smith, 1989; Harris, et al., 1985a) but may not be accepted as the primary determining factor in the differences of biotite weathering.

Literature Cited

April, R.H., M.M. Hluchy, and R.M. Newton. 1986. The nature of vermiculite in Adirondack soils and tills. Clays Clay Miner. 33:31-43.

Banfield, J.F. and R.A. Eggleton. 1988. Transmission electron microscope study of Biotite weathering. Clays Clay Miner. 36:47-60.

Cady, J.G. 1950. Rock weathering and soil formation in the North Carolin**a** Piedmont region. Soil Sci. Soc. Am. Proc. 15:337-342.

Calvert, C.S., S.W. Buol, and S.B. Weed. 1980. Mineralogical characteristics and transformations of a vertical rock-saprolite-soil sequence in the North Carolina piedmont: II. Feldspar alteration products-their transformations through the profile. Soil Sci. Soc. Am. J. 44:1104-1112.

Clark, G.M. 1968. Sorted patterned ground: New Appalachian localities south of the Glacial border. Science (Washington, DC) 161:355-357.

Clark, G.M. and E.J. Ciolkosz. 1988. Periglacial geomorphology of the Appalachian Highlands south of the glacial border – A review. Geomorphology 1:191-220.

Coen, G.M., and R.A. Arnold. 1972. Clay mineral genesis of some New York Spodosols. Soil Sci. Soc. Am. Proc. 36:342-350

Coile, T.S. 1938. Podzol soils in the southern Appalachian Mountains. Soil Sci. Soc. Am. Proc. 3:274-279

Conners, J.A. 1986. Quaternary geomorphic processes in Virginia. P.1-22. *In:* J.N. McDonald and S.O. Bird (ed.). The quaternary of Virginia – A symposium volume. Virg. Div. Min. Resour. Publ. 75, Charlottesville, VA.

Daniels, W.L., C.J. Everett, and L.W. Zelazny. 1987a. Virgin hardwood forest soils of the southern Appalachian Mountains: I. Soil morphology and geomorphology. Soil Sci. Soc. Am. J. 51:722-729.

Daniels, W.L., L.W. Zelazny, and C.J. Everett. 1987b. Virgin hardwoods forest soils of the southern Appalachian Mountains: II. Weathering, mineralogy, and chemical properties. Soil Sci. Soc. Am. J. 51:730-738.

Eggelton, R.A. and J.F. Banfield. 1985. The alteration of granitic biotite to chlorite. American Mineralogist. 70:902-910.

Eswaran, H., and W.C. Bin. 1978. A study of a deep weathering profile on granite in peninsular Malaysia: II. Mineralogy of the clay, silt and sand fractions. Soil Sci. Soc. Am. J. 42:149-153.

Eswaran, H. and Y.Y. Heng. 1976. The weathering of biotite in a profile on gneiss in Malaysia. Geoderma 16:9-20.

Fanning, D.S., V.Z. Keramidas, and M.A. El-Desoky. 1989. Micas. P. 551-634. *In* J.B. Dixon and S.B. Weed (ed.) Minerals in soil environments. 2nd ed. SSSA Book Ser. no. 1. SSSA, Madison, WI.

Farmer, V.C. and M.J. Wilson. 1970. Experimental conversion of biotite to hydrobiotite. Nature. 226:841-842.

Feldman, S.B., 1989 Taxonomy, genesis, and parent material distribution of high-elevation forest soils in the southern Appalachians. M.S. Thesis., Virginia Polytechnic Institute and State University, Blacksburg, VA.

Feldman, S.B., 1995. Pedogenesis, weathering processes, and elemental distribution Along a soil climosequence in the Southern Piedmont. Ph.D. Dissert., Virginia Polytechnic Institute and State University, Blacksburg, VA.

Feldman, S.B., L.W. Zelazny, and J.C. Baker. 1991a. High-elevation forest soils of the southern Appalachians: I. Distribution of parent materials and soil-landscape relationships. Soil Sci. Soc. Am. J. 55:1629-1637.

Feldman, S.B., L.W. Zelazny, and J.C. Baker. 1991b. High-elevation forest soils of the southern Appalachians: II. Geomorphology, pedogenesis, and clay mineralogy. Soil Sci. Soc. Am. J. 55:1629-1637.

Feldman, S.B. and L.W. Zelazny. 1998. Chemistry of soil minerals. *In:* SSSA Future prospects for soil chemistry. Soil Sci. Soc. Am. Special Pub. no. 55.

Fisher, G.W. 1970. Introduction to Section IV. The Piedmont. P. 295-298. *In:* G.W. Fisher and F.J. Pettijohn, J.C. Reed, Jr., and K.N. Weaver (ed.) Studies in Appalachian geology – Central and Southern. Interscience Publishers, New York.

Fordham, A.W. 1990. Weathering of biotite into dioctahedral clay minerals. Clay Minerals. 25:51-63.

Furman, T., P. Thompson, and B. Hatchl. 1998. Primary mineral weathering in the central Appalachians: A mass balance approach. Geochim. Cosmochim. Acta 62:2889-2904.

Ghabru, S.K., A.R. Mermut, and R.J. St. Arnaud. 1989. Layer-charge and cation exchange characteristics of vermiculite (weathered biotite) isolated from a Gray Luvisol in northwestern Saskatchewan. Clays Clay Miner. 37:164-172.

Gilkes, R.J., R.C. Young, and J.P. Quirk. 1973. Artificial weathering of biotite. I. Potassium removal by sodium chloride and sodium tetraphenylboron solutions. Soil Sci. Soc. Am. Proc. 37:25-38.

Grim, R.E. 1953. Clay Mineralogy. New York: McGraw-Hill

Harris, W.G., L.W. Zelazny, J.C. Baker, and D.C. Martens. 1985a. Biotite kaolinization in Virginia Piedmont soils: I. Extent, profile trends and grain morphological effects. Soil Sci. Soc. Am. J. 49:1290-1297.

Harris, W.G., L.W. Zelazny, F.D. Bloss. 1985b. Biotite kaolinization in Virginia Piedmont soils: II. Zonation in single grains. Soil Sci. Soc. Am. J. 49:1290-1297.

Hole, F.D. 1975. Soil-ecology tour, Great Smoky Mountains. Soil Surv. Horiz. 16(4):7-10.

Huang, P.M., L.S. Crosson, and D.A. Rennie. 1968. Chemical dynamics of potassium release from potassium minerals common in soils. Trans. 9th Int. Congr. Soil Sci. 2:705-712.

Jenny, H. 1941. Factors of soil formation. New York: McGraw-Hill.

Jeong, G.Y. 2000. The dependence of localized crystallization of halloysite and kaolinite on primary minerals in the weathering profile of granite. Clay Clay Miner. 48:196-203.

Jolicoeur, S., P. Ildefonse, and M. Bouchard. 2000. Kaolinite and gibbsite weathering of biotite within saprolites and soils of central Virginia. Soil Sci. Soc. Am. J. 64:1118-1129.

Kalpage, F.S.C.P. 1974. Tropical Soils. The Macmillan Company of India Limited.

Kittrick, J.A. 1973. Mica-derived vermiculite as unstable intermediates. Clay Clay Miner. 21:479-488.

Kogure, T., and J.F. Banfield. 2000. New insights into the mechanism for chloritization of biotite using polytype analysis. American Mineralogist. 85:1202-1208.

Lietzke, D.A., and G.A. McGuire. 1987. Characterization and classification of some soils with spodic morphology in the southern Appalachians. Soil Sci. Soc. Am. J. 51:165-170.

Likens, G.E., F.H. Bormann, R.S. Pierce, J.S. Eaton, and N.M. Johnson. 1977. Biogeochemistry of a forested ecosystem. New York: Springer-Verlag.

Losche, C.K., R.J. McCracken, and C.B. Davey. 1970. Soils of the steeply sloping Landscapes in the southern Appalachian Mountains. Soil Sci. Soc. Am. Proc. 34:473-478.

McCracken, R.J., R.E. Shanks, and E.E.C. Clebsch. 1962. Soil morphology and genesis at higher elevations of the Great Smoky Mountains National Park. Soil Sci. Soc. Am. Proc. 26:384-388.

Murphy, S.F., S.L. Brantley, A.E. Blum, A.F. White, and H. Dong. 1998. Chemical Weathering in a tropical watershed, Luquillo Mountains, Puerto Rico: II. Rate and mechanism of biotite weathering. Geochim. Cosmochim. Acta 62:227-243.

Newman, A.C.D. 1970. The synergetic effect of hydrogen ions on the cation exchange of potassium in micas. Clay Miner. 8:361-372.

Newman, A.C.D. and G. Brown. 1966. Chemical changes during the alteration of micas. Clay Miner. 6:297-310.

Norfleet, M.L., and B.R. Smith. 1989. Weathering and mineralogical classification of selected soils in the Blue Ridge Mountains of South Carolina. Soil Sci. Soc. Am. J. 53:1771-1778.

Novikoff, A., G. Tsawlossou, J.Y. Gac, F. Bourgeat, and Y. Tardy. 1972 Weathering of biotites in temperate, tropical, and equatorial countries. Sci. Geol. Bull. 25:287-306.

Ojanuga, A.G. 1973. Weathering of biotite in soils of a humid tropical climate. Soil Sci. Soc. Am. Proc. 37:644-646.

Peters, T.J. and B. Hofmann. 1984 Hydrothermal clay mineral formation in a biotite-granite in Northern Switzerland. Clay Miner. 19:579-590.

Pozzuoli, A., E. Vila, E. Franco, A. Ruiz-Amil, and C. De La Calle. 1992. Quaternary lahars from Monti Ernici, Central Italy. The Miner. Soc. pp. 175-183.

Raman, K.V. and M.L. Jackson. 1966. Layer charge relations in clay minerals and micaceous soils and sediments. Clays Clay Miner. 14:53-68.

Rebertus, R.A., S.B. Weed, and S.W. Buol. 1986. Transformations of biotite to kaolinite during saprolite-soil weathering. Soil Sci. Soc. Am. J. 50:810-819.

Rennie, P.J. 1990. Some threats to sustaining forest yields in North America: Research Challenges. *In:* Gessel, S.P., D.S. Lacate, G.F. Weetman, R.F. Powers (eds.). Sustained productivity of forest soils. Proc. 7th N. Am. Forest Soils Conf., Univ. B.C., Faculty of Forestry Publication, Vancouver, B.C. pp. 6-22.

Reynolds, R.C. 1971. Clay mineral formation in an alpine environment. Clays Clay Miner. 19:361-374.

Richter, D.M. 1973. Periglacial features in the central Great Smoky Mountains. Ph.D. diss. Univ. of Georgia, Athens. (Diss. Abstr. 73-31951).

Sanchez-Navas, A. 1999. Sequential kinetics of a muscovite-out reaction: A natural example. Am. Miner. 84:1270-1286.

Sawhney, B.L., and G.K. Voigt. 1969. Chemical and biological weathering in vermiculite from Transvall. Soil Sci. Soc. Am. Proc. 33:625-629.

Smith, H.T.U. 1949. Physical effects of Pleistocene climate changes in nonglaciated areas: Eolian phenomena, frost action, and stream terracing. Geol. Soc. Am. Bull. 60:1485-1516.

Soil Survey Staff. 1975. Soil taxonomy: A basic system of soil classification for making and interpreting soil surveys. USDA-SCS Agric. Handb. 436. U.S. Gov. Printing Office, Washington, D.C.

Springer, M.E., and J.A. Elder. 1980. Soils of Tennessee. Univ. of Tenn. Agric. Exp. Stn. Bull. 596, Knoxville.

Sridhar, K. and M.L. Jackson. 1974. Layer charge decrease by tetrahedral cation removal and silicon incorporation during natural weathering of phlogopite to saponite. Soil Sci. Soc. Am. Proc. 38:847-851.

Stoch, L. and W. Sikora. 1976. Transformation of micas in the process of kaolinization of granites and gneisses. Clays Clay Miner. 24:156-162.

Sverdrup, H. and P. Warfvinge. 1990. Calculating field weathering rates from soil mineralogy, texture and temperature. Proc. Int. Conf. Acid Deposition. Glasgow 16-21 Sept. 1990.

Taylor, A.B. and M.A. Velbel. 1991. Geochemical mass balances and weathering rates in forested watersheds of the southern Blue Ridge II. Effects of botanical uptake terms. Geoderma 51:29-50.

Ulen, B. and S. Snall. 1998. Biogeochemistry and weathering in a forest catchment and an arable field in central Sweden. Acta Agric. Scand. Sect. B. Soil and Plant Sci. 48:201-211.

Velbel, M.A. 1985. Geochemical mass balances and weathering rates in forested watersheds of the southern Blue Ridge. Am. J. Sci. 285:904-930.

Wang, C., and J.A. McKeague. 1984. Comments on proposed spodic criteria. Soil Sci. Soc. Am. J. 48:950.

White, A.F., A.E. Blum, T.D. Bullen, D.V. Vivit, M. Schulz, and J. Fitzpatrick. 1999. The effect of temperature on experimental and natural chemical weathering rates of granitoid rocks. Geochim. Cosmochim. Acta 63:3277-3291.

White, A.F., A.E. Blum, M.S. Schulz, D.V. Vivit, D.A. Stonestrom, M. Larsen, S.F. Murphy, and D. Eberl. 1998. Chemical weathering in a tropical watershed, Luquillo Mountains, Puerto Rico: I. Long-term versus short term weathering fluxes. Geochim. Cosmochim. Acta 62:209-226.

White, G.N., S.B. Feldman, and L.W. Zelazny. 1990 Rates of nutrient release by mineral weathering. *In:* Lucier, A.A. and S.G. Haines (eds.) Mechanisms of forest response to acidic deposition. New York: Springer-Verlag.

White, G.N. and L.W. Zelazny. 1986 Charge properties of soil colloids. *In:* Sparks, D.L. Soil Physical Chemistry. Boca Raton, Fl: CRC Press, Inc.

Wolfe, J.A. 1967. Forest soil characteristics as related to vegetation and bedrock in the spruce-fir zone of the Great Smoky Mountains. Ph.D. diss. Univ. of Tenn., Knoxville (Diss. Abstr. 68-9839).

Zabowski, D. 1990. Role of mineral weathering in long-term site productivity. P. 55-71 *In:* W.J. Dyck and C.A. Mees (ed.). Impact of intensive harvesting on forest site productivity. Proc. IEA/BE A3 Workshop, South Island, New Zealand, Mar 1989 IEA/BE T6/A6 Report no. 2. Forest Research Institute, Rotorua, New Zealand, FRI Bull. no. 159.

Zelazny, L.W. 1970. Temperature effects on potassium-calcium exchange and selectivity in selected soils, clay minerals, and cation exchange resins. Ph.D. diss. Virginia Polytechnic Institute and State Univ., Blacksburg, VA (Diss. Abstr. 71-0052

Chapter 2

Materials & Methods (Field Study)

Study Area

The field study was conducted in Grayson County, Virginia just north of Independence on the Elk Creek topographic quadrangle. The location was chosen because of the underlaying Striped Rock Alkaline Complex (A. Sinha, personal communication, 1999). Initial survey of the area revealed a large variation in rock outcrops, particle sizes, mineralogies and biotite. With the assistance of Dr. Jim Jerden however, specific locations of the biotite rich component of the Striped Rock pluton were discovered over the maximum elevation range on April 1st, 2000.

Two replicates (2 auger holes in close relation to each other) were taken from both a lower elevation (823m) and a higher elevation (1219m). Both samples were residuum formed on top of the grey coarse-grained, biotite granite (Riecken, 1966). All samples were taken from residuum on 25 % slopes, an azimuth of 125^{o}, and a slope length of 100-150m on a convex/convex slope.

Figure 2.1 Sampling area illustrating the difference in elevation. Stream is at 793m and the peak in the background is 1219m.

Lab Analysis

Full field descriptions were taken from each replicate at the two sites. Bulk samples for analysis were taken from the 1st mineral horizon (A), the control section (B horizon) with the greatest evidence of clay accumulation, and the C horizon at the point of contact with

rock or saprolite. At the high elevation site (replicate S-4), a sample of the saprolite was also taken for analysis.

Particle size analysis (PSA) was initially run on each of the 13 samples from the Striped Rock pluton. Then, a small, air-dry subsample of soil was weighed prior to and after oven drying over night at 110^{o} C. The difference in these weights was used to calculate the moisture content, assuming that the difference occurred from the loss of free water. In the succeeding analysis's, this percentage of moisture was used to convert all soil weights to oven-dry equivalents.

Using the Walkley-Black method (Walkley, 1947), the organic matter content of the samples was estimated. This procedure involved oxidizing the organic C in subsamples with a known volume of $Cr_2O_7^{-2}$, facilitated by heat from addition of H_2SO_4. Then the solution was titrated with standard $FeSO_4$ solution and Ferroin indicator to determine the excess $Cr_2O_7^{-2}$ not involved in the initial C oxidation. A 0.5g soil subsample was combined with 10ml of 1N $K_2Cr_2O_7$ and gently swirled. A 20mL rapid addition of concentrated H_2SO_4 followed, and then the mixture was swirled for one minute and allowed to stand for 30 minutes. Two hundred ml of water was added after this time, along with 5 drops of Ferroin indicator, and the suspension was titrated with $FeSO_4$ to a maroon-colored end point. The above procedure was then repeated with a second 0.5g subsample for replication purposes and a blank sample (same solution, no soil) to standardize the $FeSO_4$. The percent organic matter in each sample was then calculated assuming that the ratio of soil organic matter to oxidizable organic carbon is 2.

For samples, which, by quantitative analysis of organic matter resulted in organic carbon amounts of greater than 2.5%, removal of organic matter was necessary. Utilizing the method of organic matter removal via peroxide, the air-dried samples were placed in large, tall beakers, to reduce the risk of sample lost due to frothing. A 1M NaOAc buffer solution was added until a 1:1 ratio of buffer to soil existed. Thirty ml of H_2O_2 was added and the beaker was covered with a ribbed watch glass and allowed to stand overnight. Initial frothing was sustained by adding jets of water. Next, small volumes of

H_2O_2 were added (<30mL) and stirred while on the hot plate at about 65^o C for 10 minutes. After each addition, samples were allowed to stand for approximately 30 minutes to cool before the next aliquot was added. The additions continued several times until the brown color was lost. The excess water from the degradation of H_2O_2 was evaporated off until a soil-to-water ratio of about 1:2 was reached. The pH of the solution was recorded at 9.5. Clear solutions were decanted after sitting for several hours and the sample was washed one time with 1N NaCl.

Removal of free Fe oxides from each sample was performed for both quantitative analysis and for pretreatment for mineralogical analysis. The dithionite-citrate-bicarbonate (DCB) method (Holmgren, 1967) was used for both the quantitative subsamples and the mineralogical analysis of the samples. This method involved the reduction and solubilization of free Fe with dithionite ($Na_2S_2O_4$), the chelation of ferrous Fe with sodium citrate ($Na_3C_6H_5O_7$) to retain it in solution and buffering by bicarbonate ($NaHCO_3$) to keep the pH between 7.2 and 7.5 to maximize solubility of Fe.

Iron was removed by placing samples in 250mL centrifuge bottles with 60mL of 0.3M Na-citrate, 1.5g of solid dithionite, and 7.5mL of 1M $NaHCO_3$ and allowed to react for 1 hour. The samples were the mechanically shaken for 16 hours after which the suspension was centrifuged for 10 minutes at 2000 rpm. For the initial quantitative analysis, the Fe-containing supernatant was decanted into a 250mL volumetric. The precipitate was then washed with 50mL of saturated NaCl solution and centrifuged again for 10 minutes at 2000 rpm, with the supernatant being added to the 250mL volumetric. The volumetric was brought to volume with DDI water and an aliquot was analyzed for Fe content by ICP. For the bulk samples that iron was removed from, the supernatant was discarded and samples prepared for mineralogical analysis.

After all initial analysis and pretreatments were performed, samples were then fractionated into sand, silt and clay size particles. With the aid of a jet of pH 10 water, the samples were transferred from the tubes to a 270 mesh (47μm) sieve overtop a beaker. Each sample was gently stirred with a rubber policeman and the sand particles, which

were retained on the sieve, were rinsed with acetone and dried for 7 minutes in the oven at 110^{o}C.

The soil suspension that passed the 270-mesh sieve was centrifuged in a 200mL-centrifuge tube, which was marked 10 cm from the bottom of the tube. The solution was centrifuged to separate the silt and clay fractions. The centrifuge tube was consistently filled to the 10cm mark to ensure that centrifugation times and speeds resulted in the predicted level of sedimentation. The initial silt-clay suspension was centrifuged for 5 minutes at 2000 rpm and the supernatant containing the clay was decanted. The remaining solid containing silt and some clay was dispersed again with pH 10 water and centrifuged for 10 minutes at 1500 rpm and the clay supernatant again decanted. The suspension was subsequently dispersed with pH 10 water, centrifuged again and the supernatant once more decanted. This last step was repeated several more times to ensure that all the clay was removed from the sample.

The decanted clay which was collected in a large beaker was flocculated by reducing the pH to 4.0 using 6N HCl, mixing well, and allowing it to stand overnight. The clear water was then removed by siphoning. The total volume of clay was then determined. An aliquot of known volume was removed, weighed before and after drying at 110^{o}C, and used to determine weight of clay in the suspension.

After the sample was fractionated, the weight of the clay separate (in suspension) was determined. Ceramic tiles were allowed to soak for several minutes in distilled deionized water (DDI) and then placed on a suction apparatus similar to the procedures described by Gibbs (1971), and Whittig (1965). Each of the tiles was tested to see if they were sufficiently porous to allow 5 ml of DDI water to pass through quickly. Then 5-ml aliquots of the suspension were pipetted onto ceramic tiles to ensure that at least 250 mg of clay would be present on each tile. The tiles then underwent two different treatments to prepare for x-ray analysis. One tile was saturated with a KCl solution and the other tile was saturated with a $MgCl_2$ solution. A third tile was saturated with the KCl solution for the C-horizon from both elevations and the saprolite sample.

To saturate the tiles, first the aliquots of clay suspension were pipetted onto the tiles. The water in the suspension was suctioned through the tiles, leaving the clay on the surface. Once this had occurred, one tile was saturated with 1N KCl and the other was saturated with 1N $MgCl_2$. The saturations were performed with 5 ml of the respective solution applied directly to the tile, and allowed to suction through. This application was repeated a total of 5 times. After both tiles had been saturated with one of the solutions, the tiles were washed 5 times with 5 ml of DDI water, each application being allowed to result in complete suction through the tile. The tile that was saturated with $MgCl_2$ then received a 5-ml addition of a 20% glycerol solution. The second KCl-saturated tile for the C-horizons and the saprolite was then treated with formamide in the same manner as the glycerol above (Churchman, et al., 1984). All tiles were then transferred to dessicators that were designated for that saturation.

The K-saturated tile and the Mg-glys saturated tile were both analyzed on the x-ray instrument at room temperature (25^0 C). The K-sat tile was then heated overnight to temperatures of 110^0, 300^0, and 550^0 C, and the x-ray was performed after each successive heat treatment. For S-4 high elevation horizon, an extra Mg-glys sample was created and heated once more to 110^0 C. X-ray analysis was then performed on this sample to better identify the presence of montmorillonite via peak collapse from the heat treatment.

A random powder mount was also preformed using XRD. The biotite granite parent material was ground to a silt size fraction (50-2μm) and was randomly mounted using the top loading technique onto the power mount disk to prevent any orientation of the sample. The sample was then run using the x-ray diffractometer.

Non-crystalline material was estimated by use of an acid ammonium oxalate in the dark procedure (Hodges and Zelazny, 1980). About 250mg of sample were weighed into pre-weighed centrifuge tubes and dried at 110^oC. Tubes were allowed to cool in a dessicator and then re-weighed to get the dry weight of the sample. The tubes were then wrapped in

foil and acid ammonium oxalate was added. After shaking for 2 hours, the tubes were centrifuged and the supernatant discarded. The samples were washed 3 times with $(NH_4)_2CO_3$ and once with DDI water and allowed to dry overnight at 110^oC. Once tubes cooled again in the dessicator, non-crystalline material was estimated by the weight loss.

Montmorillonites and vermiculites in the samples were quantified by measurement of cation exchange capacity (CEC) via the exchange with various cations (Jackson, et al. 1986). To characterize the two minerals, 100mg of sample was weighed into a pre-weighed centrifuge tube. Samples were initially saturated with either Ca^{2+} or NH_4^+. After the weight of the entrained solution was measured, Ca^{2+} saturated samples were then exchanged with Mg^{2+} and the wash was saved for Ca^{2+} analysis. Likewise, the NH_4^+ saturated samples were weighed and exchanged with K^+ and analyzed for NH_4^+. The CEC ($cmol^+/kg$) was calculated by dividing the exchanged cations by the sample weight. The amount of vermiculite was quantified using the difference between the CEC obtained by the Ca^{2+} analysis and the CEC from the NH_4^+ analysis. The amount of montmorillonite was estimated using the CEC from the NH_4^+ analysis of the Jackson, et al. (1986) procedure.

Thermal analysis was also used to characterize these samples. To characterize the samples via thermal analysis, two small subsamples of each sample, about 10 mg each, were selected and gently ground with a mortar and pestle. One of the two subsamples from each sample was placed in a dessicator with a relative humidity of 56% by means of a $Mg(NO_3)_2$ slurry (Karathanasis and Hajek, 1982a). This was performed to enhance the quantification of the vermiculite and montmorillonite fraction. Both subsamples were placed in a small platinum dish. The TGA instrument then measured the weight loss as the temperature increased from 50^oC to 1000^oC.

External surface area, as measured by N_2-surface area, was also used to characterize the samples. About 1g of dried sample was weighed into the previously weighed surface analyzer tubes. The tubes were then placed in at 110^o C degasser and purged with N_2 gas to remove water and CO_2 from the samples. After 12 hours the samples were removed

from this degassing unit and placed on the degas port on the surface area analyzer. At this point, the samples were heated to 100^{o} C and placed under a vacuum overnight. After the analyzer indicated that the sample had been degassed sufficiently, the tube + sample was weighed to determine the degassed weight. Samples were then subjected to increasing quantities of N_2 gas and monolayer coverage calculated by application of the BET theory to determine the surface area.

Total specific surface area was obtained by following the method described by Carter, et al. (1965), after saturating the sample with $CaCl_2$. Samples were saturated by washing 3 times with 1 N $CaCl_2$, centrifuged at 1500 rpm for 10 minutes, excess salts were removed by washing with DDI water, and allowed to dry in the oven at 80^{0} C. Samples were then gently ground with a mortar and pestle until fine. These samples were then transferred to an Al dish, weighed, and about 3 ml EGME was added to each sample. The samples were allowed to equilibrate overnight in a dessicator that contained a $CaCl_2$-EGME slurry in the bottom along with a montmorillonite standard that was prepared in the same manner as above. Subsequently, these samples were placed on a vacuum apparatus at 0.25mm Hg for about 45 minutes. The dessicator was then allowed to come back to equilibrium with atmospheric pressure by allowing air to pass through a drying tube, samples were removed, weights recorded and returned to the dessicator and again vacuum applied. This procedure was repeated 3 times until samples obtained constant weight and the montmorillonite standard reached approximately its monolayer. Recorded weight values were then converted into the specific surface areas.

Scanning electron microscopy (SEM) was conducted on subsamples from selected horizons to observe morphologies of the clay minerals. Samples were gold coated to increase the conductivity and subsequently imaged.

Materials and Methods (Column Study)

Two separate column studies were performed to assess the various treatments on the weathering products of an Ontario biotite. The biotite was reconstituted and a gravity flow design used to mimic the rate of leaching for field conditions and to induce periods of reduced water content between leaching events (White, et al. 1990). One study addresses weathering with varying temperatures, surface horizons and rainfall rates as treatments and the other study addressed influences of selected acids at two simulated rainfall rates. As controls for background measurements, one blank column (no biotite) was prepared for each different type of leachate at each temperature.

Bulk samples of Ontario biotite were initially ground by use of a Waring blender to pass through a 2.5mm mesh sieve (Fisher Scientific, U.S. Standard Testing). Grinding was then continued by the use of a McCrone Micronizer with corundum tumbling elements in a water slurry for a duration of 12 minutes. Following Micronizer grinding, the biotite particle size was in the silt/clay fraction (<50μ). This biotite slurry was flocculated, washed and dried.

Eight inch long, ¾ inch diameter columns were fitted in four racks of 18 plus one tube rack with 13 columns (Figure 2.2). Each column was packed from the bottom with 0.250g glass wool, 2.500g quartz sand, 1.500g ground biotite, and topped with 2.500g of a surface horizon. The blank columns consisted of 0.250g glass wool, and 5.000g of quartz sand. A spruce-fir surface horizon was used to emulate the indigenous, undisturbed litter layer of the high elevation Blue Ridge and a hardwood surface horizon used to emulate lower elevation litter layers and the litter layer that would have once been indigenous to the Piedmont. The spruce-fir surface horizon was collected from an undisturbed stand at Whitetop Mountain, VA, and the hardwood surface horizon was collected at a virgin hardwood stand at Reynold's Homestead in the Piedmont of Virginia. These surface horizons were packed on top of the biotite layer to influence the leachate through the columns treated with these horizons.

Figure 2.2 Example of one of the racks of 18 columns, with vials to collect the leachate.

Initially 20ml of leachate was passed through all columns to ensure column moisture and equilibrate the system. Then, all columns were leached with 5 or 20ml of leachate 3 times a week for a total of 6 months. Samples of the leachate were retrieved after every four additions and analyzed for elemental content (K, Mg, Al, Si) via inductively coupled plasma (ICP) analysis, as well as measured for pH.

Organic acids can affect the dissolution of biotite in many ways; they lower the pH, form surface complexes, effect ion solubility, and allow more extensive dissolution with respect to solution/mineral equilibrium (Drever and Vance, 1993). Acids used were citric, fulvic, hydrochloric (HCl) and ascorbic, with each acid diluted to a concentration of 1mM. Citric acid was chosen because of its strong chelating abilities with Fe and Al, its ubiquity in soils due to microbial activity, and its competition with other molecules for surface edge sites (Ng Kee Kwong and Huang, 1975; Ng Kee Kwong and Huang, 1979; Boyle, et al., 1974; and Song and Huang, 1988). Citric acid was created using Na-citrate. Protonated fulvic acid was used because of its efficiency in decomposing 2:1 minerals (Tan, 1980), its common association with softwood growth (Bennett and Casey, 1993) and because of its ubiquity in virtually every soil solution, surface water, and groundwater (Drever and Vance, 1993). Fulvic acid was created using a standardized fulvic separate from Pahokee, Fl (Zelazny, 1974). One mM in respect to carboxyl groups

of the fulvic acid had a weight of 222.22mg/L. Ascorbic acid was used because it is naturally occurring due to microbial processes, a common reductant, and a chelator similar to citric acid and as a reducing agent (Eick, personal communication, 2000). Finally 0.001N HCl was used as an inorganic standard.

Upon conclusion of the six months of treatment, the columns were disassembled, and prepared for analysis of the biotite fraction. Initial disassembly was performed carefully to discourage as much mixing with the other fractions (sand and surface horizons) with the biotite. Separations were then performed similar to that described in the field study. X-ray analysis of Mg-saturated, glycerol solvated samples was performed on selected replicates. Due to small sample sizes, the samples were mounted on glass slides. To do this, samples in suspension were washed 5 times with $MgCl_2$ and 5 times with water. Incorporating an eyedropper, samples were transferred to Wards petrographic glass slides and allowed to air dry. This drying encouraged gravity settling of the clays so the finer clays would dry on the surface of the mount and be most prominent when x-rayed. No other analyses were used to characterize the column clays.

Literature Cited

Alexiades, C.A., and M.L. Jackson. 1965. Quantitative determination of vermiculite in soils. Soil Sci. Soc. Am. Proc. 29:522-527.

Bennett, P.C. and W. Casey. 1993. Chemistry and mechanisms of low-temperature dissolution of silicates by organic acids. *In:* Pittman, E.D. and M.D. Lewan (eds.). Organic Acids in Geological Processes. New York: Springer-Verlag. pp. 162-200.

Boyle, J.R., G.K. Voigt, and B.L. Sawhney. 1974. Chemical weathering of biotite by organic acids. Soil Sci. 117(1):42-45.

Carter, D.L., M.D. Heilman, and C.L. Gonzalez. 1965. Ethylene glycol monoethyl ether for determining surface area of silicate minerals. Soil Sci. 100:356-360.

Churchman, G.J., J.S. Whitton, G.C.C. Claridge, and B.K.G. Theng. 1984. Intercalation method using formamide for differentiating halloysite and kaolinite. Clays Clay Mineral. 32:241-248.

Drever, J.I. and G.F. Vance. 1993. Role of soil organic acids in mineral weathering processes. *In:* Pittman, E.D. and M.D. Lewan (eds.). Organic Acids in Geological Processes. New York: Springer-Verlag. pp. 139-161.

Gibbs, R.J. 1971. X-ray diffraction mounts. (In) R. E. Carver. Procedure in sedimentary petrology, Wiley-Interscience. pp. 533-534.

Karathanasis, A.D., and B.F. Hajek. 1982a. Revised methods for rapid quantitative determination of minerals in soil clays. Soil Sci. Soc. Am. J. 46:419-425.

Holmgren, G.G.S. 1967. A rapid citrate-dithionite extractable iron procedure. Soil Sci. Soc. Am. Proc. 31:210-211.

Ng Kee Kwong, K.F. and P.M. Huang. 1975. Influence of citric acid on the crystallization of aluminum hydroxide. Clays Clay Miner. 23:164-165.

Ng Kee Kwong, K.F. and P.M. Huang. 1979. Surface reactivity of aluminum hydroxides precipitated in the presence of low molecular weight organic acids. Soil Sci. Soc. Am. J. 43:1107-1113.

Riecken, C.C. 1966. Petrography of the Striped Rock Granite and Surrounding Rocks, Grayson County, Virginia. Ph.D. Diss. VPI&SU., Blacksburg, VA.

Song, S.K., and P.M. Huang. 1988. Dynamics of potassium release from potassium-bearing minerals as influenced by oxalic and citric acids. Soil Sci. Soc. Am. J. 52:383-390.

Tan, K.H. 1980. The release of silicon, aluminum, and potassium during decomposition of soil minerals by humic acid. Soil Sci. 129(1):5-11.

Walkley, A. 1947. A critical examination of a rapid method for determining organic carbon in soils: Effect of variations in digestion conditions and of inorganic soil constituents. Soil Sci. 63:251-38. *In:* Page, A.L., R.H. Miller and D.R. Keeney (eds.). Methods of Soil Analysis. 1986. Madison, WI: ASA and SSSA. pp.570-571.

White, G.N., S.B. Feldman, and L.W. Zelazny. 1990. Rates of nutrient release by mineral weathering. *In:* Lucier, A.A. and S.G. Haines (eds.) Mechanisms of forest response to acidic deposition. New York: Springer-Verlag. pp. 108-162.

Whittig, L.D., and W.R. Allardice. 1986. X-ray diffraction techniques. ASA, pp.331-362.

Zelazny, L.W. and V.W. Carlisle. 1974. Physical, chemical, elemental and oxygen-containing functional group analysis of selected Florida Histisols. p. 63-78. *In:* A.R. Aandahl, S.W. Boul, D.E. Hill, and H.H. Bailey (ed.) Histosols: Their characteristics, classification, and use. Soil Sci. Soc. Am. Spec. Pub. No. 6. ASA, Madison, WI.

Chapter 3

Results and Discussion (Field Study)

These soils possess characteristics of young soils, evidenced by their classification as Inceptisols, typical of the Blue Ridge province in Virginia. Field descriptions of the profiles the soils from both sites, the high elevation and low elevation, were used to classify the soils as mixed, active, Typic Dystrudepts. The upper elevation site (1219m) was identified as the Peaks series, characteristic of the ridge top / shoulder slope topography, 1066mm of mean annual precipitation, and a mean annual temperature of 12.78^{o}C. The lower elevation site (822m) was identified as the Edneyville series, also characteristic of ridges and shoulder slopes in the Blue Ridge, with a higher mean annual precipitation (1651mm a year) and a higher mean annual temperature (13.33^{o}C). The high elevation site (Peaks) was observed to have many more large roots, due to the forested vegetation, and large rocks, as the profile was augered. Both sites were formed from residuum parent material. The stable, nonmetamorphosed granite parent material led to a solum with limited weathering throughout the profile. The weathering of these soils at both sites was minimal, because of the low amount of iron oxides, low clay content, and the presence of unstable clay minerals. To determine the initial stages of the weathering process, only the clay fraction was analyzed since it should be most susceptible to weathering. The clay mineralogy of all the samples, both at the high and low elevation, shared similar mineral suites. This is a result of the criteria for choosing the sites, keeping slope, aspect, and parent material as constant as possible while changing elevation and vegetation (Table 3.1.). Several 2:1 type minerals were common in the surface horizon including biotite, despite its unstable nature in soil environments. Gibbsite, micas, and quartz commonly occurred together in these soils, with some accumulations of kaolinite in the lower horizons and some feldspars throughout. By studying the clay fractions of these samples, the weathering differences in biotite are observed between two different vegetations and microclimates. Several analyses were used to study the weathering differences since one single analysis may give incomplete

mineralogical information. The discussion of the strengths and weaknesses of each analysis will be presented along with how it may compliment other tests.

Table 3.1 Summary of sampling characteristics at each elevation site replicate.

	Low Elevation		**High Elevation**	
ID	*s1*	*s2*	*s3*	*s4*
Series	Edneyville	Edneyville	Peaks	Peaks
Elevation (m)	822	822	1219	1219
Parent Material	Srb* Granite	Srb* Granite	Srb* Granite	Srb* Granite
Vegetation	Pasture	Pasture	Oak	Oak
Slope (%)	27	27	25	25
Azimuth (deg.)	125^{o}	125^{o}	125^{o}	125^{o}
Landscape Position	Shoulder	Shoulder	Shoulder	Shoulder

***Striped rock biotite granite.**

Initial Soil Analysis

The Particle Size Analysis (PSA) reveals that all four sites had very similar sandy loam (SL) textures, except for the C-horizon from the second site (S-2) and the saprolite horizon of the fourth site, which were loamy sand (LS). Percent silt and clay quantification of iron and carbon, as well as the percent moisture are presented in Table 3.2. All of the high elevation sites have greater values for moisture, iron and carbon.

Table 3.2 Summary of initial soil analysis for each horizon at the two elevations sites. Standard deviation shown in parentheses beside the mean value.

Site #	*% moist*	*%OC*	*% Fe*	*% Silt*	*% Clay*	*Ratio %Fe/ %Clay*	*Depth of Horizon (cm)*
				A-Horizon			
s1	1.34	3.15	1.07	29.70	1.70	0.63	5.08
s2	1.42	4.24	1.12	35.20	2.40	0.47	5.08
mean	1.38 (0.17)	3.69(0.67)	1.09(0.04)	32.45(3.89)	2.05(0.49)	0.55(0.11)	5.08(0.00)
s3†	2.38	5.18	1.52	25.90	7.50	0.20	7.62
s4†	2.33	3.79	1.65	25.80	7.60	0.22	15.24
mean	2.35(0.11)	4.48(0.81)	1.59(0.16)	25.85(0.07)	7.55(0.07)	0.21(0.01)	11.43(5.39)
				B-Horizon			
s1†	1.76	1.06	1.05	29.10	4.80	0.22	30.48
s2†	2.08	1.10	0.97	25.20	5.90	0.16	40.64
mean	1.92(0.34)	1.08(0.04)	1.01(0.06)	27.15(2.76)	5.35(0.78)	0.19(0.04)	35.56(7.18)
s3†	3.12	2.15	1.77	28.40	11.50	0.15	15.24
s4†	2.56	1.61	1.71	26.00	13.70	0.12	27.94
mean	2.84(0.41)	1.88(0.33)	1.74(0.09)	27.20(1.70)	12.60(1.56)	0.14(0.02)	21.59(8.98)
				C-Horizon			
s1†	1.56	0.77	1.14	18.10	14.10	0.08	40.64
s2†	1.13	0.78	0.84	21.60	1.80	0.47	45.72
mean	1.34(0.26)	0.78(0.12)	0.99(0.19)	19.85(2.47)	7.95(8.70)	0.27(0.27)	43.18(3.59)
s3†	2.28	1.12	1.29	16.60	13.80	0.09	20.32
s4†	2.09	1.13	1.90	19.90	9.30	0.20	20.32
mean	2.18(0.20)	1.13(0.05)	1.59(0.36)	18.25(2.33)	11.55(3.18)	0.15(0.08)	20.32(0.00)
Sapr*	1.94	0.90	0.78	16.30	4.00	0.19	15.24

†sample identification, s1 and s2 are low elevation samples; s3 and s4 are high elevation samples

***saprolite**

X-Ray

X-ray analysis of the three major horizons for each replicated site allowed identification of the clay mineral suites. Noncrystalline materials and iron oxides were not accounted for in these analyses. The surface horizons were dominated by hydroxy-interlayered vermiculite (HIV), vermiculite, and some kaolinite. The HIV has a distinct peak characterized by a peak at 14Å d-spacing (thickness of one unit cell) at room temperature

collapsing to 11Å when heated to 500^{o}C. A 14Å peak at room temperature collapsing completely to 10Å at 500^{o}C similarly identifies the vermiculite. The kaolinite and gibbsite are characterized by 7.4Å / 3.5Å and 4.83Å / 4.34Å peaks respectively. Halloysite may also be indicated by the 7Å peak, therefore separating halloysite from kaolinite is necessary by using a saturation with KCl-formamide treatment. The formamide treatment results in selective intercalation in the halloysite structure, expanding it to 10Å. This expansion facilitates the quantification of kaolinite and halloysite. Montmorillonite, present in some samples, is identified by its 18Å peak with Mg-saturation, glycerol solvated (Mg-glys) treatment that collapses to 14Å upon K^{+} saturation. Since x-ray background may be intense in this region, it can additionally be identified by observation of the 14Å-peak intensity after the Mg-glys sample is heated to 110^{o}C. Peak intensity is measured in counts per second (CPS).

Many subtle differences were evident by x-ray identification of the clays between the high elevation and low elevation sites. Examination of the A horizon of the four sites reveals 3 apparent differences between these seemingly similar soils. As illustrated in Figure 3.1. at room temperature with Mg-glys treatment, the high elevation site replicate, S-3, has a stronger montmorillonite peak (18Å) after the Mg-glys treatment. The other high elevation site replicate, S-4, does not appear to have a montmorillonite peak after the Mg-glys treatment, but this could be due to masking of the peak by the onset on the low angle side.

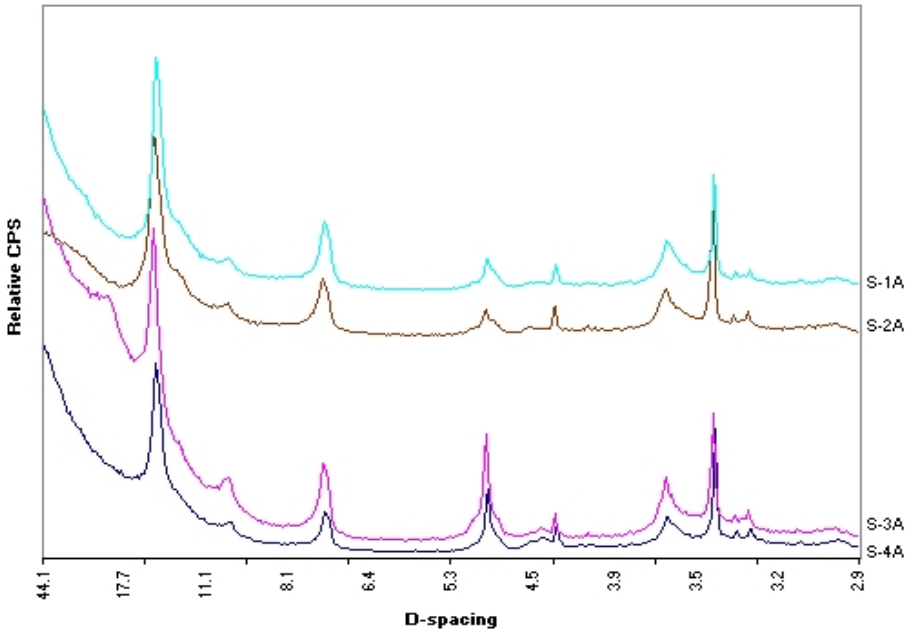

Figure 3.1 Clay (<2µ) mineralogy of the A-horizon replicates of both elevations. All samples were Mg-glys treated and analyzed at 25°C. Peak intensity in counts per second (CPS).

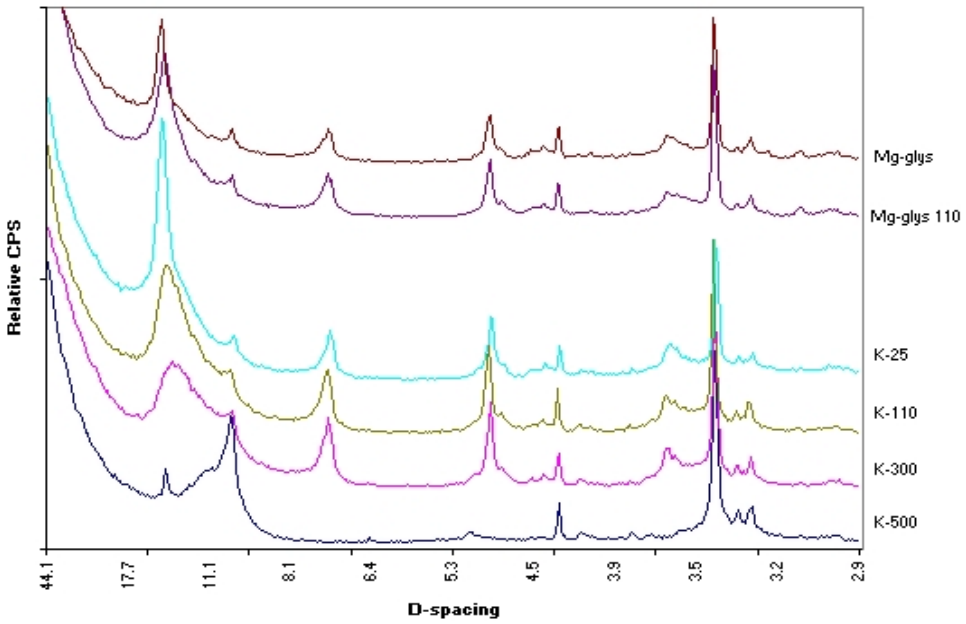

Figure 3.2 X-ray diffractograms of the clay (<2µ) fraction of the A-horizon S-4 replicate. Samples treated with Mg-glys or KCl as indicated at various temperatures.

Figure 3.2 illustrates the five x-ray treatments for S-4 and the progression of peak collapse. Although the montmorillonite peak is not as evident after Mg-glys treatment, an

additional treatment was added to this sample to better interpret the presence of montmorillonite. Following Mg-glys treatment, the sample was heated to 110°C. Since the heating causes montmorillonite to collapse to approximately 14Å, the 14Å peak of a sample containing montmorillonite would increase in intensity, increase in peak area, and the ratio of peak height to peak area would decrease. All of the 14Å peak features (Table 3.3) from heating the Mg-glys treatment of the S-4 replicate indicate that montmorillonite is present in the S-4 replicate.

Table 3.3 Effects of Mg-glys saturation at 25°C and 110°C for the A horizon S-4 replicate 14Å peak.

	Heat Treatment (°C)	
	25	*110*
14Å peak intensity (CPS)	1396.5	1585.8
Peak Area $(units)^2$	327.9	648.5
Peak Height / Peak Area	2.56	1.42

Montmorillonite appears to be a product of biotite weathering after a vermiculite intermediate phase. This indicates that the high elevation surface horizons have different weathering factors than the low elevation samples, which do not exhibit the presence of montmorillonite. The existence of montmorillonite is inconsistent with the high leaching, acid environment, however, high base saturation and the presence of slow leaching microenvironments can allow montmorillonite to form and exist in their high leaching environment.

The higher elevation sites also appear to have more intense gibbsite peaks (4.83Å and 4.34Å) relative to the lower elevation (Figure 3.1). The higher intensity gibbsite peaks indicate a more intense weathering environment that has caused the dissolution of phyllosilicates or feldspars with reprecipitation of Al-oxides. Chlorite, a possible product

of biotite weathering is also identified in all the samples by a 14Å peak that remains after the 500°C treatment.

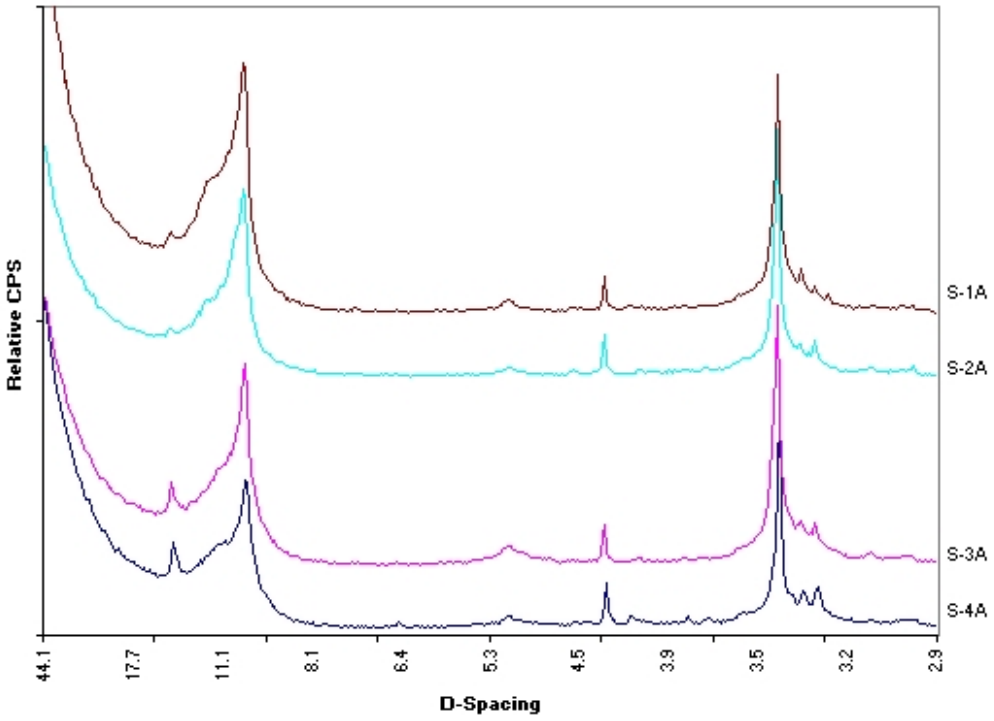

Figure 3.3 Clay (<2µ) mineralogy of the A-horizon replicates of both elevations. All samples were KCl-saturated and analyzed at 500°C.

.

The differences found in the B-horizon resemble that of the A horizons but to a more pronounced extent. The existence of montmorillonite in the high elevation samples, identified by the 18Å peak with Mg-glys saturation (Figure 3.4), and the complete lack thereof in the lower elevation is very evident in the sample of this horizon.

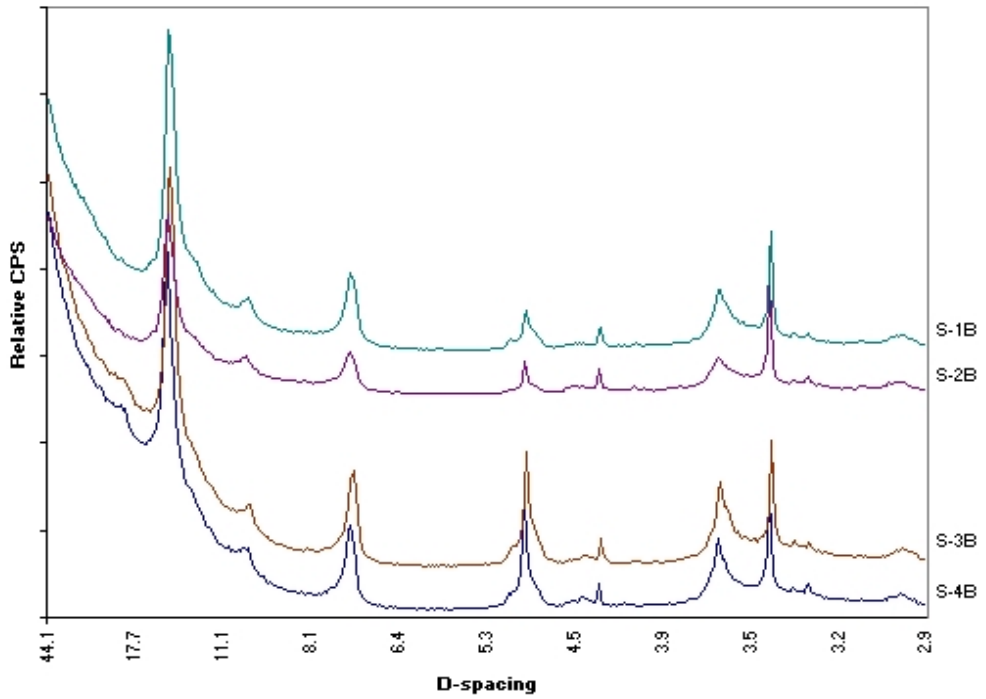

Figure 3.4 Clay (<2µ) mineralogy of the B-horizon replicates of both elevations. All samples were Mg-glys treated and analyzed at 25°C.

The 500°C treatment illustrates the strong presence of chlorite in the higher elevation samples while the chlorite peaks are broad and less intense in the lower elevation samples. Finally, the same treatment shows a difference in the peaks collapsing towards 10Å (Fig. 3.5). The higher elevation 10Å peaks are very skewed and broad, apparently with many hydroxy-interlayer minerals or montmorillonite relative to the vermiculite concentration in the sample. The lower elevation peaks, though skewed to the low angle side (greater d-spacing), also produce intense, sharp peaks at 10Å, suggesting much of what was identified in this sample is vermiculite. This would imply that the higher elevation samples have weathered through the vermiculite intermediate to more advanced weathering products such as montmorillonite and HIV. . The 4.83Å gibbsite peak is much more intense in the high elevation sites again.

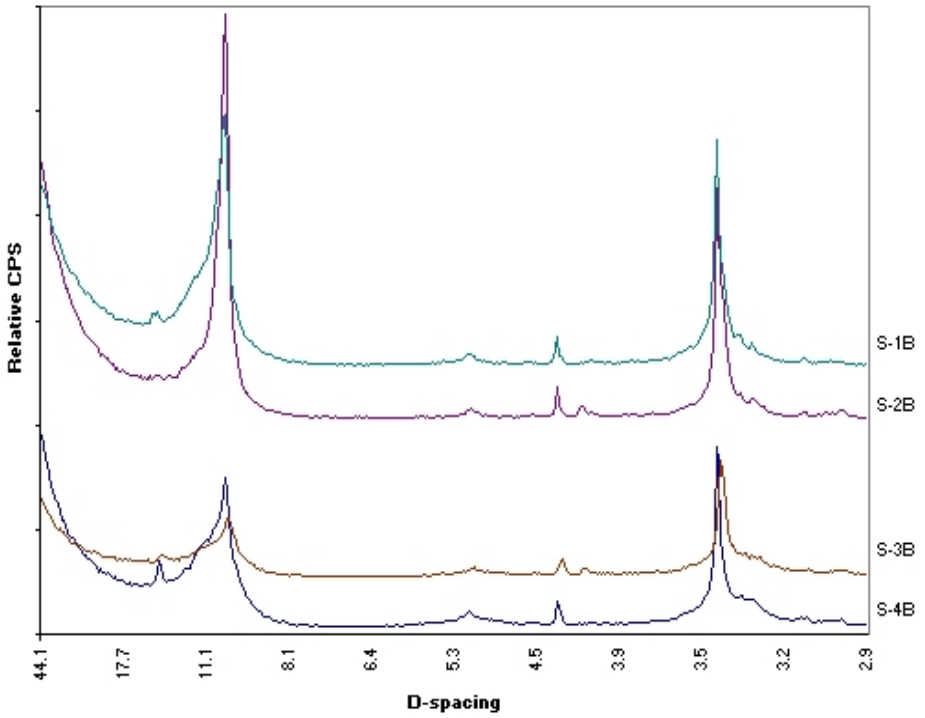

Figure 3.5 Clay (<2μ) mineralogy of the B-horizon replicates of both elevations. All samples were KCl-saturated and analyzed at 500°C.

The C-horizon illustrates one significant difference between the two elevations upon initial observation of x-ray patterns. At Mg-glys room temperature, the 14Å peak at the lower elevation is much more intense than the higher elevation (Fig. 3.6). Proceeding through the heat treatments, the peaks collapse to a final d spacing of 10Å at 500° C, therefore identifying this peak as primarily vermiculite at the lower elevation (Fig. 3.7). The low intensity, broad peaks of the higher elevation samples do indicate the strong presence of vermiculite as well, but to a much lower degree than the low elevation samples. There is no evidence of intergrade minerals, citing the lack of skewedness of the 10Å peak at the 500° C heat treatments. The saprolite horizon, from the high elevation, (Fig. 3.8) exhibits similar trends to the high elevation C-horizons at the Mg-glys and 500° C treatments.

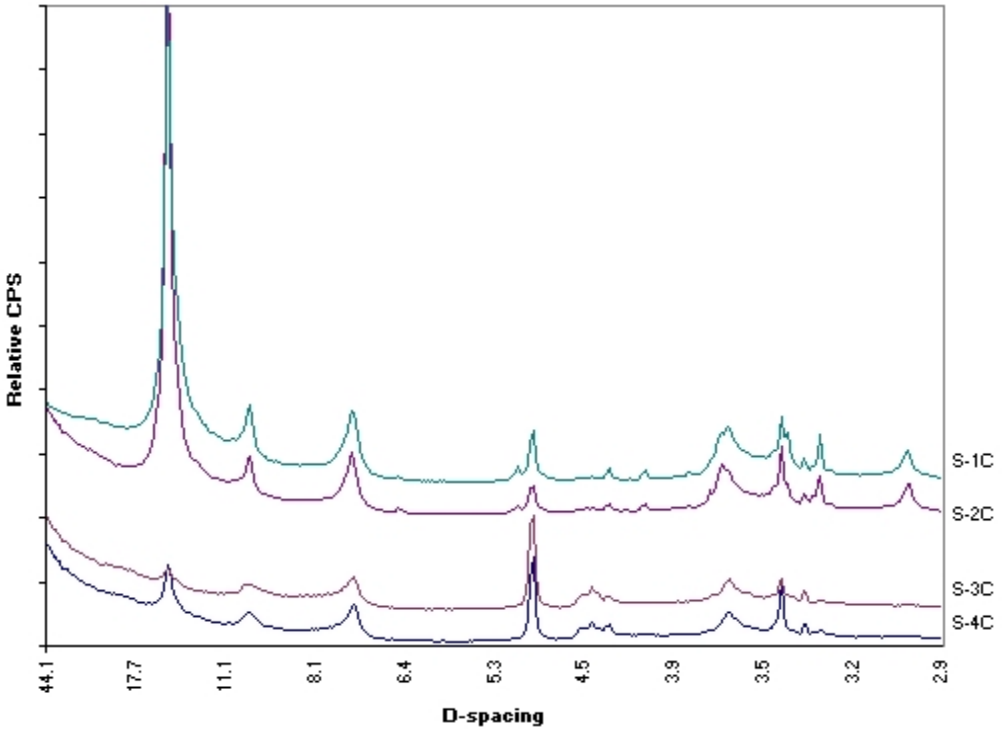

Figure 3.6 Clay (<2µ) mineralogy of the C-horizon replicates of both elevations. All samples were Mg-glys treated and analyzed at 25°C.

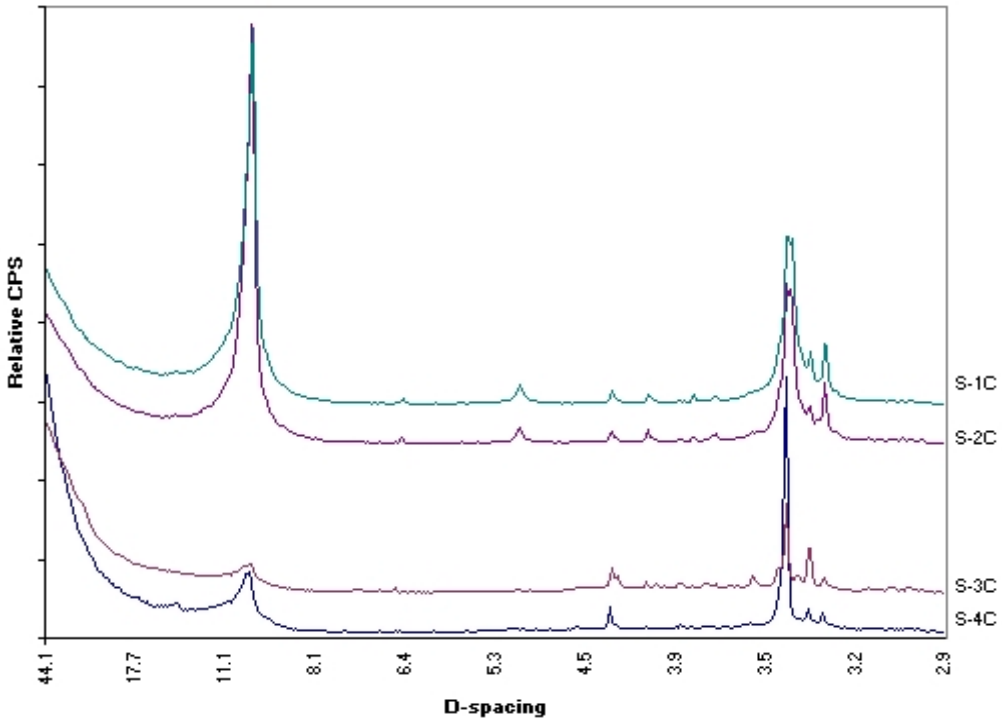

Figure 3.7 Clay (<2µ) mineralogy of the C-horizon replicates of both elevations. All samples were KCl-saturated and analyzed at 500°C.

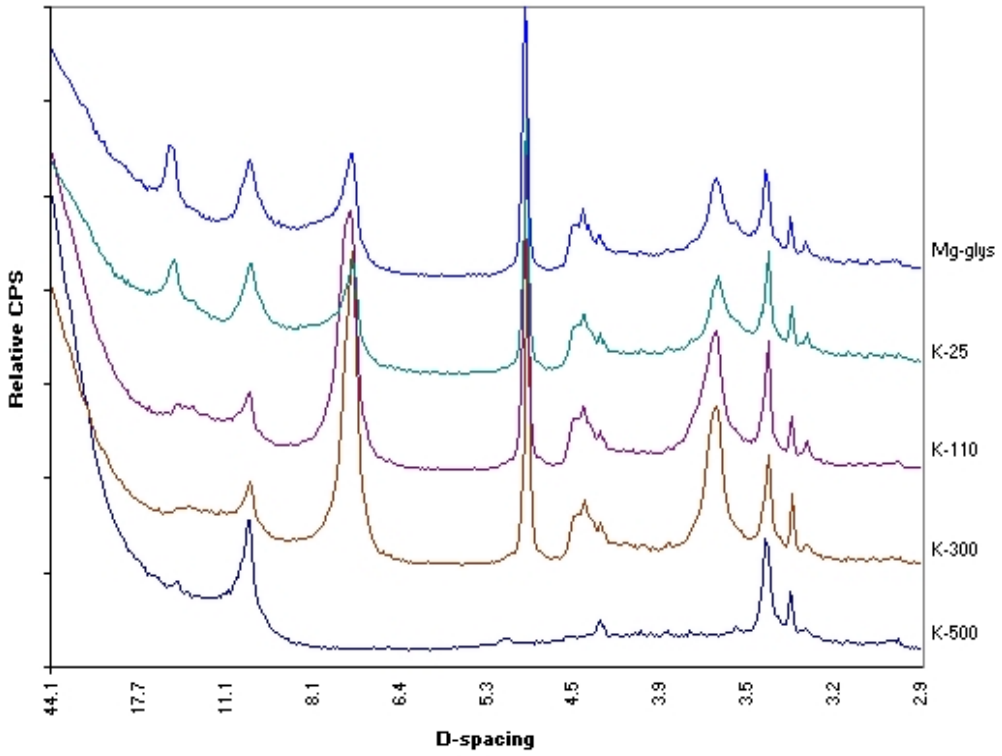

Figure 3.8 X-ray diffractograms of the clay (<2μ) fraction of the saprolite horizon from the high elevation. Samples treated with Mg-glys or KCl as indicated at various temperatures.

The progression of the saprolite sample through the treatments indicates that this sample has vermiculite with little to no intergrade and has a large amount of kaolinite and halloysite. The successive increase of the 7Å-peak intensity up to the 300^{o}C treatment is an indication that there may be a large proportion of halloysite in the saprolite and possibly in the C-horizons as well. SEM images also show a noticeable amount of halloysite (tubular structure) in the saprolite and high elevation C that will be presented later. The KCl-formamide treatment was used in the C-horizons and the saprolite to quantify the amount of halloysite and kaolinite. Halloysite is not a large portion of the 1:1 type minerals in the two low elevation horizons as illustrated by the formamide treatments in Figure 3.9;

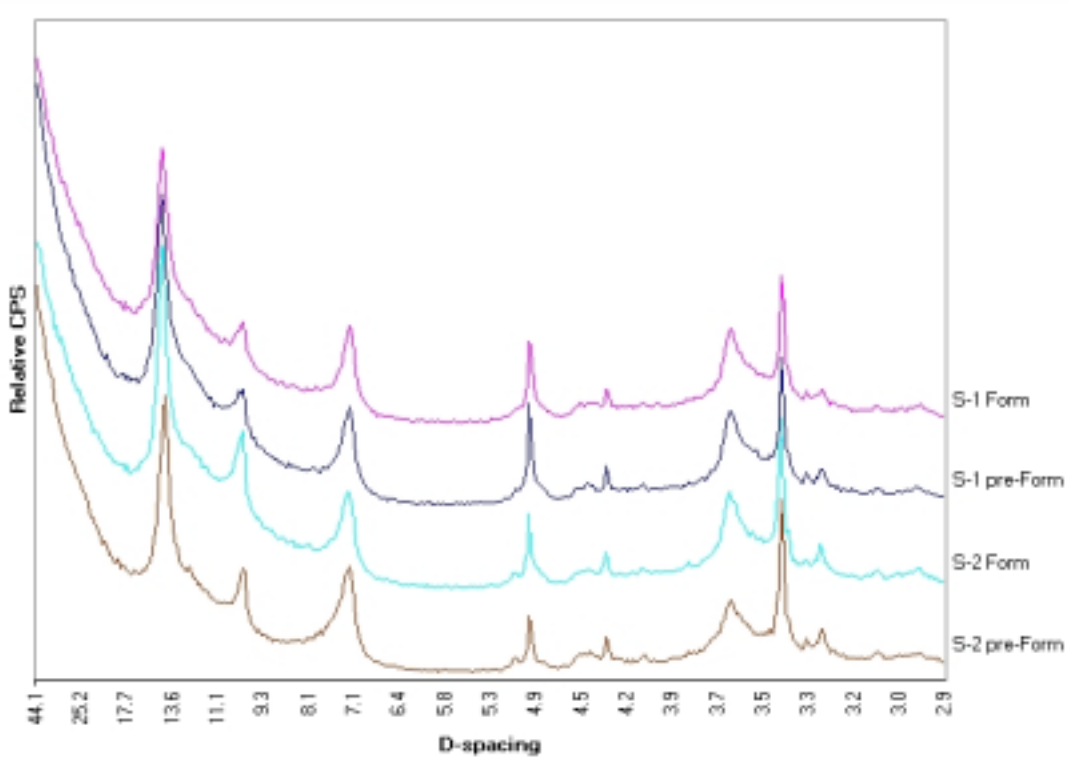

Figure 3.9 X-ray diffractograms of the clay (<2μ) fraction from the low elevation C-horizons. Comparison of formamide treated samples (Form) with untreated samples (pre-Form) show subtle changes in the 7Å and 10Å peaks.

however, the high elevation replicates have a much larger proportion of halloysite, as indicated in Figure 3.10,

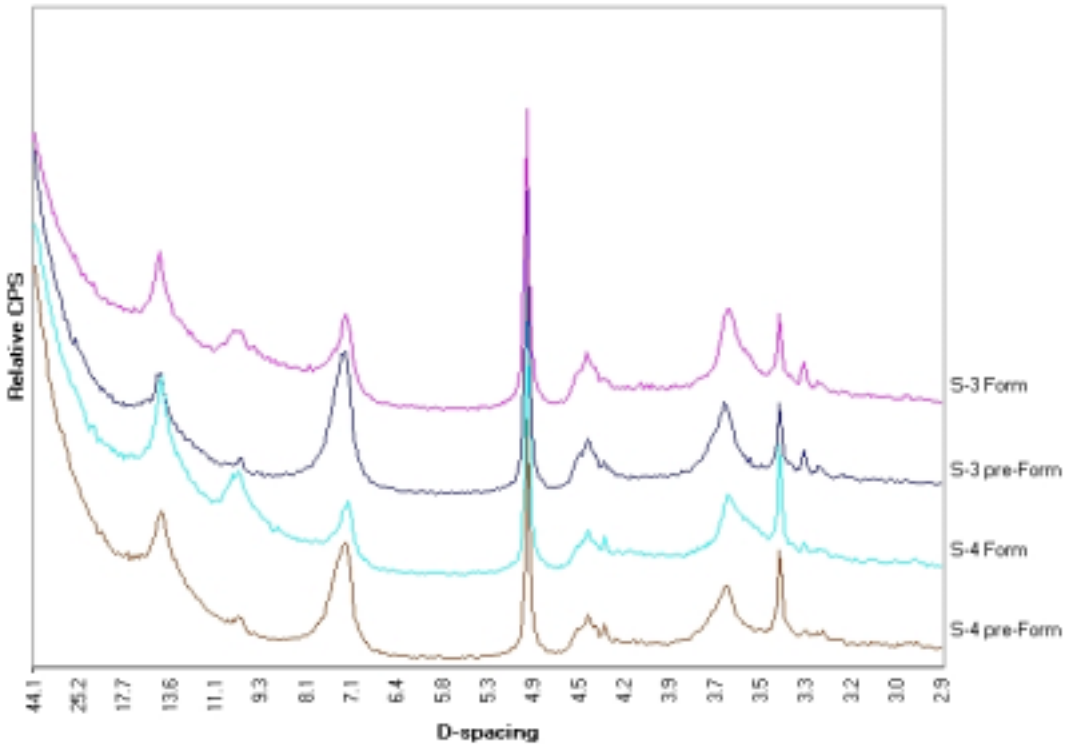

Figure 3.10 X-ray diffractograms of the clay (<2μ) fraction from the high elevation C-horizons. Comparison of formamide treated samples (Form) with untreated sample (pre-Form) show a significant amount of halloysite in the higher elevation samples.

while the saprolite horizon exhibited the greatest amount of halloysite, apparent in Figure 3.11.

Using the change in the 7Å peak areas before and after formamide treatment, the percentage of kaolinite comprising the 7Å peak was calculated (Table 3.4). The amount of kaolinite was adjusted to a clay fraction basis by incorporating TGA results (also discussed later). The values were also adjusted to a whole soil basis.

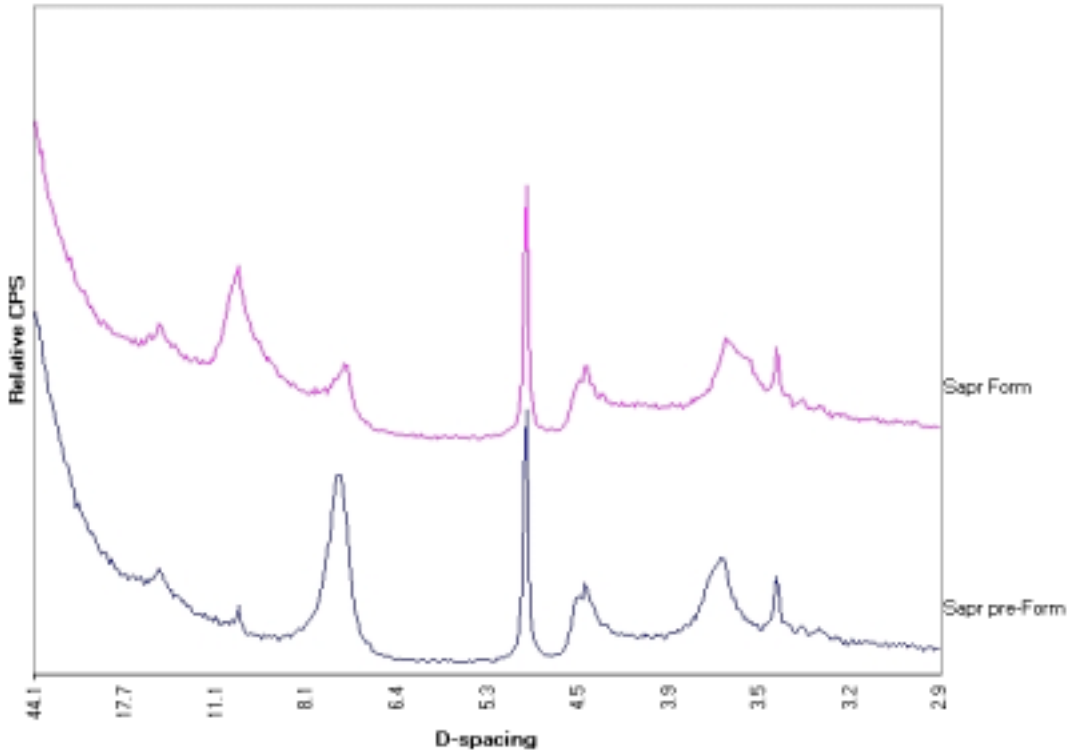

Figure 3.11 X-ray diffractograms of the clay (<2μ) fraction from the saprolite horizon. Comparison of formamide treated samples (Form) with untreated samples (pre-Form) show halloysite dominating the 1:1 character of the saprolite.

Table 3.4 Summary of the KCl-formamide treatment on the C horizons and saprolite 7Å peak.

	7Å peak area			clay fraction		whole soil	
	KCl	KCl + formamide	% kaolinite in 7A peak	% kaolinite	% halloysite	% kaolinite	% halloysite
S-1	268.5	257.9	96	29	1	4	<1
S-2	298.9	234.1	78	24	7	<1	<1
S-3	621.3	280.2	45	18	23	2	3
S-4	521.3	197.5	38	16	25	2	3
saprolite	711.9	161.5	23	12	42	1	2

The recrystallization of halloysite deep in a profile is the result of pseudomorphic transformation of both biotite and sodic plagioclase. Halloysite at the saprolite contact is typical, however, it commonly recrystallizes to kaolinite higher in the profile. The dominance of halloysite in the high elevation samples corresponds to the higher weathering intensity observed in these horizons.

Furthermore, the halloysite, kaolinite and vermiculite characterized in the C-horizon are all pedogenic. X-ray inspection of the parent material reveals that it is primarily quartz ≈ orthoclase > biotite >> plagioclase (Fig 3.12). The weathering difference between the low elevation and high elevation samples can be related to the difference in leaching intensities rather than temperature. Assuming that the 2:1's in the C-horizons are a result of biotite weathering from the parent material, this would suggest that biotite kaolinization versus biotite vermiculitization is controlled by factor such as leaching more so than temperature.

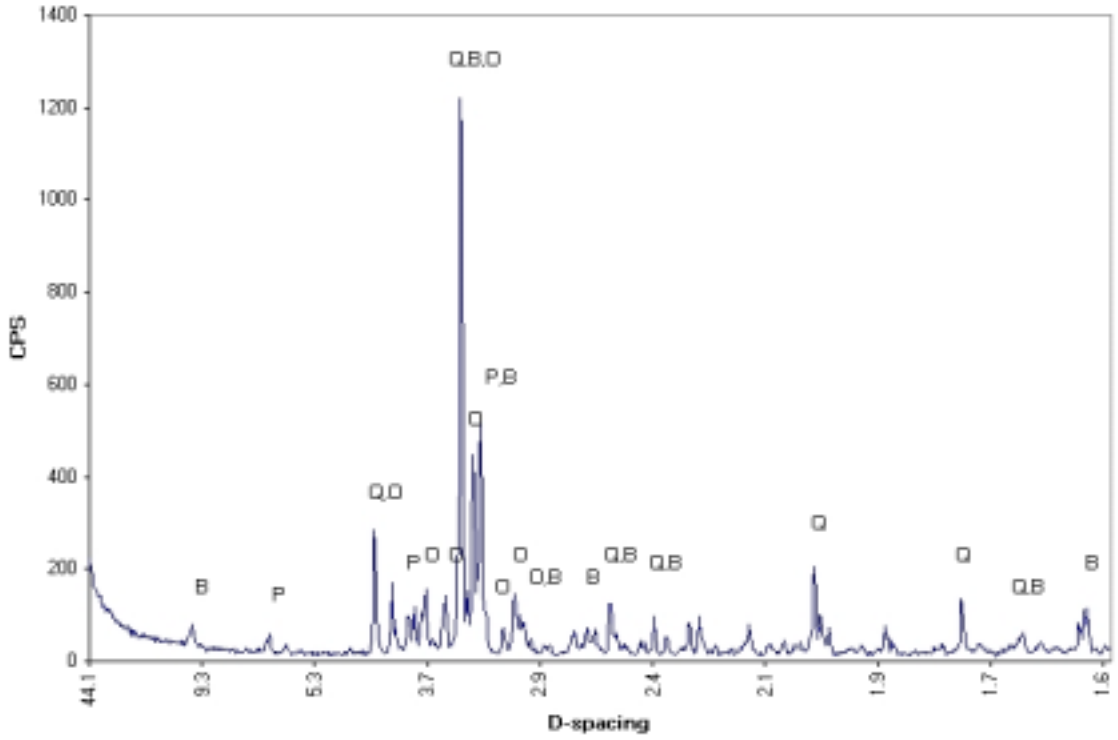

Figure 3.12 Oriented powder mount of silt (<20μ) size mineralogy of ground Striped Rock Biotite Granite. Major peaks are explained by the presence of quartz (Q), orthoclase (O), biotite (B), and plagioclase (P).

Cation Exchange Capacity (CEC) and Non-Crystalline Material Determination

The cation exchange capacity (CEC) was used as a method of quantification for the montmorillonite and vermiculite minerals in the clay fraction of the sample. The CEC resulting from the exchange of Ca^{2+} by Mg^{2+} is relatively low (Table 3.5). This initially suggests that the amount of low charge minerals such as montmorillonite and vermiculite in the clay fraction is small and that the clay fraction is dominated by minerals that don't have interlayers (kaolinites, micas) or minerals in which the interlayer is occupied (HIV, chlorites). Likewise, the monovalent exchange of K^+ for NH_4^+ exhibits a low CEC. Assuming charges of 1.54/unit cell and 1.05/unit cell for vermiculite and montmorillonite respectively, the difference between the Ca^{2+}-derived CEC values and the NH_4^+-derived CEC values was used to calculate the relative amounts of vermiculite and montmorillonite (Table 3.5). Both amounts are low, reflectant upon the low CEC, however, the vermiculite estimation is much lower than expected. Mineral quantities less than 5% are often difficult to identify via x-ray diffraction (Zelazny, personal communication, 2000), however, intense vermiculite peaks were observed in many of the x-ray analysis. Failure of NH_4^+ to become fixed in the interlayers of vermiculite, or a false assumption of the charge on vermiculite could both explain the low observed values. Vermiculite and montmorillonite charge can vary greatly from the assumed values, possibly resulting in error in quantification by the CEC method.

Analysis of the non-crystalline material by acid ammonium oxalate decomposition in the dark (AOD) revealed low amounts of non-crystalline material in all samples (Table 3.5). These low values are considered insignificant in the succeeding mineralogical analysis.

Table 3.5 Summary of CEC analysis of the clay fraction (<2µm) for each horizon and estimation of relative amounts of vermiculite, montmorillonite, and non-crystalline material at the two elevations sites. Standard deviation shown in parentheses beside the mean value.

Site #	*Ca-Mg CEC* $cmol^+/kg$	*NH_4-K CEC* $cmol^+/kg$	*% Vermiculite*	*% Montmorillonite*	*% Non-crystalline*
			A-Horizon		
s1	10.37(0.18)	7.66(--)	1.76	7.30	3.15
s2	9.03(0.58)	7.48(1.17)	1.01	7.12	3.02
s3	18.32(0.63)	14.36(0.69)	2.57	13.68	3.02
s4	12.29(0.01)	12.70(0.76)	0.00	12.10	2.85
			B-Horizon		
s1	13.16(0.02)	7.90(0.24)	3.42	7.52	2.44
s2	15.17(0.48)	8.50(0.67)	4.33	8.10	2.51
s3	16.60(0.33)	12.62(0.00)	2.59	12.02	2.57
s4	16.15(0.15)	13.87(0.14)	1.48	13.21	2.68
			C-Horizon		
s1	12.36(0.42)	10.20(0.15)	1.41	9.71	2.32
s2	12.31(0.94)	9.83(0.78)	1.60	9.37	2.94
s3	6.61(0.27)	4.35(0.56)	1.46	4.14	2.07
s4	10.45(0.31)	7.26(0.05)	2.07	6.91	2.89
Sapr*	6.57(0.51)	3.23(0.25)	2.17	3.08	2.98

***Saprolite**

Thermogravimetric Analysis (TGA)

The observed thermogravimetrics data for the field samples reinforces much of the results from XRD identification and CEC. Quantitative analysis, particularly of 1:1's and gibbsite is best performed with TGA. The distinctive peak of gibbsite, occurring around 220-240^o C was evident in all samples. Kaolinite and/or halloysite was also present in all samples but not easily distinguishable so the weight loss due to kaolinite (14% at about 400^o C) was used for calculations. Subsamples were equilibrated at a relative humidity of 56% to facilitate a separation between the amount of HIV and the montmorillonite/vermiculite component.

The results of both the dry TGA and the TGA of samples equilibrated at 56% relative humidity are expressed in Figure 3.14. The quantification of vermiculite and montmorillonite agrees relatively well with the CEC results except for the A and B-horizons of the high elevation site. Comparing these results to the CEC and XRD analysis, the TGA results seem to have underestimated the quantities of these two minerals. This could be due to the Na-saturation of samples inhibiting water from entering the interlayers in the 56% relative humidity samples, or a significant proportion of this interlayer water may have been lost below 50^{o}C before the instrument begins detection. The dominance of kaolinite, mica and/or HIV in the samples (Fig. 3.13) suggests why the CEC was so low.

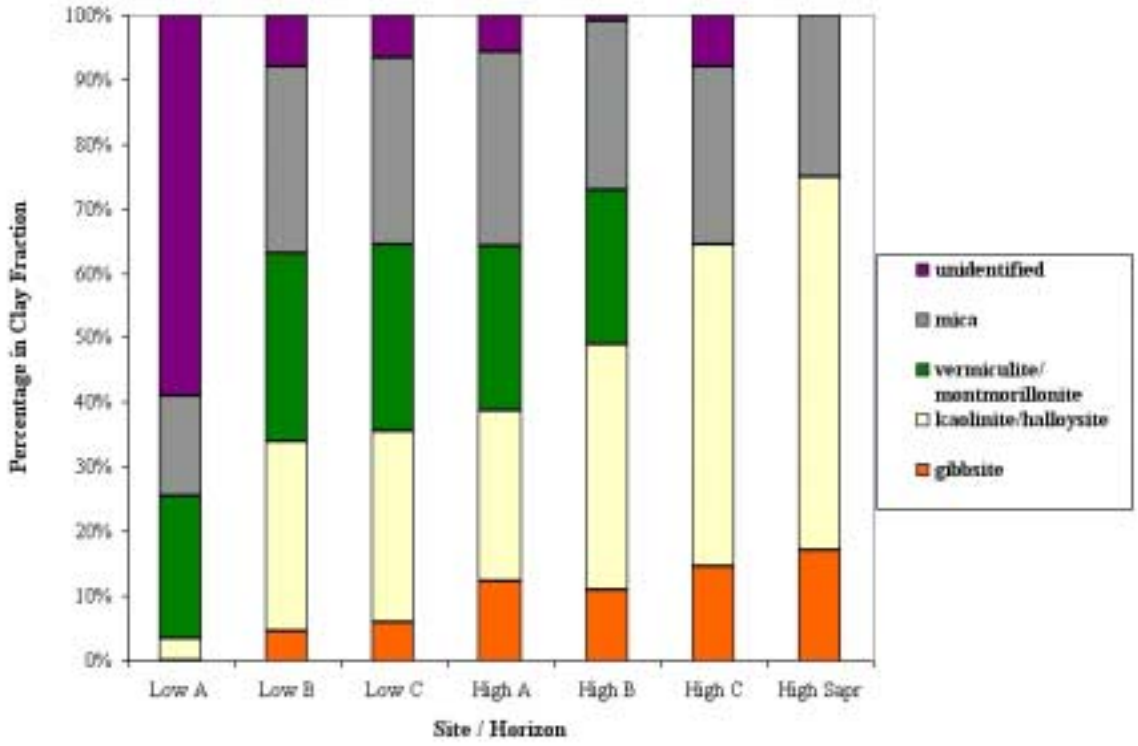

Figure 3.13 Average mineralogical distribution of horizons from high and low elevations by TGA.

The low and high elevation A horizons exhibit one primary difference, the amount of gibbsite in the clay fraction. The lower elevation has a much lower amount of gibbsite present. This indicates that the high elevation surface horizon may have been exposed to a greater weathering intensity at some point in the pedogenesis. Aside from the different

gibbsite amount, the surface horizons have similar quantities of the minerals, suggesting that the exposure to the surface has allowed similar weathering factors to influence the character of both sites.

The shape of the A horizon TGA curves (Fig. 3.14) shows that the samples experience weight loss at the same temperatures, however, there is a difference in the magnitudes. This difference in magnitude is attributed to the greater weight loss at temperatures between 225^{o}-250^{o}C, diagnostic of gibbsite.

The low and high elevation B-horizons had similar shaped TGA curves (Fig. 3.15) however, the quantities identified varied. The high elevations again have a greater weight loss in the range of gibbsite, reflected also in Figure 3.14 and the s-4 replicate experiences a greater initial weight loss, usually attributed to samples having a higher non-structural water content. The low elevation B has a much lower amount of gibbsite, a characteristic noted in the x-ray patterns and in the surface horizons. The B-horizon for the lower elevation also has a larger amount of unidentified material than the high elevation. The contrasting B-horizons have about the same mica content, though this quantification cannot be separated into biotite and muscovite. There is a similar problem with the vermiculite / montmorillonite amounts when comparing the B-horizons. The high elevation B-horizon has a slightly higher amount of vermiculite / montmorillonite character, likely due to the presence of montmorillonite observed in the x-ray patterns and the CEC quantification methods.

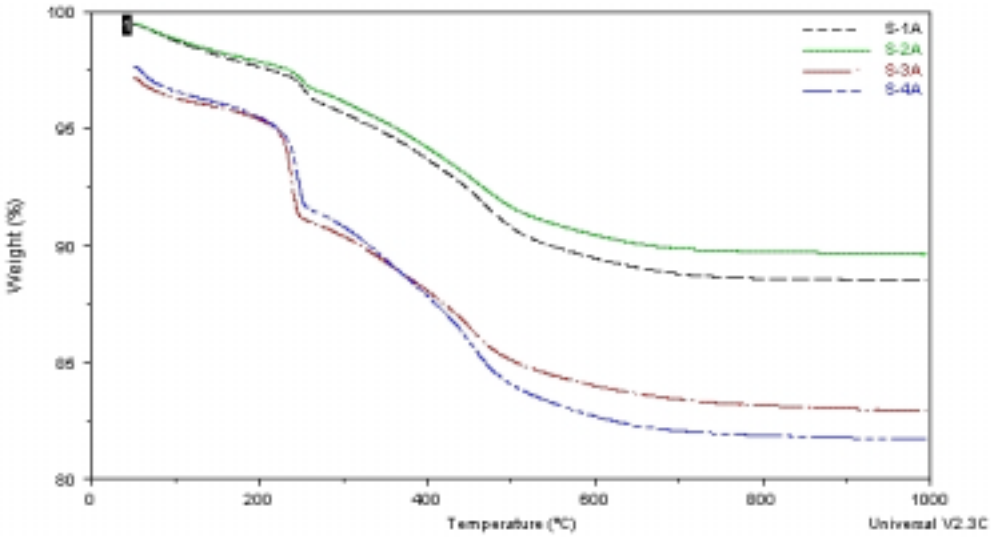

Figure 3.14 TGA curves of the four A-horizon samples showing the similarity in the shape of the curves, but varying magnitudes of weight loss.

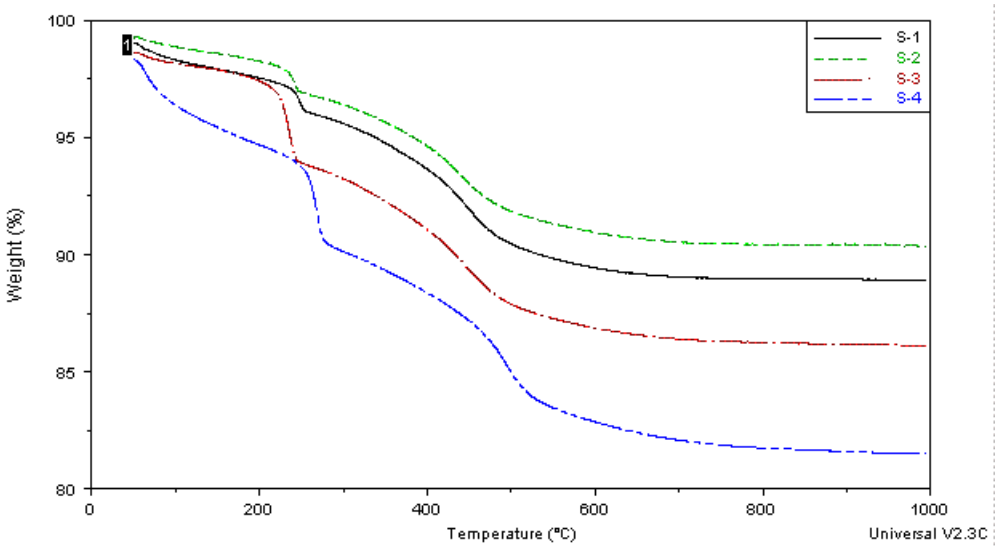

Figure 3.15 TGA curves of the four B-horizon samples showing the similarity in the shape of the curves, but varying magnitudes of weight loss.

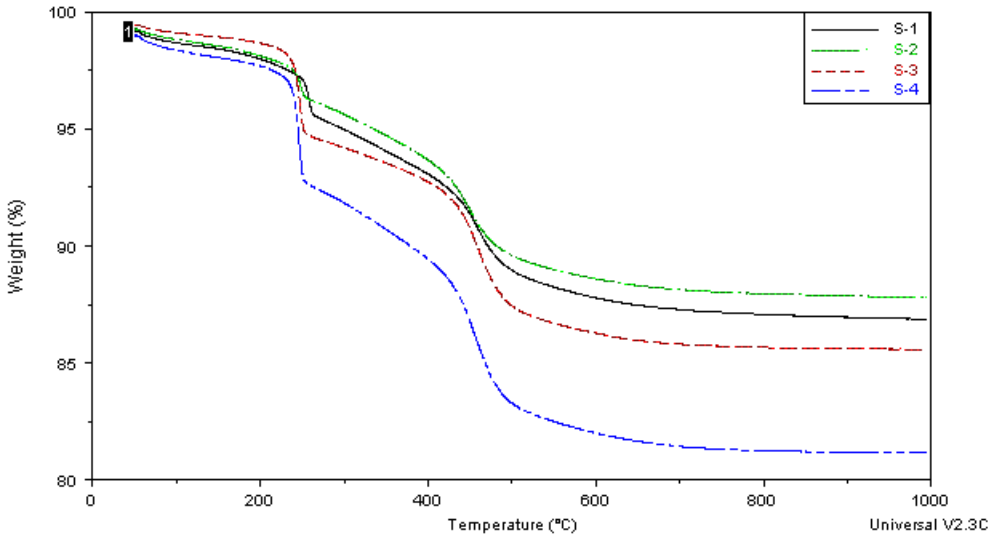

Figure 3.16 TGA curves of the four C-horizon samples showing the similarity in the shape of the curves, but varying magnitudes of weight loss.

The TGA curves for the C horizons (Fig. 3.16) again illustrate similar patterns of weight loss, however, the s-4 replicate again exhibits a greater weight loss than the other samples.

The C-horizons of the two elevation sites both show an increase in 1:1's compared to the respective B-horizon. Since no kaolinite or halloysite identified in the granite, all of it in the soil must be pedogenic. Regardless of whether the kaolinite and / or halloysite occurs from biotite or feldspar weathering, it is formed in the C-horizons more than any other horizon. No HIV was quantified for the high elevation horizons since x-ray analysis illustrated an absence of these intergrade minerals, however, some vermiculite and montmorillonite were detected by TGA and CEC analysis. Again, the high elevation site has greater gibbsite amounts, however the lower elevation site appears to show a trend of increasing gibbsite with depth. The trends suggest greater or different weathering intensity with greater depth. Intuitively this is a contradiction, however, a change in the direction and magnitude of water movement may cause the deeper depths to be subject to a different weathering environment. Again, this could be an indication that the leaching environment controls the weathering products of biotite more so than temperature or vegetation. The relatively higher amount of kaolinite and gibbsite in the high elevation

samples would indicate that these horizons have still undergone more intense weathering conditions. The high amount of feldspars, particularly orthoclase (K-feldspar), in the granite parent material, predecessors for kaolinite formation, creates a problem associating kaolinite levels with biotite weathering. However, the resistance of feldspars to weathering and the relatively low amount of plagioclase in the C-horizon suggest that the increase in the 1:1 clay mineral content be attributed to biotite weathering. Finally, the saprolite horizon has similar gibbsite and mica amounts relative to the C-horizons, but greater kaolinite and less vermiculite/montmorillonite than the above horizons.

Surface Area Analysis

The nitrogen purged clay samples were analyzed for external surface area at liquid nitrogen temperatures and the surface areas determined by the BET monolayer adsorption of molecular nitrogen. The EGME saturated clay samples were analyzed for total surface areas determined when EGME had reached monolayer coverage of the clays. The average results of the two surface area determinations are expressed graphically in Figure 3.17. The ratio of interlayer surfaces for all the samples is about 1:1, yet the surface area values vary greatly. This can be attributed to particle size if the mineralogies of all samples are the same, or mineralogy if the particle sizes are constant, or some combination of the two.

The two surface horizons agree with earlier results. The low elevation A horizon has a low surface area which could be the result of less complete weathering. Though this suggestion does not agree with the TGA, since the majority of the material was unidentified, it is related to the lower gibbsite content, and lack of montmorillonite and less weathering. The high elevation A, however, did exhibit some montmorillonite, which could substantially increase the surface area of the clay. The greater external surface area itself suggests that the high elevation surface horizon has some minerals with smaller particle size, which would typically include montmorillonite.

The B-horizons of both sites are also compliant with the other results. The XRD illustrates an increase in montmorillonite in the high elevation B, and the TGA suggests,

by the presence of gibbsite and montmorillonite / vermiculite that the high elevation is more weathered than the low elevation. Both low and high elevations of the B-horizon increase in surface area relative to the A, suggesting both have experienced a degree of alleviation and they are the horizons of maximum soil development.

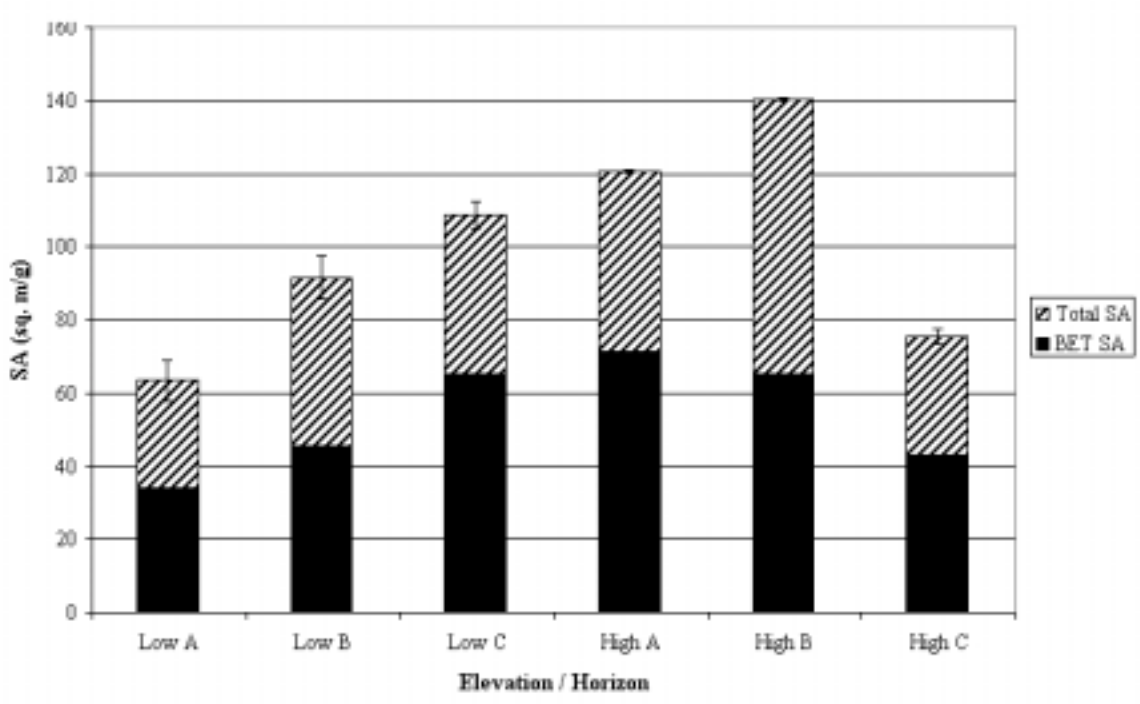

Figure 3.17 Average external (BET) and total clay fraction surface areas of sampled horizons at low and high elevations. Error bars indicate the 95% confidence interval.

The C-horizons of the low and high elevation sites tend to agree with the x-ray patterns, and show some of the trend that the TGA indicated. The low elevation C continues to increase in both types of surface area, correlating well with the substantial increase in vermiculite seen in the x-ray pattern. The high elevation values decrease from the B-horizon, likened to the "clay bulge" trend often observed in horizon textures. This trend implies a more advanced weathering scheme relative to the low elevation soils. This corresponds well to the TGA results. The lower surface area due to the lower vermiculite and higher halloysite amounts agrees with that observed by thermogravimetrics and x-ray. The high amount of surface area in the low elevation site is presumably from the vermiculite derived from the micas in the parent material as in the discussion of the TGA and x-ray.

Scanning Electron Microscopy (SEM)

Scanning electron microscopy (SEM) imaging was used as a supplemental analysis. Since identification via SEM can be ambiguous at the clay size fraction and quantification only subjective, SEM images were only used to support the information derived from XRD, TGA, and surface area measurements. Images of one replicate from each horizon of both sites were taken at various magnification to illustrate any visual differences between like horizons at the two elevations. Images that were not considered significant can be found in Appendix A.

The A horizons did not appear to differ much except an example of montmorillonite can be observed in the high elevation surface horizon. The images appear slightly different because of different quantities of sample mounted for imaging, however, by SEM imaging, there is no obvious reason why the mineral suites (from TGA) and surface area measurements would differ.

The B-horizons show a difference between the low and high elevations as seen in Figure 3.18. (low) and Figure 3.19. (high). Both samples exhibit some platy minerals and some halloysite. The halloysite was not identified by x-ray because there was such a small amount that there was no x-ray reinforcement to create a peak. The low elevation B is dominated by large, platy, clay particles, accounting for its lower surface area compared to the high elevation B. These particles can be kaolinite, micas, or vermiculite. There are finer particles present in the low elevation B, however, these particles are not dominant and they appear to have the same platy character. The high elevation B, as mentioned above, does have some large, platy clays, but there is a dominance of fine minerals, some of which resemble the fines observed in the low elevation B, but in much greater number. The resolution of the magnification did not allow further inspection. These could be montmorillonite that appear in the x-ray patterns and which influenced the TGA and surface area measurements.

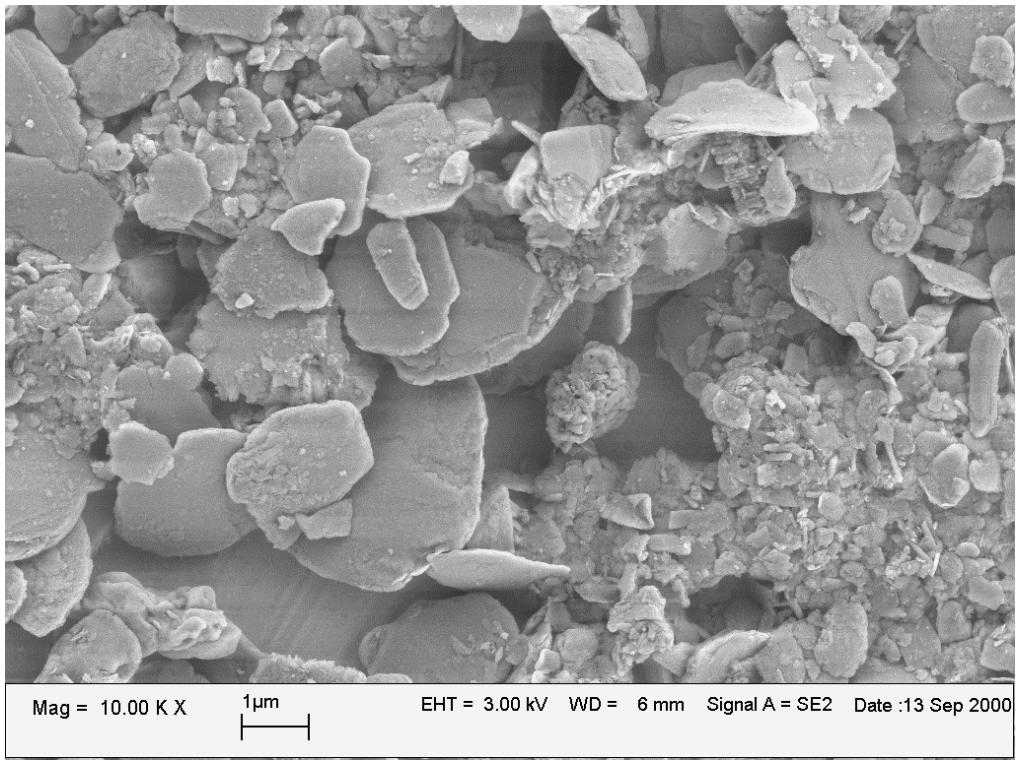

Figure 3.18 SEM of the clay (<2µ) fraction of the low elevation B-horizon.

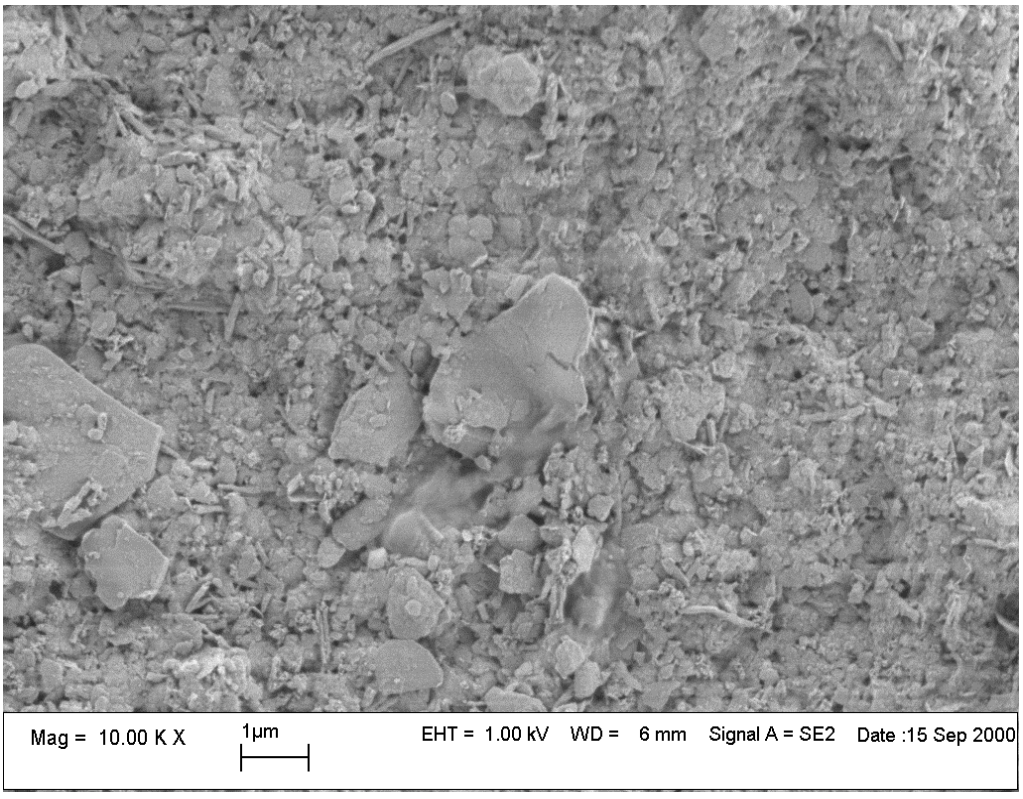

Figure 3.19 SEM of the clay (<2µ) fraction of the high elevation B-horizon.

The two C horizons showed some difference in the texture of the clay fraction. The low elevation sample, apparently dominated by vermiculite, is illustrated in Figure 3.20. The smaller particle size relative to the B horizon of the low elevation suggests why the surface area was higher at a deeper depth. This image resembles more the B horizon of the high elevation. There is also a small amount of halloysite present in this sample but in such small amounts, it was not identified by x-ray. The dominance of vermiculite in the low elevation C again suggests that it has not experienced a sufficient weathering intensity to induce the formation of halloysite. The high elevation sample (Fig. 3.21), however, exhibits many tube-like structures characteristic of halloysite, thereby supporting the x-ray diffraction data.

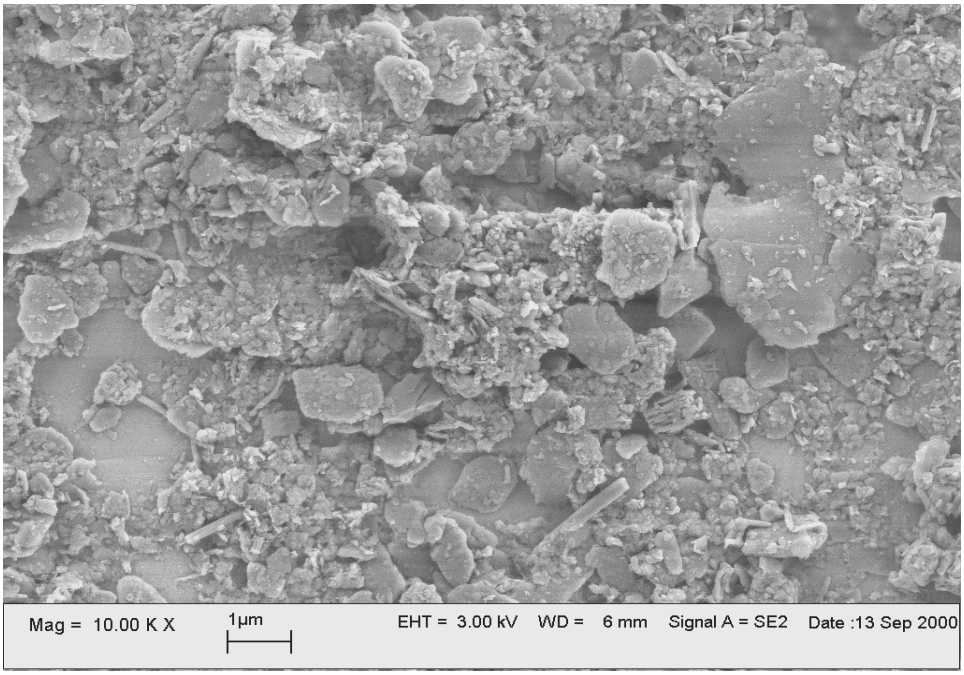

Figure 3.20 SEM of the clay (<2µ) fraction of the low elevation C-horizon.

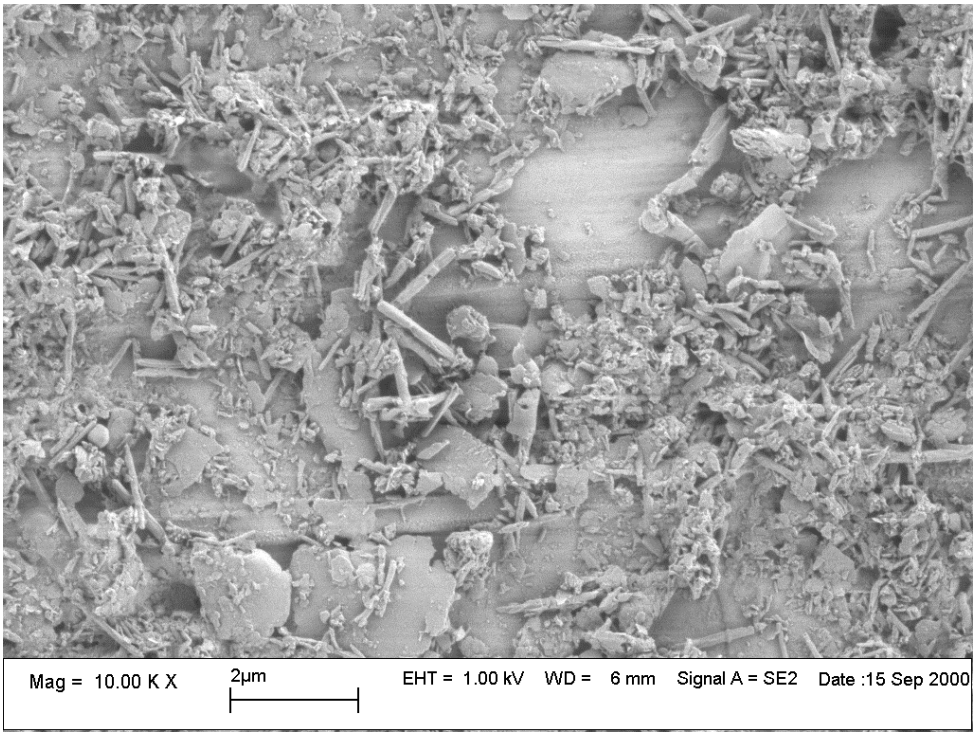

Figure 3.21 SEM of the clay (<2µ) fraction of the low elevation C-horizon.

Final Mineralogical Estimations

Clay mineralogy of a sample is not well quantified by a single analysis. This is why various analysis are often used for complete mineralogical investigation. Mineralogical approximations from a compilation of techniques such as x-ray, surface area, CEC, TGA, and SEM are made with much greater confidence. Table 3.6 offers estimates for the mineralogies of the low and high elevation samples collected over the Striped Rock Biotite Granite. TGA was used as a basis for the values of gibbsite, mica, kaolinite/halloysite, and HIV. Gibbsite and mica values were supported by x-ray and CEC analysis. The formamide treatment in the x-ray analysis was used to quantify kaolinite and halloysite. The vermiculite and montmorillonite were initially estimated from the CEC results, then changed, considering x-ray and surface area analysis. The HIV/vermiculite ratio was estimated by using the total CEC and inspection of the x-rays, understanding that not all HIV is prevented from collapsing to 10Å. Non-crystalline material was estimated solely from AOD and the chlorite and feldspars were estimated strictly from the peaks in x-ray analysis.

The trends within the profiles and the differences between the two elevations suggest different relative weathering intensities. The increase in kaolinite, gibbsite, halloysite, and vermiculite in the low elevation profile indicate increasing stages of soil development with depth. The high elevation has an increase in gibbsite with depth again suggesting a higher weathering intensity, a maximum montmorillonite content in the B horizon, indicating favorable conditions for the continued weathering of vermiculite and neoformation of the montmorillonite, and an increasing dominance of halloysite in the C horizon and saprolite indicating high weathering intensities and an environment allowing reprecipitation. All of the trends in the mineralogies between the two sites suggest that the high elevation site has undergone a more intense weathering, as previously discussed. We attribute the difference in the weathering to leaching intensity and vegetation differences between the two elevations.

Table 3.6 Final approximations (in percent) of mineral suites for the clay fraction (<2µm) of the low and high elevation sites based on complete mineralogical analysis.

	Gibbsite	Mica	Kaolinite	Halloysite	HIV / intergrade	Vermiculite	Montmorillonite	Chlorite	Feldspar	Non-crystalline
Low A	3	27	21	<1	21	10	7	1	2	3
High A	10	25	24	<1	15	6	12	3	2	3
Low B	5	24	21	<1	21	12	8	1	1	2
High B	10	25	23	<1	8	10	14	2	1	3
Low C	5	30	25	3	14	16	3	<1	3	2
High C	14	28	16	26	<1	5	5	<1	2	2
Saprolite	16	27	10	38	<1	2	2	<1	4	3

Chapter 4

Results and Discussion (Columns)

X-ray analysis of samples from both the acid and temperature studies did not exhibit any weathering products from the original biotite. Effluent analysis of the columns from both studies, however, revealed significant differences between treatments. The pH fluctuation and cation release trends overtime are interpreted as well as the average pH and total elemental loss for each treatment or treatment combination.

Acid Study

Leaching of the columns with selected acids produced no observable by-products of biotite weathering in x-ray analysis (Figure 4.1). These samples were Mg-saturated; glycerol solvated (Mg-glys) to promote maximum differences between samples; however none were observed. Therefore, no subsequent mineralogical analyses were performed.

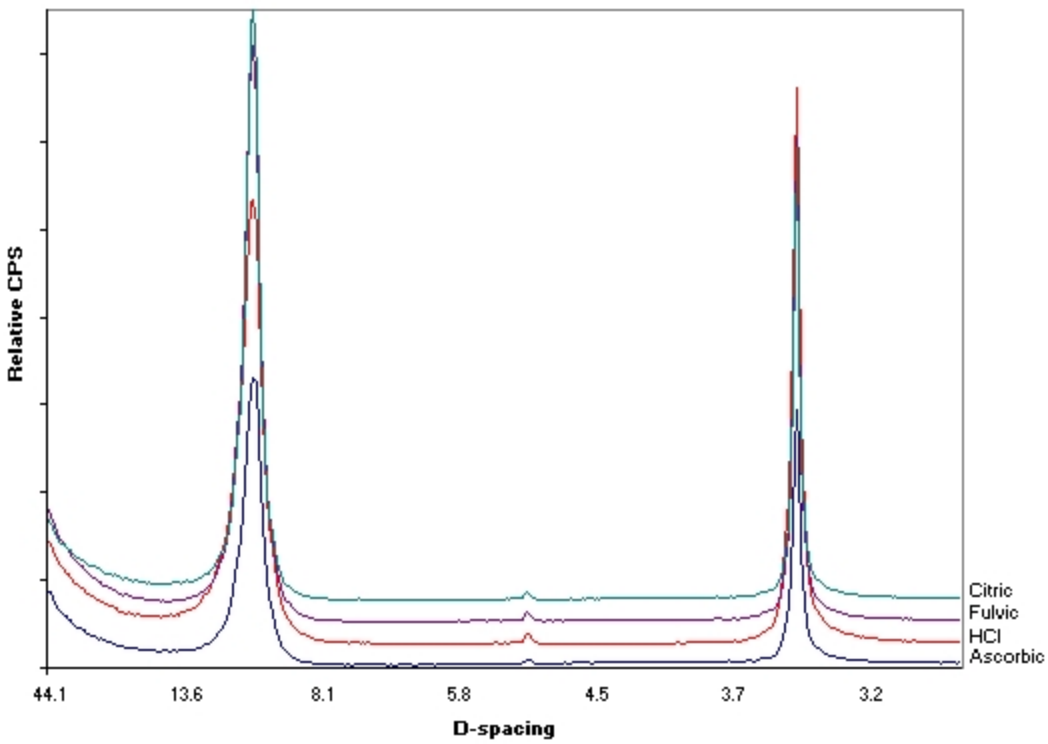

Figure 4.1 X-ray diffractograms of biotite clay (<0.2μm) representative samples for each selected acid, treated with Mg-glys.

The fluctuations in pH overtime for the acid treated columns exhibit similar trends at the two leachate rates (Figure 4.2). The ascorbic, citric and fulvic treatments are higher in pH at the low leachate rate, possibly due to continuing hydrolysis reactions even at the later dates.

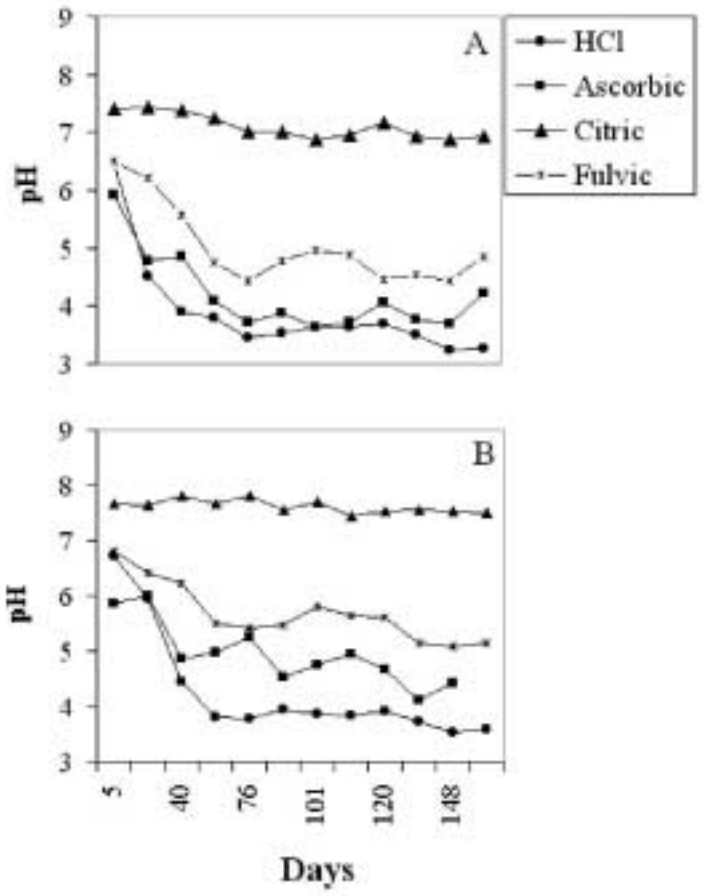

Figure 4.2 Trends in pH as a function of time for columns leached with selected acids at (A) 60ml/week and (B) 15ml/week leachate rates.

Each acid is significantly different from one another at both the high and low leachate rates (Table 4.1), suggesting each undergoes a specific reaction within the column to produce a specific, reproducible pH. Initial pH of the acid solutions are 6.6 for citric, 4.0 for fulvic, 3.7 for ascorbic, and 3.2 for HCl. The leachates are also significantly different between the two leachates for each acid, which implies the steady state may not have been reached. The high pH of the citric acid in both leachate treatments could be attributed to a higher initial pH of the leachate since it was made with Na-citrate

The inability of the columns that were treated with low leachates rates to reach a steady state is further demonstrated by the Al^{3+} release (Fig. 4.3) as well as Fe^{2+}, Si^{4+}, and K^{+} releases trends (Figures 4.4, 4.5, 4.6 respectively).

Table 4.1 Mean pH values and estimated least squared mean difference between selected acid treatments at (A) 60ml/week and (B) 15ml/week leachate rates.

	Mean pH	HCl A	Ascorbic A	Citric A	Fulvic A	HCl B	Ascorbic B	Citric B
HCl A	3.81							
Ascorbic A	4.20	-0.39*						
Citric A	7.09	-3.28*	-2.90*					
Fulvic A	5.00	-1.19*	-0.81*	2.09*				
HCl B	4.26	-0.45*						
Ascorbic B	4.94		-0.74*			-0.68*		
Citric B	7.62			-0.52*		-3.36*	-2.68*	
Fulvic B	5.69				-0.69*	-1.43*	-0.75*	1.93*

*** Significant at the 0.05 level of probability.**

A peak is observed at the 68 day reading for both high and low leachate rates under ascorbic and citric acid treatments. This spike in all cation levels can be related to an extra addition of toluene added prior to day 68 to reduce microbial growth. In both the low and high leachate rates, the Al^{3+} release seems to be least variable with the hydrochloric acid (HCl) treatment. All of the organic acids (ascorbic, citric, and fulvic) at high leachate rates release significantly higher amounts of Al^{3+} than the HCl treatment (Table 4.2). This may be due to the specific chelating abilities of the organic acids resulting from their higher amounts of functional groups associated with their structures. Table 4.3 represents the stablility constants of these selected acids with Al^{3+} and Fe^{2+}. These functional groups are able to bind with the Al^{3+} and remove it from the biotite stucture. At the low leachate rates, only the citric acid treatment exhibits strong enough affinity for the Al^{3+} ion to remove significantly more than the HCl. Additionally, all of the organic acids remove a significantly greater amount of Al^{3+} from the biotite at high leachate rates than low leachate rates. The inorganic acids does not show a significant difference between leachate rates, suggesting that the interaction of organic acids with higher rainfall would weather more Al^{3+} from biotite.

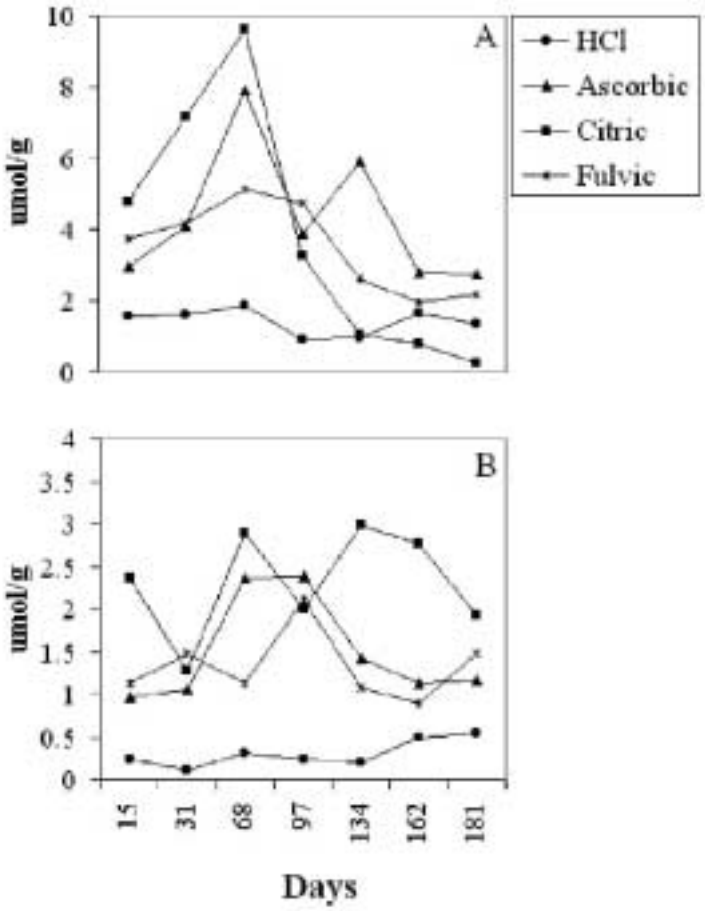

Figure 4.3 Release of Al^{3+} over time from the biotite columns leached with selected acids at (A) 60ml/week and (B) 15ml/week leachate rates.

Table 4.2 Total Al^{3+} released and estimated least squared mean difference (µmol/g) between total Al^{3+} release of different acids after 181 days at (A) 60ml/week and (B) 15ml/week leachate rates.

	Total Al^{3+} (µmol/g)	HCl A	Ascorbic A	Citric A	Fulvic A	HCl B	Ascorbic B	Citric B
HCl A	9.86							
Ascorbic A	30.28	-20.42*						
Citric A	26.94	-17.08*	3.34					
Fulvic A	24.50	-14.64*	5.78	2.44				
HCl B	2.11	7.74						
Ascorbic B	10.50		19.78*			-8.38		
Citric B	16.18			10.75*		-14.07*	-5.69	
Fulvic B	9.26				15.24*	-7.14	1.24	6.93

* Significant at the 0.05 level of probability.

Table 4.3 Stability constants of selected acid / metal complexes, assuming a metal-ligand bond at 25°C.

	Stability Constant (log K)	
Acid	Al3+	Fe2+
Citric[1]	7.87	4.56
Ascorbic[2]	3.55	1.99
Fulvic[3]*	6.06	2.3
HCl[4]	0	0

***EDTA values substituted for Fulvic, behavior assumed to be similar.**
[1] Smith, R.M. and A.E. Martell, 1989
[2] Martell, A.E. and R.M. Smith, 1977
[3] IUPAC, Perrin, D.D., 1979
[4] HCl has no chelating ability due to lack of ligand groups.

The loss of Fe^{2+} from biotite over time exhibits similar trends as the Al^{3+} loss but to a slightly greater magnitude (Fig. 4.4). This suggests that the organic acids are strong chelators of Fe^{2+}, increasing its solubility and allowing it to be removed with the solution. This incongruent loss suggests the octahedral layer is more highly substituted with Fe^{2+} than Al^{3+} and as the octahedral layers experience dissolution, more Fe^{2+} is released. Again, the high leachate rates show greater Fe^{2+} loss from organic acids than the inorganic acid (Table 4.4) thereby reinforcing the idea that the interaction of organic acids and leachate rates significantly influence the initial weathering processes of biotite. Also, both ascorbic and citric acid treatments show significantly greater loss of Fe^{2+} at the low leachates rates. This would continue to suggest that Fe^{2+} is either in greater amounts in the octahedral layer of this Ontario biotite, or that it is preferentially lost before Al^{3+}. Finally, all of the organic acids exhibited significant differences between low and high leachate rates, while the inorganic (HCl) acid treatment did not.

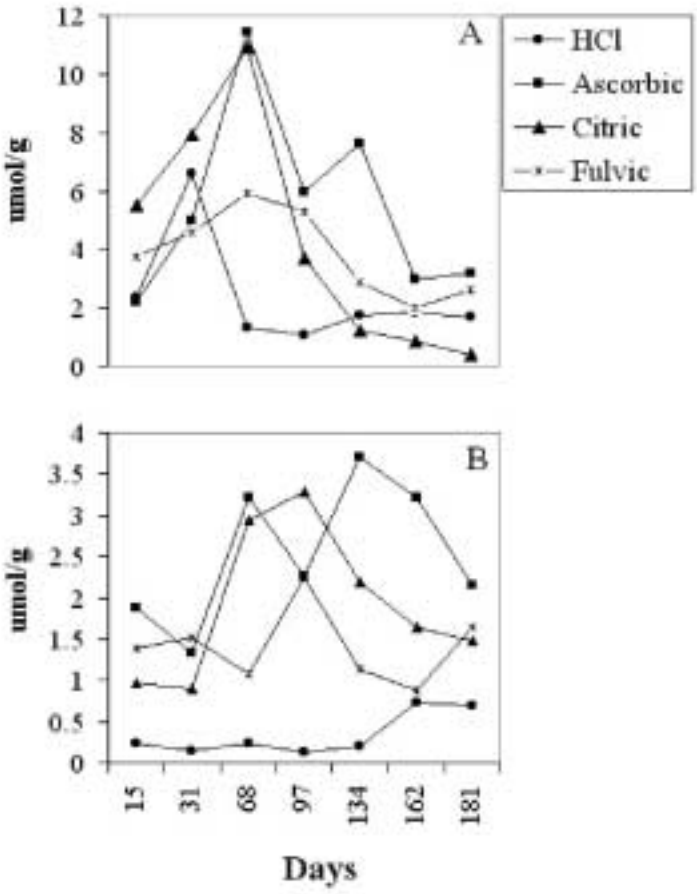

Figure 4.4 Release of Fe^{2+} over time from the biotite columns leached with selected acids at (A) 60ml/week and (B) 15ml/week leachate rates.

Table 4.4 Total Fe^{2+} released and estimated least squared mean difference (µmol/g) between total Fe^{2+} release of different acids after 181 days at (A) 60ml/week and (B) 15ml/week leachate rates.

	Total Fe^{2+} (µmol/g)	HCl A	Ascorbic A	Citric A	Fulvic A	HCl B	Ascorbic B	Citric B
HCl A	16.73							
Ascorbic A	38.43	-21.71*						
Citric A	30.64	-13.91*	7.80					
Fulvic A	27.16	-10.44*	11.27*	3.47				
HCl B	2.37	14.35						
Ascorbic B	13.42		25.02*			-11.05*		
Citric B	17.78			12.85*		-15.41*	-4.37	
Fulvic B	9.88				17.28*	-7.51	3.53	7.90

*** Significant at the 0.05 level of probability.**

Silica in solution occurs as $H_2SO_4^-$, however, it was detected as Si by ICP analysis. The loss of Si is similar in trends to Al^{3+} and Fe^{2+} however; the magnitude is much greater (Fig. 4.5). Observed blanks (no biotite) for the acid treatments only released nominal amounts of Si (<0.5 μmol/g) therefore all Si loss can be attributed to dissolution of the tetrahedral layer. If both tetrahedral layers of biotite were dissolving simultaneously as the octahedral is being degraded, this would explain the higher release of Si as $H_2SiO_4^-$ observed. Furthermore, this effect would be increased in the presence of ultrafine particles that could have resulted from the grinding processes. The organic acid treatments continue to release significantly greater amounts of $H_2SiO_4^-$ also (Table 4.5) at the high leachate rates. The citric acid treatment influences a significantly greater release of Si than the HCl at low leachate rates as similarly observed in the Al^{3+} release. The high leachate rate results in a greater Si release than the low leachate rates for all of the organic acids.

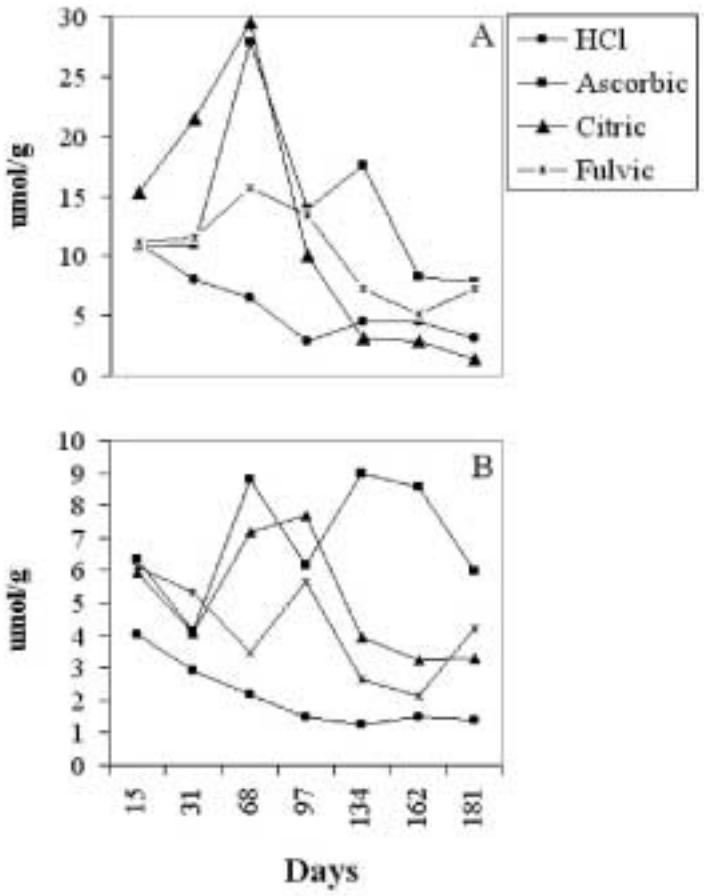

Figure 4.5 Release of Si over time from the biotite columns leached with selected acids at (A) 60ml/week and (B) 15ml/week leachate rates.

Table 4.5 Total Si released and estimated least squared mean difference (µmol/g) between total Si release of different acids after 181 days at (A) 60ml/week and (B) 15ml/week leachate rates.

	Total Si^{4+} (µmol/g)	HCl A	Ascorbic A	Citric A	Fulvic A	HCl B	Ascorbic B	Citric B
HCl A	40.73							
Ascorbic A	97.24	-56.51*						
Citric A	83.58	-42.85*	13.66					
Fulvic A	71.69	-30.96*	25.54	11.89				
HCl B	14.74	-25.99						
Ascorbic B	35.34		-61.90*			-20.60		
Citric B	48.99			-34.59*		-34.25*	-13.65	
Fulvic B	29.57				-42.12*	-14.83	5.77	19.42

*** Significant at the 0.05 level of probability.**

The overall trends in K^+ loss exhibit a slightly different trend in release as compared to Al^{3+}, Fe^{2+}, and Si^{4+} losses. The K^+ release is unexpectedly low, since K^+ is held in the interlayers of mica and thought to be lost rapidly and incongruently in relation to other cations. The high leachate rates do show a steady state of release though (Fig. 4.6) and are similar in K^+ release, except for the ascorbic acid treatment, which is significantly higher than the other treatments (Table 4.6). This is a different phenomenon than observed for the previous cations. Ascorbic acid acts as a reducing agent. The reduction of ferric iron may cause the repulsion of K^+ and release from interlayers. At low leachate rates, there are no differences between treatments, suggesting that K^+ will weather from the biotite structure regardless of the acid character of the solution at low leachate rates. This is again suggested when comparing of all four acid treatments at the two leachate rates since the high leachate rates release significantly higher amounts of K^+.

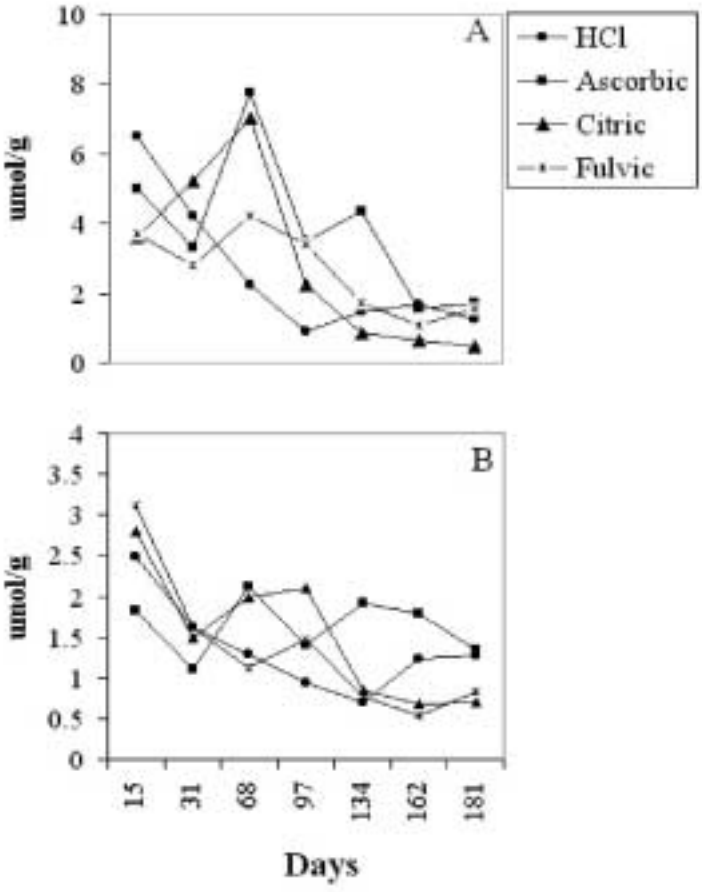

Figure 4.6 Release of K^+ over time from the biotite columns leached with selected acids at (A) 60ml/week and (B) 15ml/week leachate rates.

Table 4.6 Total K^+ released and estimated least squared mean difference (µmol/g) between total K^+ release of different acids after 181 days at (A) 60ml/week and (B) 15ml/week leachate rates.

	Total K^+ (µmol/g)	HCl A	Ascorbic A	Citric A	Fulvic A	HCl B	Ascorbic B	Citric B
HCl A	18.33							
Ascorbic A	27.22	-8.90*						
Citric A	20.14	-1.81	7.09*					
Fulvic A	18.52	-0.20	8.70*	1.61				
HCl B	9.57	8.76*						
Ascorbic B	10.61		16.61*			-1.04		
Citric B	11.50			8.64*		-1.93	-0.89	
Fulvic B	9.47				9.05*	0.09	1.13	2.02

*** Significant at the 0.05 level of probability.**

In summary, the pH of the acid study columns appears to reach a steady state of equilibrium in the acid treatments at the high leachate rate, however, not all acid treatments have reached a steady state at the low leachate rate of 15ml/week after 166 days. This steady state status is reflected in the release of Al^{3+}, Fe^{2+}, Si^{4+}, and K^+ from the biotite columns over 181 days. Organic acids, at higher rates of leaching, increase the loss of Al^{3+}, Fe^{2+}, and Si^{4+} compared to the inorganic acid (HCl) because of the ability of the functional groups in the organic to chelate Al^{3+} and Fe^{2+}, and electrostatically attract Si^{4+}. The release of K^+ is not influenced by the difference between organic and inorganic acids; however, K^+ loss from ascorbic acid leaching was significantly greater than the rest of the treatments. This can be attributed to the reducing agent character of ascorbic acid. Any Fe^{3+} that may be present in the octahedral layer of the biotite would be reduced, resulting in a greater electrostatic repulsion with the K^+ in the interlayer, allowing K^+ to be lost more readily. High leachate rates resulted in significantly higher cation release concentration with the organic acid treatments and a significantly higher K^+ rate with the HCl treatment. The high leachate rates provide a dilute column solution, not allowing the cations to reach the critical concentration in the column solution to slow down their release. This in turn results in greater dissolution.

Temperature Study

X-ray analysis of the biotite in the columns treated with different surface horizons at selected temperatures show that the six month duration of the experiment was not sufficient to promote weathering products from biotite (Figure 4.7). These samples were Mg-saturated; glycerol solvated (Mg-glys) to encourage maximum differences between samples; however none were observed. Therefore, no subsequent mineralogical analyses were performed.

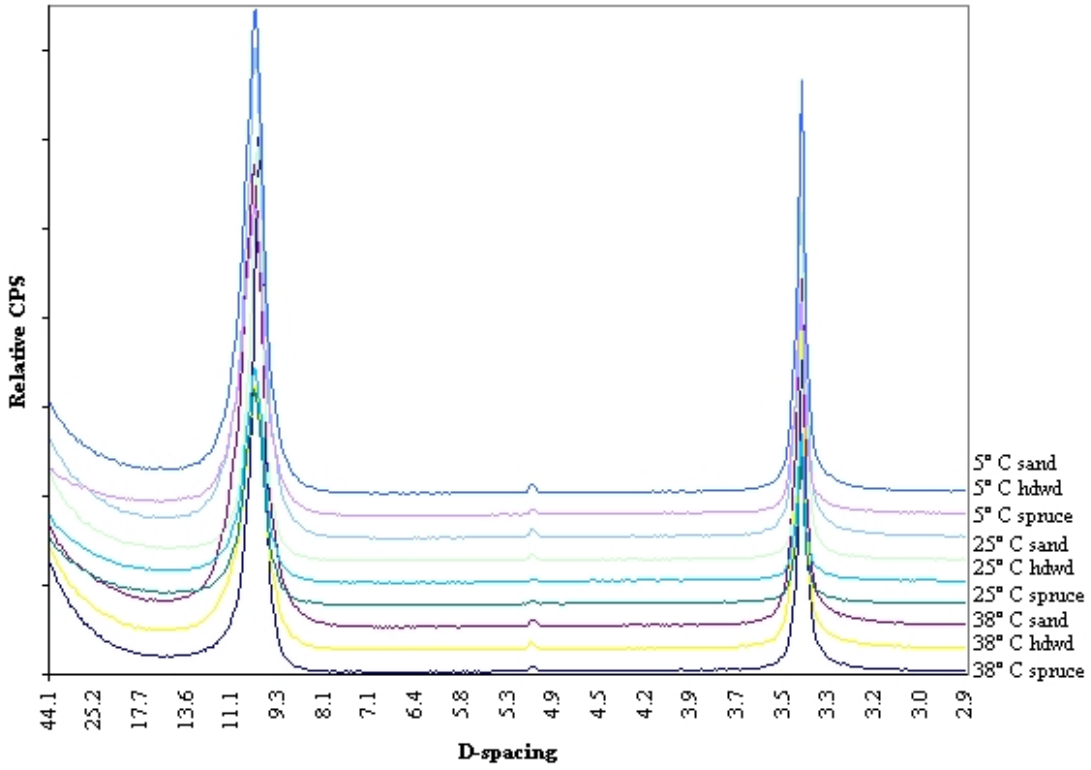

Figure 4.7 X-ray diffractograms of biotite clay (<0.2µm) representative samples for each temperature and selected surface horizon, treated with Mg-glys.

Fluctuations in pH (Figure 4.8) over time for the surface horizons and temperatures exhibit some steady state conditions and others that are still relatively variable. The low temperature treatments all appear to remain at a steady state, however, as temperature increases, especially when treated with low leachates, the pH of the different surface horizons begins to deviate. The high leachate rate, spruce-fir surface horizon treatment

pH is significantly lower than the other surface horizon treatments at every temperature (Table 4.7). This may be due to the organic acids that are released specifically by this type of organic matter. The low leachate spruce-fir horizon also exhibits a lower pH at all temperatures than the sand horizon and a lower pH than the hardwood horizon at the 25°C and 38°C treatments. The hardwood surface horizon treatments have a lower pH than the sand at the high temperature with both leachate rates and at 25°C under the low leachate rate conditions. The high leachate rates influence a lower mean pH at 25°C for all surface horizon treatments and a lower average pH at 38°C for sand and spruce-fir surface horizon treatment.

Table 4.7 Mean pH values and estimated least squared mean difference between selected surface horizon treatments at 4°, 25°, and 38°C and (A) 60ml/week and (B) 15ml/week leachate rates.

		Mean pH	Hardwd A	Sand A	Spruce A	Sand B	Hardwd B
4	Hardwd A	6.06					
	Sand A	6.23	-0.16				
	Spruce A	5.48	**0.58*** **	**0.75*** **			
	Hardwd B	6.29	-0.23			-0.13	
	Sand B	6.42		-0.19			
	Spruce B	5.63			-0.15	**0.79*** **	**0.66*** **
25	Hardwd A	6.23					
	Sand A	6.33	-0.11				
	Spruce A	6.17	**0.65*** **	**0.76*** **			
	Hardwd B	6.70	**-0.47*** **			**-0.65*** **	
	Sand B	7.35		**-1.01*** **			
	Spruce B	5.10			**0.67*** **	**2.43*** **	**1.78*** **
38	Hardwd A	5.37					
	Sand A	7.33	**-1.8*** **				
	Spruce A	4.90	**0.34*** **	**2.14*** **			
	Hardwd B	5.36	0.17			**-3.38*** **	
	Sand B	8.74		**-1.41*** **			
	Spruce B	4.55			**0.67*** **	**4.23*** **	**0.85*** **

***** Significant at the 0.0005 level of probability.**

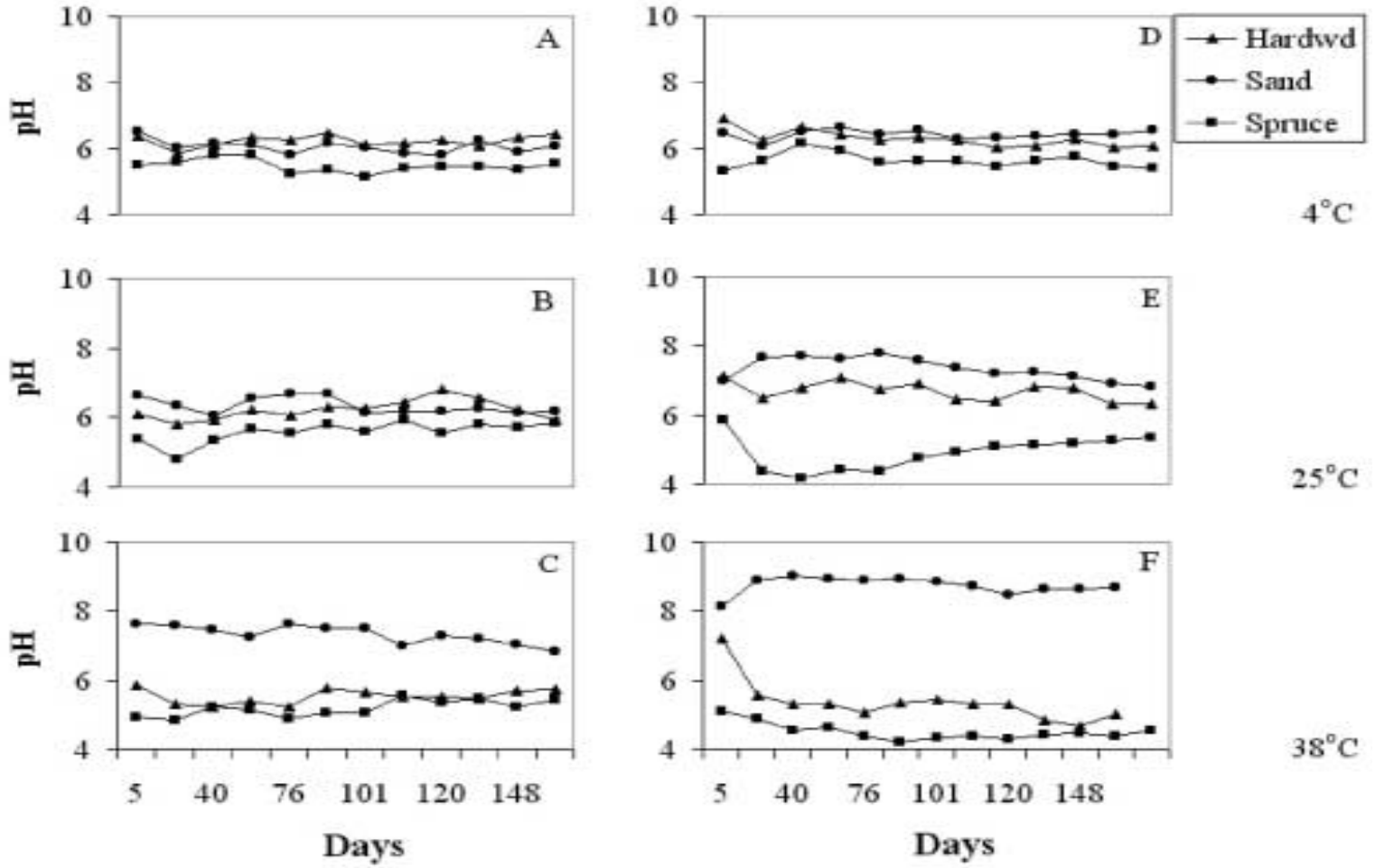

Figure 4.8 Trends in pH as a function of time for columns treated with selected surface horizons at 4°, 25°, and 38° and at (A, B, C) 60ml/week and (D, E, F) 15ml/week leachate rates.

The loss of all cations overtime (Figures 4.9, 4.10, 4.11, 4.12) again exhibit a peak at 68 days, as observed in the acid study, for all temperatures at the high leachate rate and at 4^{o}C at the low leachate rate. This phenomenon can again be attributed to the addition of extra toluene to the columns to inhibit microbe growth. The 25^{o} and 38^{o}C blocks of the low leachate rate treatments may not exhibit this trend due to a resistance to toluene or the volatilization of the toluene before it could be effective.

Loss of Al^{+3} over time (Fig. 4.9) for the selected temperatures shows that the trends of both the high leachate and low leachate treatments change with increasing temperature. The high leachate treatments have a greater average total amount of Al^{3+} lost (Table 4.8) at 4^{o}C than at 25^{o} or 38^{o}C for every surface horizon (Table 4.9). None of the high leachate rate surface horizon treatments at 25^{o}C are different from the 38^{o}C treatments. The spruce-fir surface horizon at 4^{o}, 25^{o}, and 38^{o}C, releases a significantly greater amount of Al^{3+} than the hardwood or sand surface horizons (Table 4.10) at the high leachate rate.

Comparing the low leachate rate results, only the hardwood surface horizon influences a greater Al^{3+} release at 4^{o}C than the other temperatures (Table 4.9). The release of Al^{3+} with columns packed with the spruce-fir horizon increases between 25^{o}C and 38^{o}C (Table 4.9). The spruce-fir horizon releases greater amounts of Al^{3+} than sand at 4^{o}C and both sand and hardwood at 38^{o}C (Table 4.10). This suggests the spruce-fir horizon may leach compounds that are able to chelate the Al^{3+}. The increased release could also be due to the lower pH expressed by the spruce-fir horizon. The hardwood surface horizon does not express any difference between the high and low leachate rates and therefore is not expressed in the Table 4.10. Spruce-fir and sand however, exhibit significantly greater amounts of Al^{3+} release in the high leachate treatments (Table 4.9) at 4^{o}C and spruce-fir at 38^{o}C (Table 4.10).

Table 4.8 Average element release (µmol/g) after 181 days for selected surface horizons at 4°, 25°, and 38°C at leachate rates of (A) 60ml/week and (B) 15ml/week.

		Hardwood		Sand		Spruce	
		A	B	A	B	A	B
4	Al	8.65	7.96	11.14	3.05	14.75	7.52
	Fe	10.07	8.93	15.22	3.81	14.08	6.90
	K	13.13	11.90	13.75	4.88	16.64	12.77
	Si	34.04	29.75	44.68	13.71	41.65	21.00
25	Al	1.99	1.01	1.26	1.39	7.00	3.52
	Fe	5.42	2.54	1.42	1.54	11.18	5.20
	K	7.07	7.27	5.58	4.67	11.37	8.53
	Si	29.76	23.72	13.95	41.37	35.17	21.57
38	Al	3.10	2.30	4.09	0.21	8.43	9.81
	Fe	4.52	4.76	2.54	0.18	11.71	11.79
	K	6.99	8.78	5.80	2.56	10.25	12.89
	Si	45.25	47.23	117.84	160.93	46.22	47.32

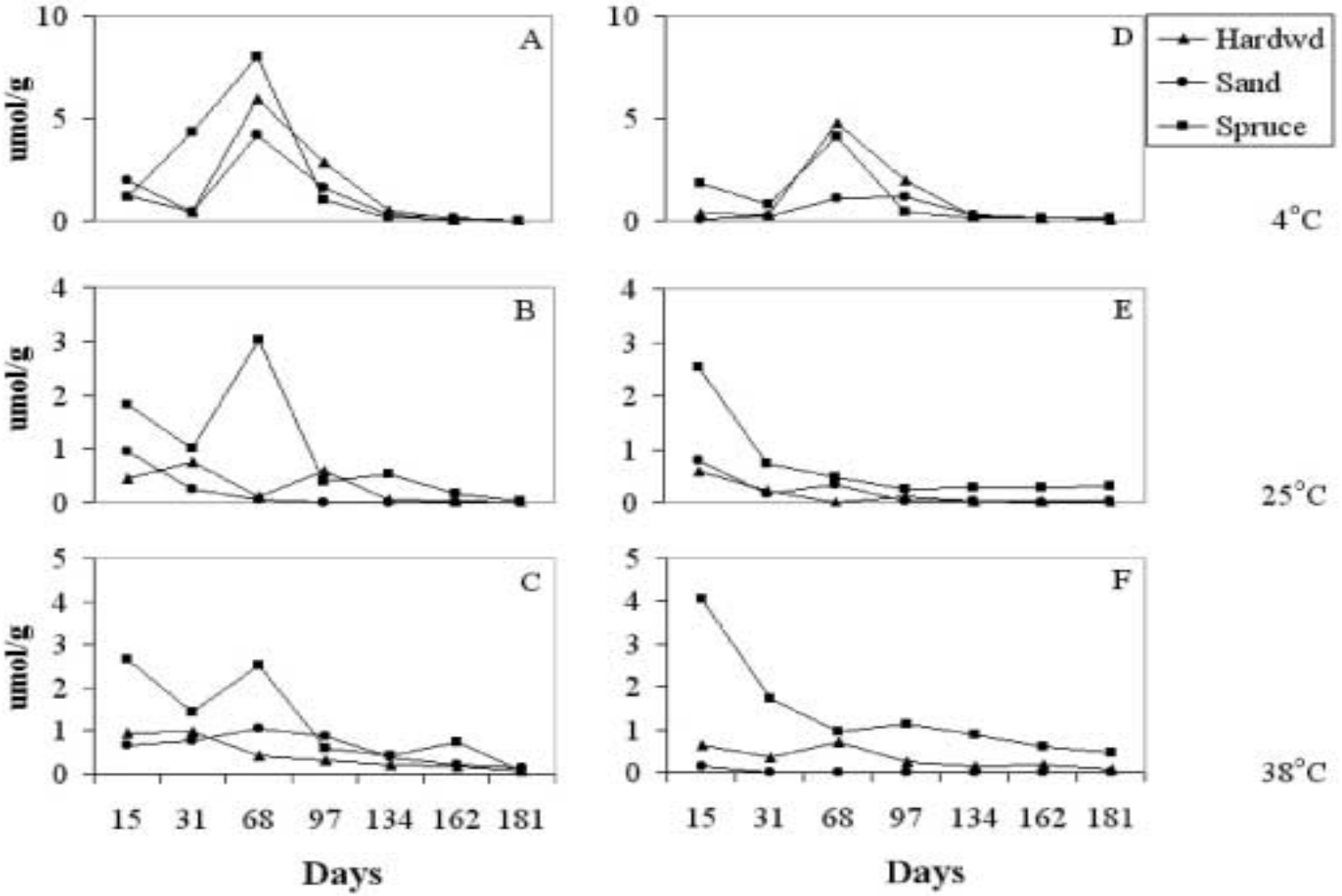

Figure 4.9 Loss of Al^{3+} (μmol/g) for selected surface horizons and temperatures for (A,B,C) high leachate rates and (D,E,F) low leachate rates.

Table 4.9 Comparison of temperature effects on Al^{3+} release (µmol/g) at selected temperatures by estimated least square mean differences at (A) 60ml/week and (B) 15ml/week leachate rates for 3 different surface horizons.

			4						25					
			Hardwood A	Hardwood B	Sand A	Sand B	Spruce A	Spruce B	Hardwood A	Hardwood B	Sand A	Sand B	Spruce A	Spruce B
25	Hardwood	A	**6.66*** **											
	Hardwood	B		**6.94*** **										
	Sand	A			**9.88*** **									
	Sand	B				1.65								
	Spruce	A					**7.75*** **							
	Spruce	B						2.66						
38	Hardwood	A	**5.55** **						-1.11					
	Hardwood	B		**5.66*** **						-1.29				
	Sand	A			**7.05*** **						-2.83			
	Sand	B				2.84						1.18		
	Spruce	A					**6.32*** **						-1.43	
	Spruce	B						-2.29						**-4.95** **

*** Significant at the 0.05 level of probability.**
**** Significant at the 0.005 level of probability.**
***** Significant at the 0.0005 level of probability.**

Table 4.10 Comparison of estimated least square mean difference (µmol/g) between selected surfaces at the same temperature at leachate rates of (A) 60ml/week and (B) 15ml/week.

			Al				Fe				K				Si			
			Spruce		Sand		Spruce		Sand		Spruce		Sand		Spruce		Sand	
			A	B	A	B	A	B	A	B	A	B	A	B	A	B	A	B
	Hardwood	A	**-6.10*** **		-2.49		-4.01		-5.15		-3.51		-0.62		-7.61		-10.64	
	Hardwood	B		0.44		**4.91** **		2.03		5.12		-0.88		**7.02*** **		8.75		16.04
4	Sand	A	-3.61				1.14				-2.89				3.03			
	Sand	B		**-4.47***	**8.09*** **			-3.09	**11.40*** **			-7.90	**8.88*** **			-7.29	30.97	
	Spruce	B	**7.24*** **				**7.18** **				**3.87***				20.65			
	Hardwood	A	**-5.02** **		0.73		**-5.77***		4.00		**-4.30** **		1.49		-5.41		15.81	
	Hardwood	B		-3.85		-0.38		-2.66		1.00		-1.26		2.60		2.15		-17.66
25	Sand	A	**-5.74*** **				**-9.76*** **				**-5.79*** **				-21.22			
	Sand	B		-3.47	-0.13			-3.66	-0.12			-3.86	0.91			19.80	-27.42	
	Spruce	B	2.15				**5.99***				2.84				13.60			
	Hardwood	A	**-5.34** **		-0.99		**-7.18** **		1.99		-3.27		1.19		-0.96		**-72.59*** **	
	Hardwood	B		**-7.51*** **		2.09		**-7.02** **		4.58		**-4.11***		**6.23*** **		-0.09		**-113.70*** **
38	Sand	A	**-4.35***				**-9.17*** **				**-4.45** **				**71.62*** **			
	Sand	B		**-9.60*** **	3.88			**-11.60*** **	2.36			**-10.34*** **	3.24			**113.61*** **	**-43.09*** **	
	Spruce	B	-1.37				-0.08				-2.64				-1.10			

*** Significant at the 0.05 level of probability.**
**** Significant at the 0.005 level of probability.**
***** Significant at the 0.0005 level of probability.**

Loss of Fe^{2+} over time (Fig. 4.10) for the selected temperatures shows that trends that are very similar to that of Al^{+3} the way both the high leachate and low leachate treatments change with increasing temperature. The high leachate treatments have a greater average total amount of Fe^{2+} lost (Table 4.8) at 4°C than at 25° or 38°C for the sand surface horizon only (Table 4.11). None of the high leachate rate surface horizon treatments at 25°C are different from the 38°C treatments. The spruce-fir surface horizons at 25°, and 38°C also release a significantly greater amount of Fe^{2+} than the hardwood or sand surface horizons (Table 4.10).

Comparing the low leachate rate results, only the hardwood surface horizon influence a greater Fe^{2+} release at 4°C than the other temperatures (Table 4.11). The release of Fe^{2+} with columns packed with the spruce-fir horizon increases between 25°C and 38°C (Table 4.11). The spruce-fir horizon releases greater amounts of Fe^{2+} than sand and hardwood horizons at 38°C (Table 4.10). This suggest the spruce-fir again acts as chelator and removes the Fe^{2+} with the soil solution as the leachate is passed through. The hardwood surface horizon does not express any difference between the high and low leachate rates and therefore is not expressed in the Table 4.10. Sand however, exhibits significantly greater amounts of Fe^{2+} release in the high leachate treatment (Table 4.11) at 4°C. This could be due to the higher permeability of the sand, allowing a faster relative leaching rate through the columns and promoting more dissolution.

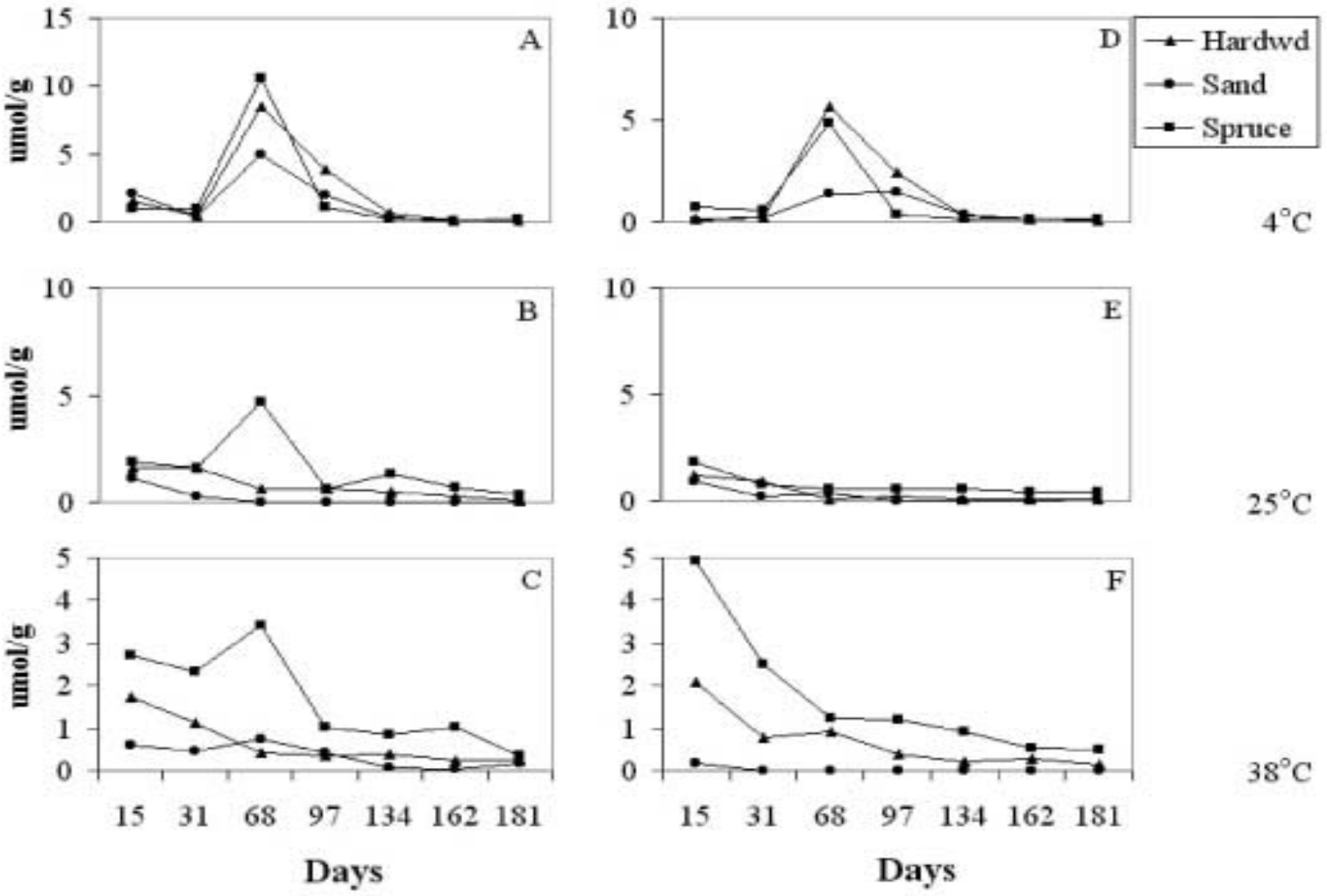

Figure 4.10 Loss of Fe^{2+} (μmol/g) for selected surface horizons and temperatures for (A,B,C) high leachate rates and (D,E,F) low leachate rates.

Table 4.11 Comparison of temperature effects on Fe^{2+} release (µmol/g) at selected temperatures by estimated least square mean differences at (A) 60ml/week and (B) 15ml/week leachate rates for 3 different surface horizons.

			4						25					
			Hardwood A	Hardwood B	Sand A	Sand B	Spruce A	Spruce B	Hardwood A	Hardwood B	Sand A	Sand B	Spruce A	Spruce B
25	Hardwood	A	4.65											
	Hardwood	B		**6.39***										
	Sand	A			**13.80*****									
	Sand	B				2.28								
	Spruce	A					2.89							
	Spruce	B						1.70						
38	Hardwood	A	5.54						0.89					
	Hardwood	B		4.17						-2.22				
	Sand	A			**12.68*****						-1.12			
	Sand	B				3.63						1.35		
	Spruce	A					2.37						-0.52	
	Spruce	B						-4.89						**-6.59****

*** Significant at the 0.05 level of probability.**
**** Significant at the 0.005 level of probability.**
***** Significant at the 0.0005 level of probability.**

Loss of Si over time (Fig. 4.11) for the selected temperatures exhibits similar trends to that of Fe^{2+} and Al^{3+} at 4^{o} and 25^{o}C, however, at 38^{o}C the trend is very different for both the high leachate and low leachate treatments. The high leachate treatments of the sand surface horizon treatment have a greater average total amount of Si lost (Table 4.8) at 4^{o}C that 25^{o} or 38^{o}C (Table 4.12). The high leachate rate sand surface horizon treatment at 25^{o}C is different from the same treatment at 38^{o}C. Both the hardwood and spruce-fir surface horizon treatments lose significantly less Si than the sand at the 38^{o}C treatment only (Table 4.10). This increased loss is likely due to the sand dissolution releasing Si at the high temperatures as observed in blank columns (no biotite).

Comparing the low leachate rate results, only the sand surface horizon influences a greater Si release at 4^{o}C than both of the other temperatures (Table 4.12), however the spruce-fir horizon lost a significantly greater amount at 4^{o}C than at 38^{o}C. Each surface horizon lost a significantly greater amount at the low leachate rates at 38^{o}C than the same treatment at 25^{o}C (Table 4.12). The sand horizon releases greater amounts of Si than spruce-fir and hardwood at 38^{o}C (Table 4.10). Only the sand horizon exhibits a difference in Si^{4+} between high and low leachate rates strictly at 38^{o}C.

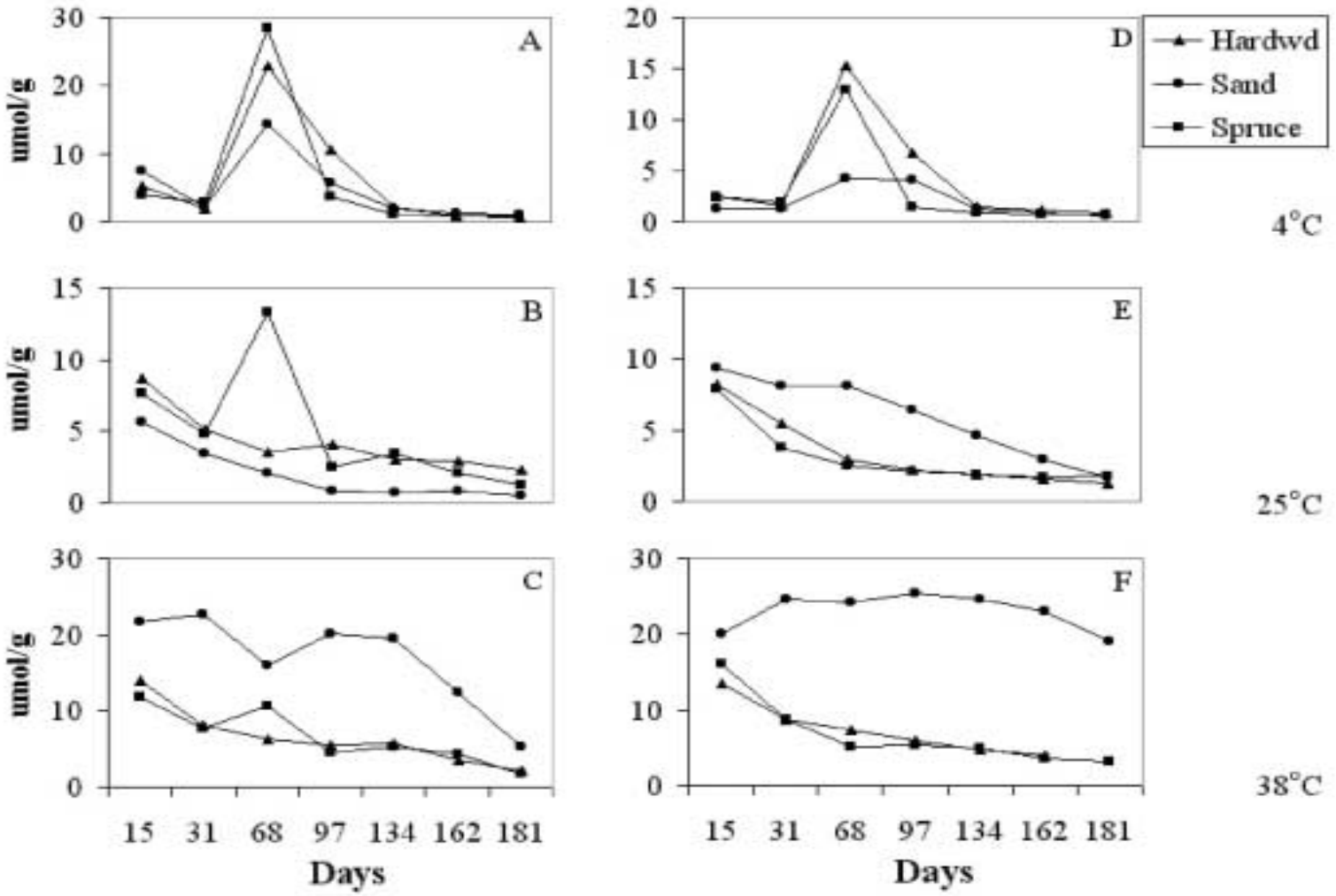

Figure 4.11 Loss of Si (μmol/g) for selected surface horizons and temperatures for (A,B,C) high leachate rates and (D,E,F) low leachate rates.

Table 4.12 Comparison of temperature effects on Si release (µmol/g) at selected temperatures by estimated least square mean differences at (A) 60ml/week and (B) 15ml/week leachate rates for 3 different surface horizons.

			4						25					
			Hardwood A	Hardwood B	Sand A	Sand B	Spruce A	Spruce B	Hardwood A	Hardwood B	Sand A	Sand B	Spruce A	Spruce B
25	Hardwood	A	4.28											
	Hardwood	B		6.04										
	Sand	A			**30.73****									
	Sand	B				**-27.66****								
	Spruce	A					6.48							
	Spruce	B						-0.56						
38	Hardwood	A	-11.21						-15.49					
	Hardwood	B		-17.48						**-23.52***				
	Sand	A			**-73.16*****						**-103.89*****			
	Sand	B				**-147.22*****						**-119.56*****		
	Spruce	A					-4.56						-11.05	
	Spruce	B						**-26.31***						**-25.75***

*** Significant at the 0.05 level of probability.**
**** Significant at the 0.005 level of probability.**
***** Significant at the 0.0005 level of probability.**

Loss of K^+ over time (Fig. 4.12) for the selected temperatures shows that trends that are very similar to that of Al^{3+} and Fe^{2+}, the manner which the high leachate and low leachate treatments change with increasing temperature. The high leachate treatments have a greater average total amount of K^+ lost (Table 4.8) at 4°C that 25° or 38°C for the sand, spruce-fir, and hardwood surface horizons (Table 4.13). None of the high leachate rate surface horizon treatments at 25°C are different from the 38°C treatments. The spruce-fir surface horizons at 25°C release a significantly greater amount of K^+ than the hardwood or sand surface horizons and at 38°C spruce-fir released more than the sand horizon (Table 4.10).

Comparing the low leachate rate results, the hardwood surface horizon influence a greater K^+ release at 4°C than at 25°C and spruce-fir horizon releases a greater amount at 4°C than 25° and 38°C (Table 4.13). This could be attributed to greater microbial growth at the higher temperatures than 4°C. The release of K^+ with columns packed with the spruce-fir horizon also increases between 25°C and 38°C (Table 4.13). The spruce-fir horizon releases greater amounts of K^+ than sand and hardwood horizons at 38°C and the hardwood releases a greater amount than the sand horizon (Table 4.10). The hardwood surface horizon also releases a significantly higher amount of K^+ than the sand horizon at the 4°C treatment. The hardwood surface horizon does not express any difference between the high and low leachate rates and therefore is not expressed in the Table 4.10. Sand and spruce-fir surface horizon treatments however, exhibit significantly greater amounts of K^+ release in the high leachate treatment (Table 4.13) at 4°C.

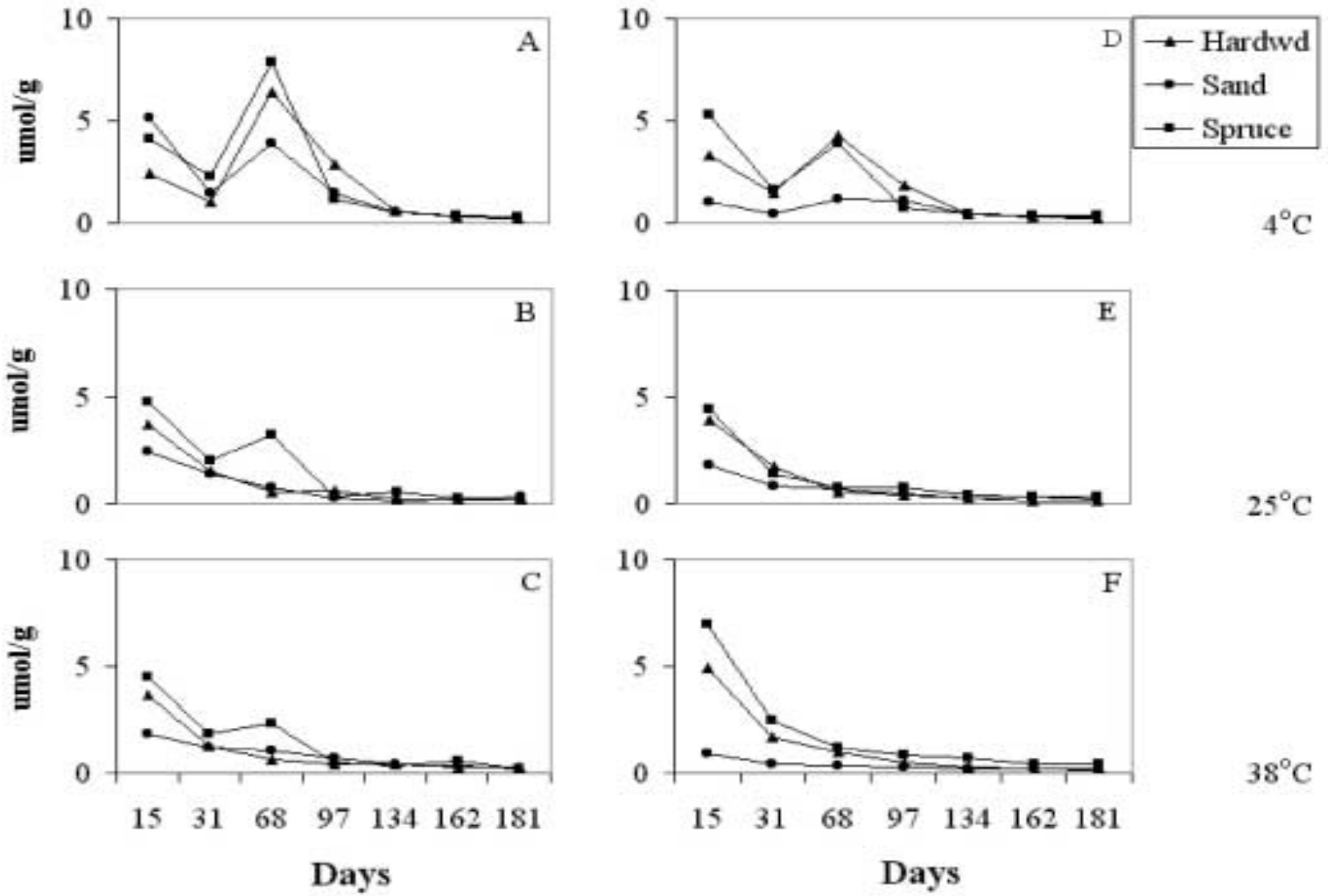

Figure 4.12 Loss of K^+ (μmol/g) for selected surface horizons and temperatures for (A,B,C) high leachate rates and (D,E,F) low leachate rates.

Table 4.13 Comparison of temperature effects on K^+ release (µmol/g) at selected temperatures by estimated least square mean differences at (A) 60ml/week and (B) 15ml/week leachate rates for 3 different surface horizons.

			4						25					
			Hardwood A	Hardwood B	Sand A	Sand B	Spruce A	Spruce B	Hardwood A	Hardwood B	Sand A	Sand B	Spruce A	Spruce B
25	Hardwood	A	**6.06*** **											
	Hardwood	B		**4.63** **										
	Sand	A			**8.18*** **									
	Sand	B				0.21								
	Spruce	A					**5.27*** **							
	Spruce	B						**4.24** **						
38	Hardwood	A	**6.14*** **						0.08					
	Hardwood	B		3.11						-1.51				
	Sand	A			**7.96*** **						-0.22			
	Sand	B				2.32						2.11		
	Spruce	A					**6.39*** **						1.12	
	Spruce	B						-0.12						**-4.36** **

*** Significant at the 0.05 level of probability.**
**** Significant at the 0.005 level of probability.**
***** Significant at the 0.0005 level of probability.**

To summarize, the influence of the spruce-fir surface horizon versus the hardwood surface horizon is first observed in the pH measurements. The lower pH of the spruce-fir horizon may explain the variation in release of base cations. High leachate rates again significantly increase the release of most of the base cations, especially under the spruce-fir and hardwood surface horizon treatments. This suggests that any undisturbed, forest litter layer in the Southeast will promote greater dissolution than a disturbed, plowed surface layer. The influence of high leachate rates, with interaction of the surface horizons, also seen in the acid treatments, suggest that the chelating ability of the functional groups of organic acids removes the cation from solution creating a positive potential for enhanced cation release. The greater cation loss observed for the high leachate rates at the 4^{o}C temperature could be due to an influence of microbial growth in all the columns. At the low temperature, the growth of microorganisms is kept to a minimum and therefore any release of nutrients from dissolution of biotite will remain in soil solution. Also, the microbes would influence the breakdown of organic acids in the columns. The 25^{o}C temperature may provide ideal conditions for these microbes; therefore, they would remove nutrients from the soil solution as they grow. Finally, many cations, especially in the columns packed with the spruce-fir horizon at the low leachate rate, exhibit an increase in cations in solution at 38^{o}C. This temperature may, in effect, be too hot for the microbes to grow as well and more cations will remain in solution.

Literature Cited

Perrin, D.D., 1979. Stability constants of metal-ion complexes. Part B. Organic Ligands. IUPAC, Pergamon Press, New York. pp.26-30.

Martell, A.E., and Smith, R.M. 1977. Critical stability constants. Volume 3: Other organic ligands. Plenum Press, New York. pp.265

Smith, R.M. and Martell, A.E. 1989. Critical stability constants. Volume 6: Second supplement. Plenum Press, New York. pp.356-358.

Chapter 5

Conclusions

The weathering of biotite is controlled by pedogenic factors. However, the mechanisms of biotite weathering can vary depending upon the weathering environment and often result in the formation of several different phyllosilicate minerals. For example, biotite has been observed to weather directly to kaolinite in the Piedmont of Virginia and hydroxy-interlayered vermiculite in the Blue Ridge, suggesting a temperature dependence. To accurately determine whether or not there is a temperature dependence, all other soil forming factors would have to be held constant. However, the heterogeneity of natural systems makes this very difficult. In this study, the selection of sites ontop of a continuous granite rock with little variation in composition allowed time, and parent material to remain constant. Furthermore, sampling from residuum soils in similar landscape positions with similar slopes and azimuth allowed other soil forming factors such as relief to remain constant. The only variation between the sites was elevation and vegetation. The difference in elevation allowed for diffrerences in climate (i.e. temperature and rainfall) while differences in vegetation could result in different organic acids, soil structure, porosity and permeability. Accordingly a detailed mineralogical analysis was performed on the clay fractions of soil samples from each site in an attempt to observe differences in biotite weathering from sites with different climates and vegetation.

Mineralogical analysis shows that the higher elevation soils:

1) have a higher gibbsite content in the clay fraction,
2) have evidence of later stages of weathering in the clay fractions of the A and B horizons, as evidenced by the greater amounts of gibbsite, montmorillonite, soluble Fe, higher surface area, and finer particle size in the clay fraction of the B-horizon,
3) have a dominance of halloysite in the C horizons with little evidence of original mineralogy of the parent material.

These results suggest that the high elevation site experienced a greater weathering intensity. This is counterintuitive, since it is commonly accepted that an increase in elevation or a decrease in temperature will result in less weathered soils. The greater weathering of the minerals in the high elevation suggests that differences in vegetation (oak vs. pasture), higher leaching rates due to greater porosity, or differences in the quantity of rainfall controlled the difference in biotite weathering.

Concurrent with the filed study, a laboratory column study was included to examine the influence of leaching intensity, soluble organic acids from selected vegetation, and temperature on biotite weathering. However, the column study did not result in any detedtable difference in biotite weathering products. It was concluded that 6 months may not be a long enough duration of weathering to identify the secondary mineral formation using various chemical and mineralogical techniques. The cation release throughout the study does offer valuable data, which supports the field study conclusions. The presence of organic acids and the interaction of organic acids with higher leachate rates release a greater amount of cations from the biotite structure. This suggests that the vegetation may be responsible for a greater weathering of the biotite observed at the high elevation, especially with the higher rainfall rate. Furthermore, the presence and type of organic horizon may cause a reduction in soil solution pH due to production of organic acids, thus promoting greater dissolution. Moreover, a reduction in pH coupled with a higher leaching rate may significantly increase the cation release from the biotite. Finally, the temperature study was inconclusive possibly due to differences in microbial activity.

Though many field studies suggest that biotite weathering is temperature dependent, there is not significant evidence in the soils derived from the Striped Rock Biotite Granite to support this, possibly due to minimal temperature differences. However, this study suggests the weathering of biotite is dependent on the type of vegetation and leaching environment.

APPENDIX A

Figures Used In Mineralogical Analysis

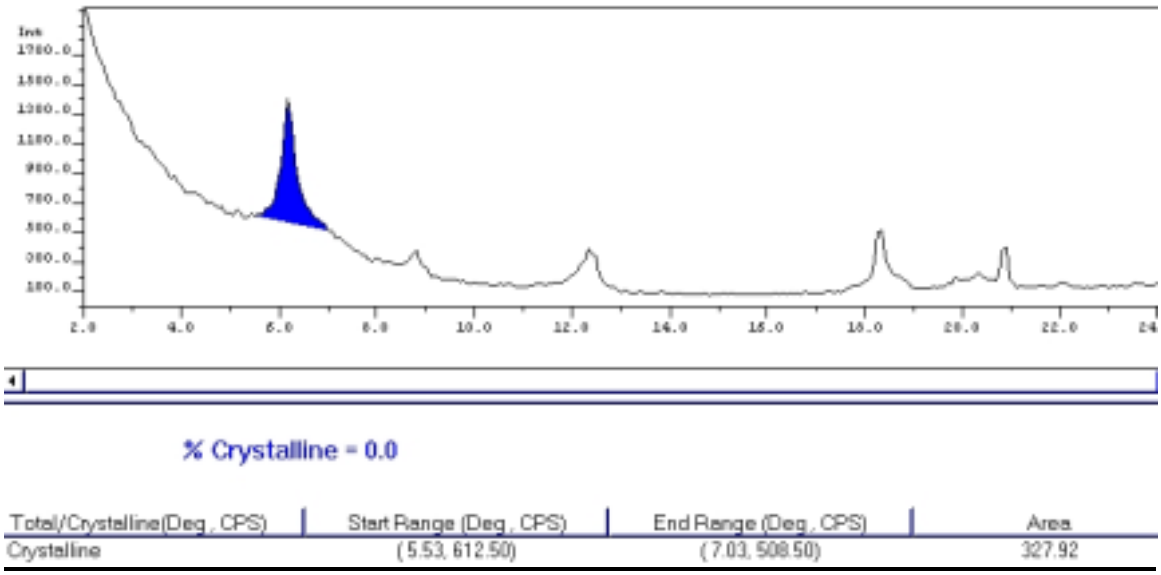

Figure A.1_X-ray pattern and peak area determination of the S-4A Mg-saturated, glycerol solvated clay fraction sample at 25°C for the 14Å peak. Used to help identify montmorillonite.

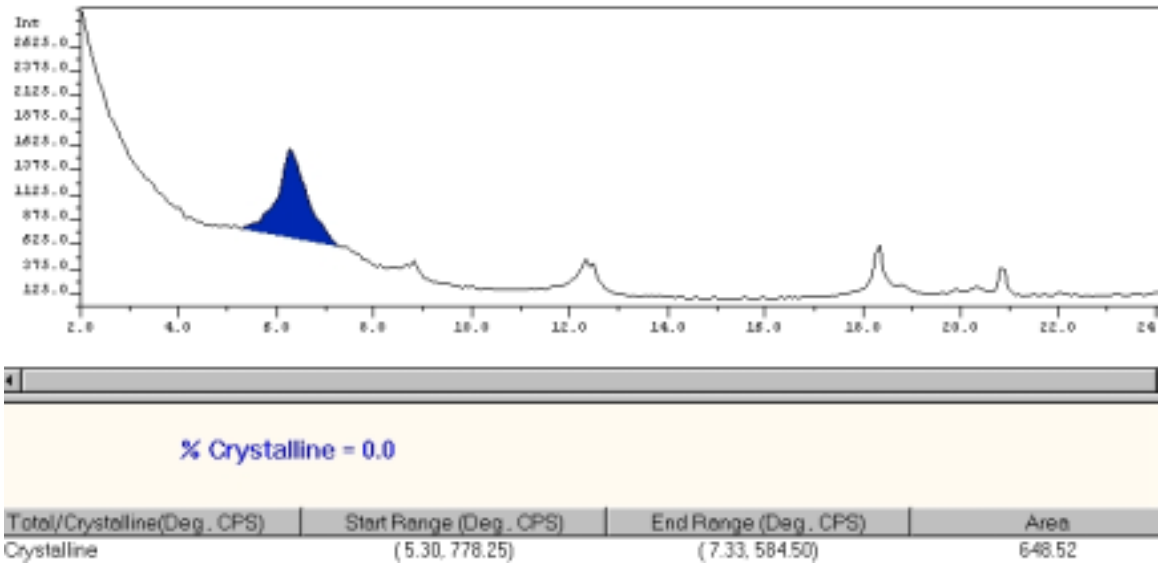

Figure A.2 X-ray pattern and peak area determination of the S-4A Mg-saturated, glycerol solvated clay fraction sample at 110°C for the 14Å peak. Used to help identify montmorillonite.

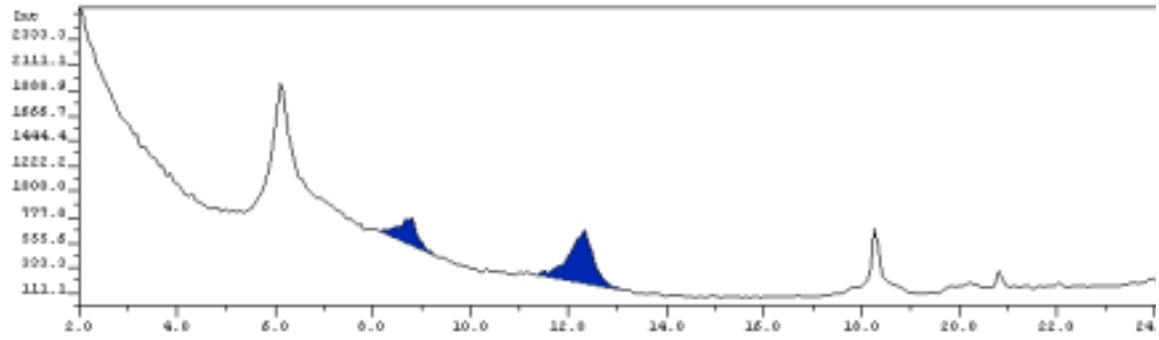

% Crystalline = 0.0

Total/Crystaline(Deg., CPS)	Start Range (Deg., CPS)	End Range (Deg., CPS)	Area
Crystaline	(8.15, 642.75)	(9.28, 424.50)	117.31
Crystaline	(11.38, 263.00)	(13.10, 130.25)	271.94

Figure A.3 X-ray pattern and peak area determination of S-1C, K^+-saturated clay fraction sample to determine 10Å and 7Å peak areas prior to treatment with formamide. Used to determine relative amounts of kaolinite and halloysite.

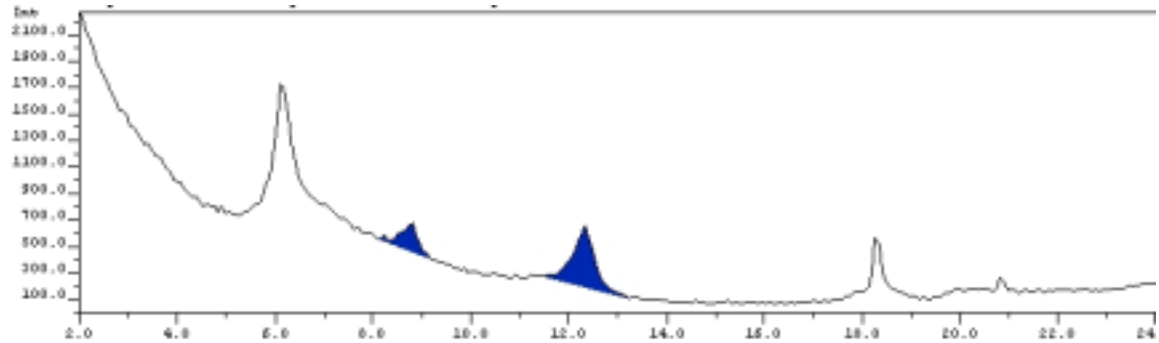

% Crystalline = 0.0

Total/Crystaline(Deg., CPS)	Start Range (Deg., CPS)	End Range (Deg., CPS)	Area
Crystaline	(8.15, 551.25)	(9.35, 371.25)	96.49
Crystaline	(11.45, 264.75)	(13.25, 100.50)	259.43

Figure A.4 X-ray pattern and peak area determination of S-1C, K^+-saturated, formamide treated clay fraction sample to determine 10Å and 7Å peak areas after treatment to compare to the untreated peak areas. Used to determine relative amounts of kaolinite and halloysite.

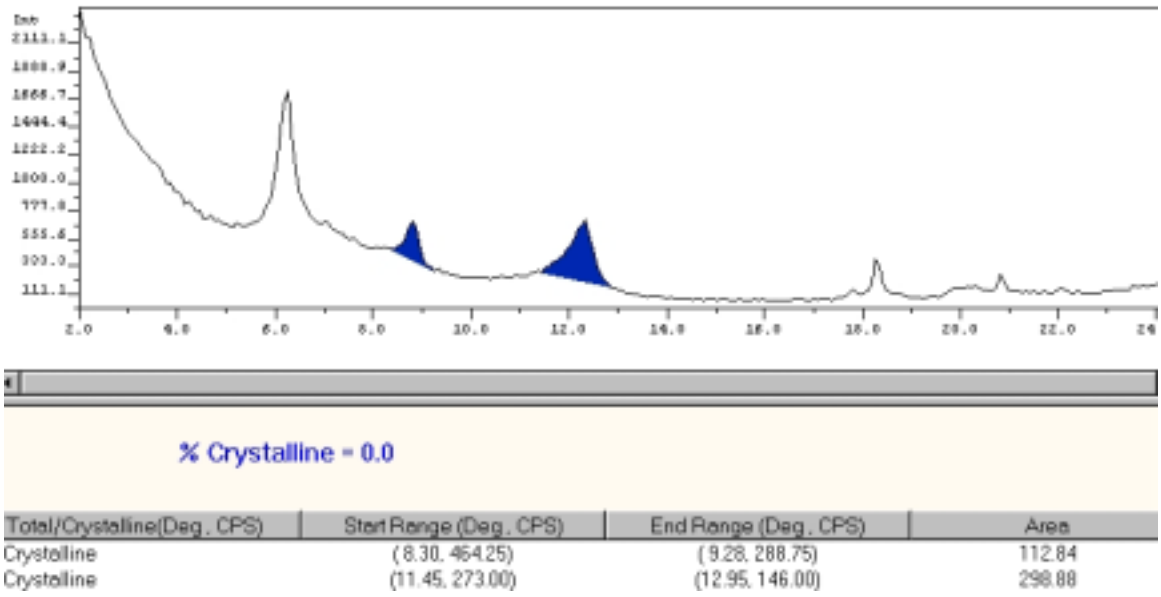

Figure A.5 X-ray pattern and peak area determination of S-2C, K^+-saturated clay fraction sample to determine 10Å and 7Å peak areas prior to treatment with formamide. Used to determine relative amounts of kaolinite and halloysite.

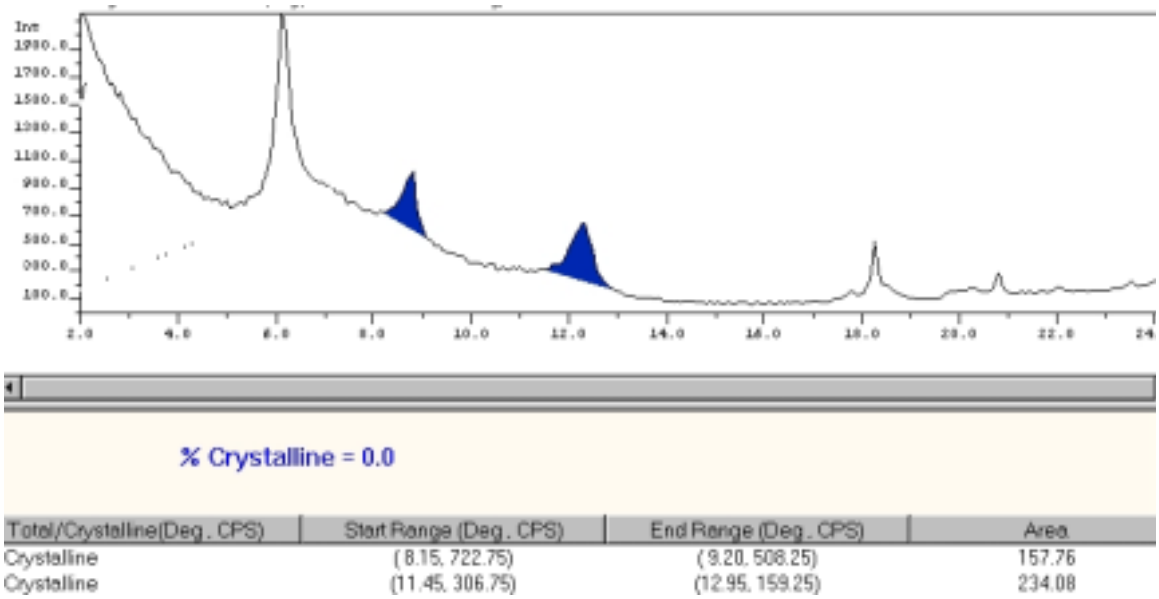

Figure A.6 X-ray pattern and peak area determination of S-2C, K^+-saturated, formamide treated clay fraction sample to determine 10Å and 7Å peak areas after treatment to compare to the untreated peak areas. Used to determine relative amounts of kaolinite and halloysite.

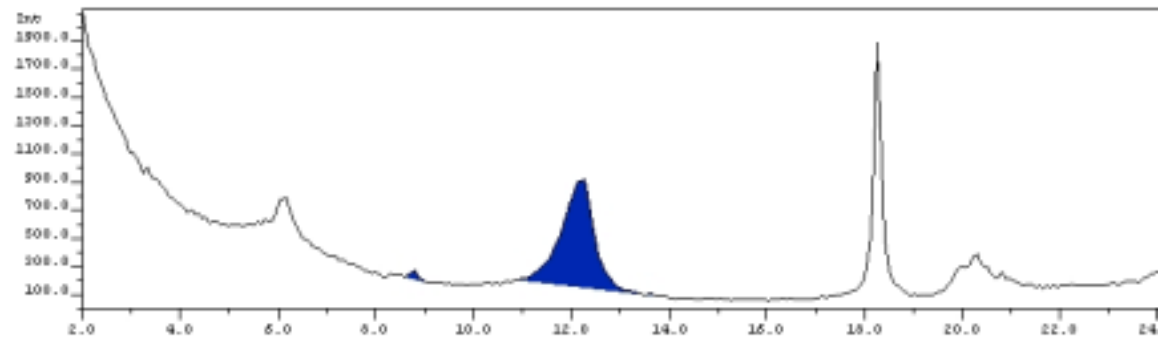

% Crystalline = 0.0

Total/Crystalline(Deg., CPS)	Start Range (Deg., CPS)	End Range (Deg., CPS)	Area
Crystaline	(9.05, 181.00)	(9.05, 181.00)	0.00
Crystaline	(8.45, 228.25)	(9.05, 181.00)	15.86
Crystaline	(10.85, 195.00)	(13.78, 85.50)	620.40

Figure A.7 X-ray pattern and peak area determination of S-3C, K^+-saturated clay fraction sample to determine 10Å and 7Å peak areas prior to treatment with formamide. Used to determine relative amounts of kaolinite and halloysite.

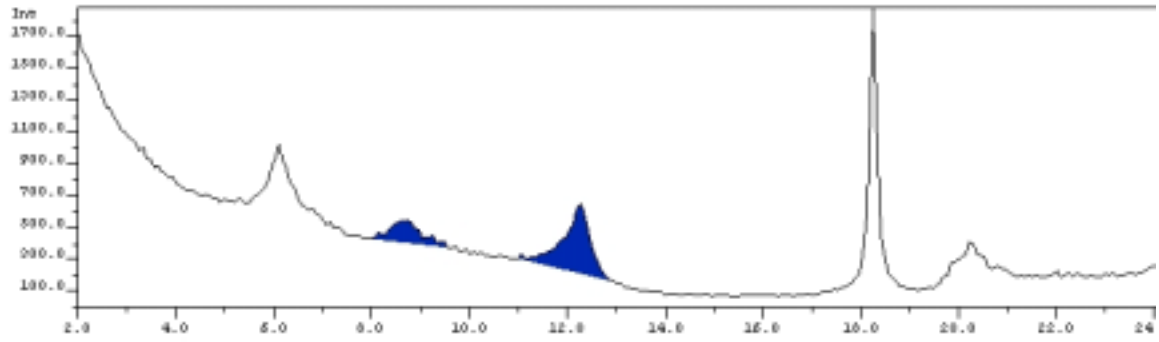

% Crystalline = 0.0

Total/Crystalline(Deg., CPS)	Start Range (Deg., CPS)	End Range (Deg., CPS)	Area
Crystaline	(8.00, 426.75)	(9.65, 370.75)	105.62
Crystaline	(11.00, 301.75)	(12.95, 158.25)	280.24

Figure A.8 X-ray pattern and peak area determination of S-3C, K^+-saturated, formamide treated clay fraction sample to determine 10Å and 7Å peak areas after treatment to compare to the untreated peak areas. Used to determine relative amounts of kaolinite and halloysite.

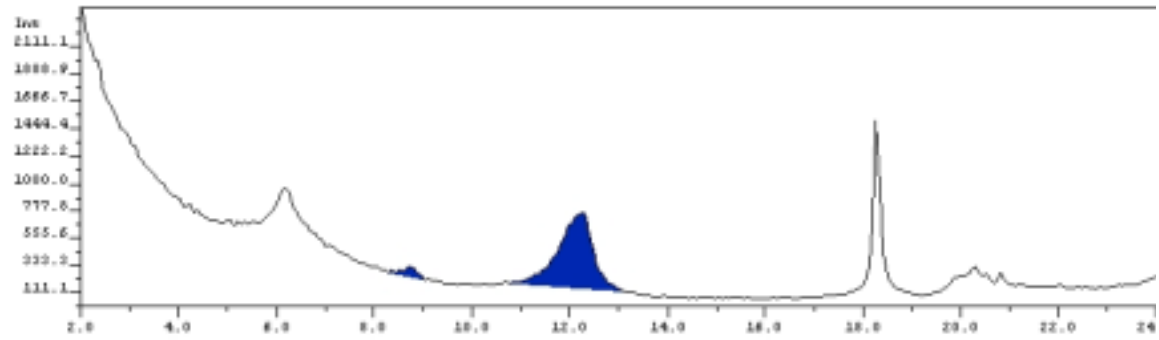

% Crystalline = 0.0

Total/Crystalline(Deg., CPS)	Start Range (Deg., CPS)	End Range (Deg., CPS)	Area
Crystalline	(8.30, 268.50)	(9.05, 206.00)	32.32
Crystalline	(10.78, 177.50)	(13.32, 104.25)	521.08

Figure A.9 X-ray pattern and peak area determination of S-4C, K^+-saturated clay fraction sample to determine 10Å and 7Å peak areas prior to treatment with formamide. Used to determine relative amounts of kaolinite and halloysite.

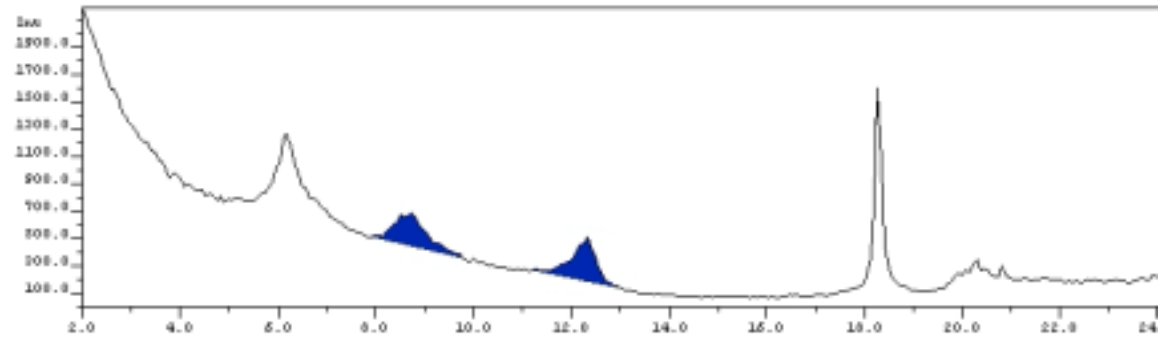

% Crystalline = 0.0

Total/Crystalline(Deg., CPS)	Start Range (Deg., CPS)	End Range (Deg., CPS)	Area
Crystalline	(7.92, 504.25)	(9.80, 353.75)	188.96
Crystalline	(11.23, 261.25)	(13.18, 111.25)	197.48

Figure A.10 X-ray pattern and peak area determination of S-4C, K^+-saturated, formamide treated clay fraction sample to determine 10Å and 7Å peak areas after treatment to compare to the untreated peak areas. Used to determine relative amounts of kaolinite and halloysite.

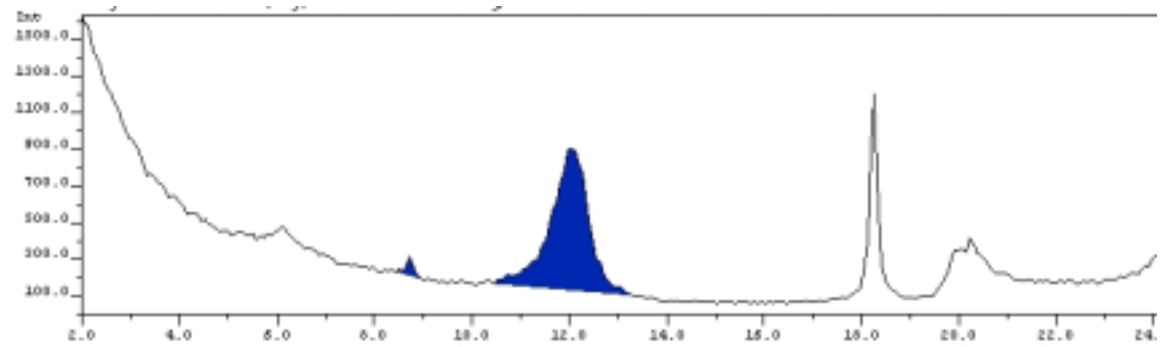

% Crystalline = 0.0

Total/Crystalline(Deg., CPS)	Start Range (Deg., CPS)	End Range (Deg., CPS)	Area
Crystalline	(8.45, 224.75)	(8.97, 187.75)	20.91
Crystalline	(10.48, 162.00)	(13.40, 94.50)	711.94

Figure A.11 X-ray pattern and peak area determination of saprolite, K^+-saturated clay fraction sample to determine 10Å and 7Å peak areas prior to treatment with formamide. Used to determine relative amounts of kaolinite and halloysite.

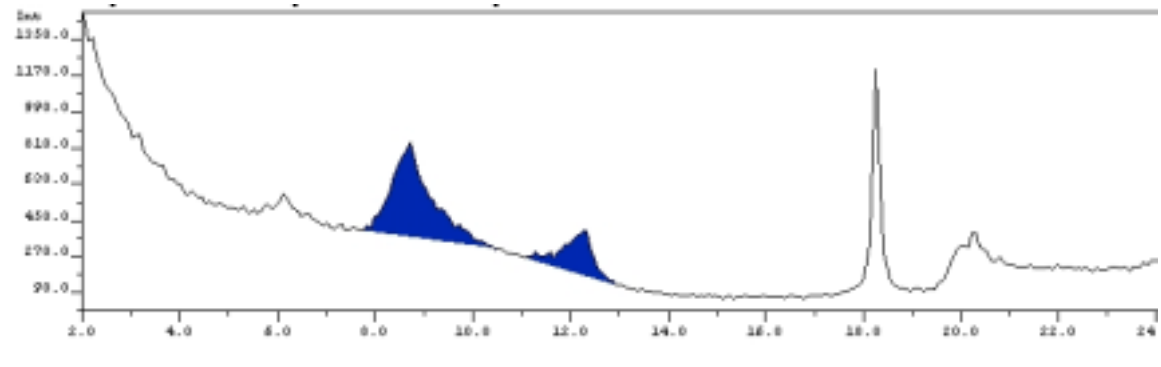

% Crystalline = 0.0

Total/Crystalline(Deg., CPS)	Start Range (Deg., CPS)	End Range (Deg., CPS)	Area
Crystalline	(7.78, 396.00)	(10.55, 306.75)	433.38
Crystalline	(11.07, 258.75)	(12.95, 126.00)	161.47

Figure A.12 X-ray pattern and peak area determination of saprolite, K^+-saturated, formamide treated clay fraction sample to determine 10Å and 7Å peak areas after treatment to compare to the untreated peak areas. Used to determine relative amounts of kaolinite and halloysite.

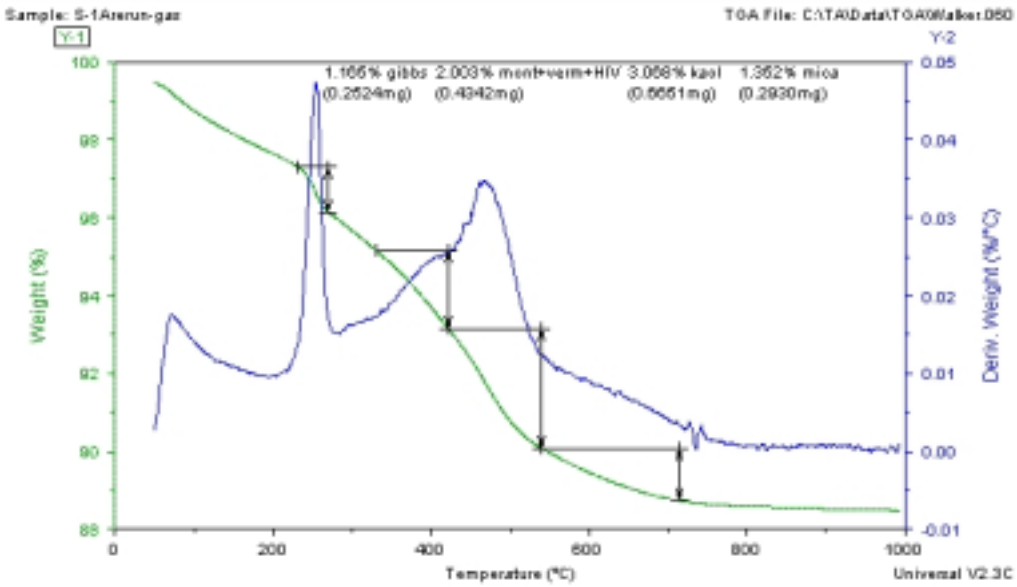

Figure A.13 TGA curve with derivative weight loss and approximated weight loss due to indicated minerals for the S-1A sample.

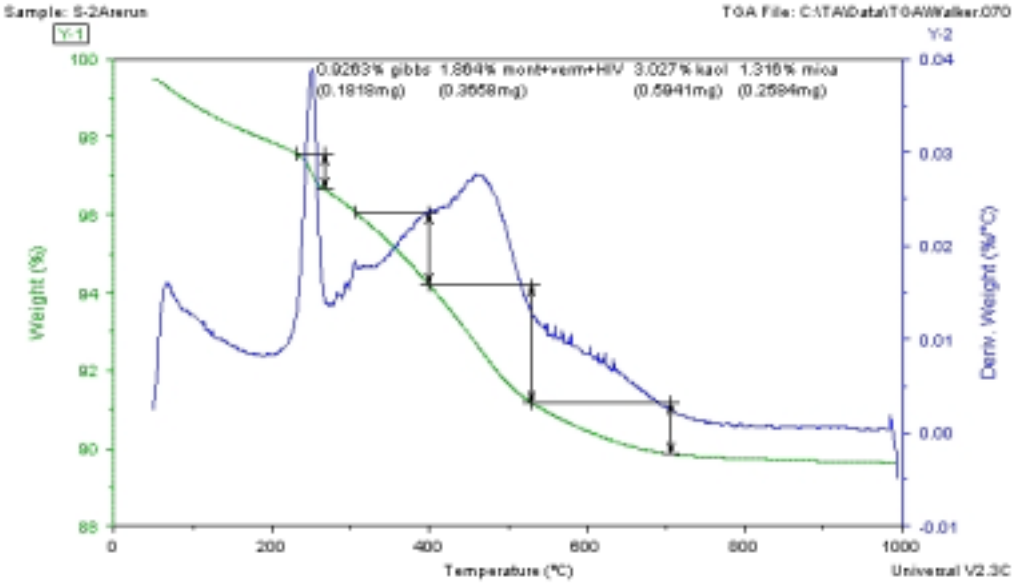

Figure A.14 TGA curve with derivative weight loss and approximated weight loss due to indicated minerals for the S-2A sample.

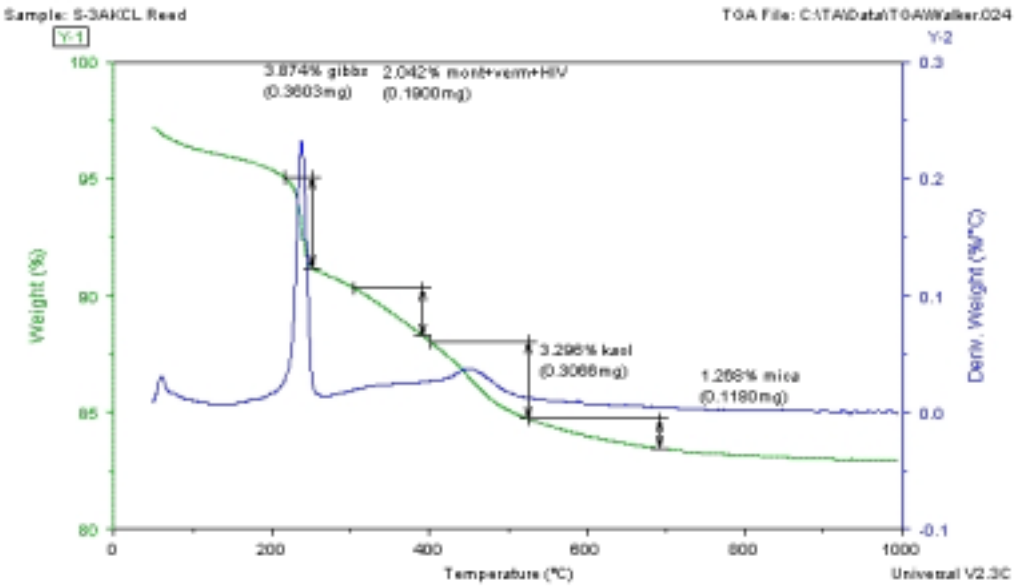

Figure A.15 TGA curve with derivative weight loss and approximated weight loss due to indicated minerals for the S-3A sample.

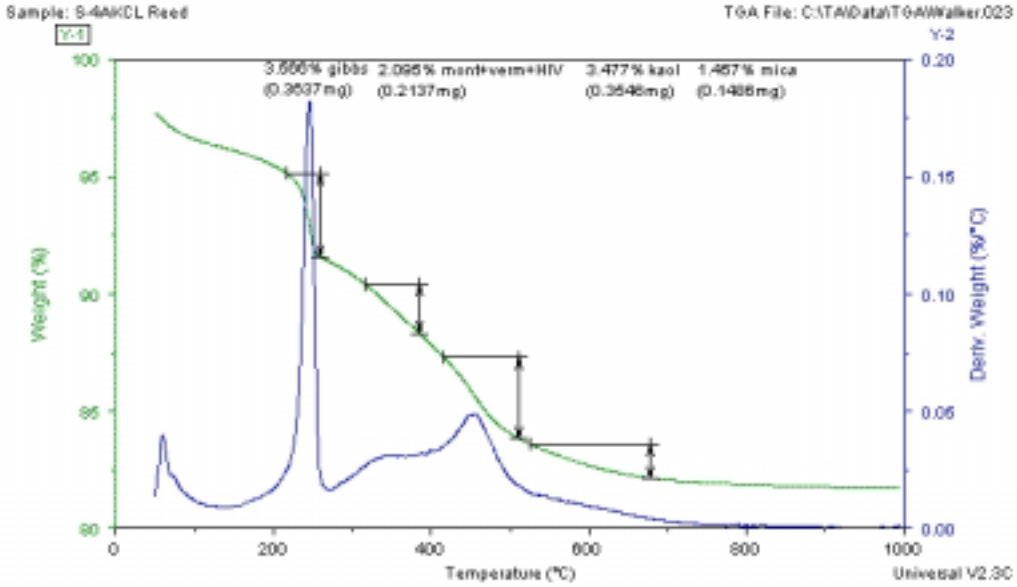

Figure A.16 TGA curve with derivative weight loss and approximated weight loss due to indicated minerals for the S-4A sample.

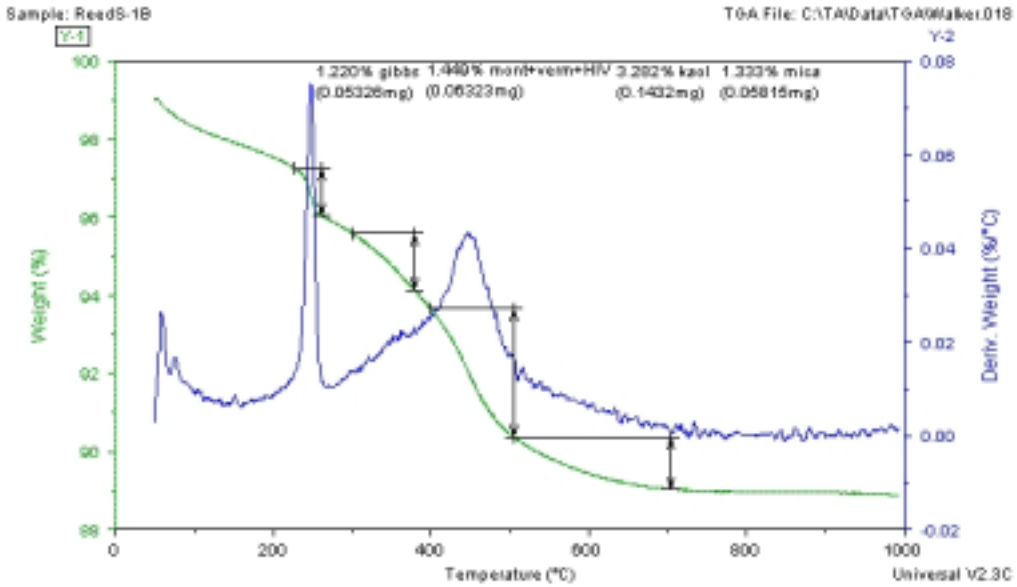

Figure A.17 TGA curve with derivative weight loss and approximated weight loss due to indicated minerals for the S-1B sample.

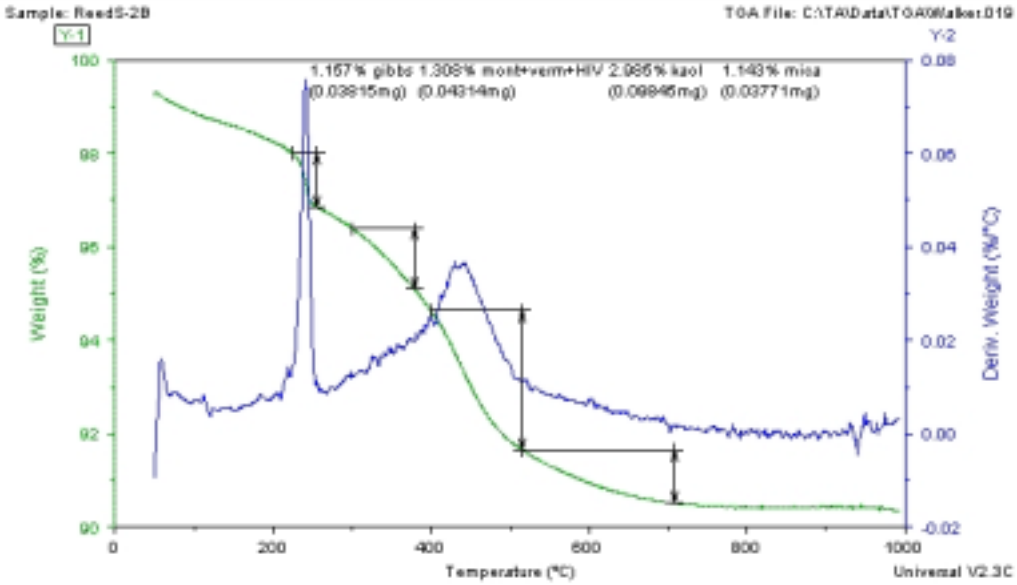

Figure A.18 TGA curve with derivative weight loss and approximated weight loss due to indicated minerals for the S-2B sample.

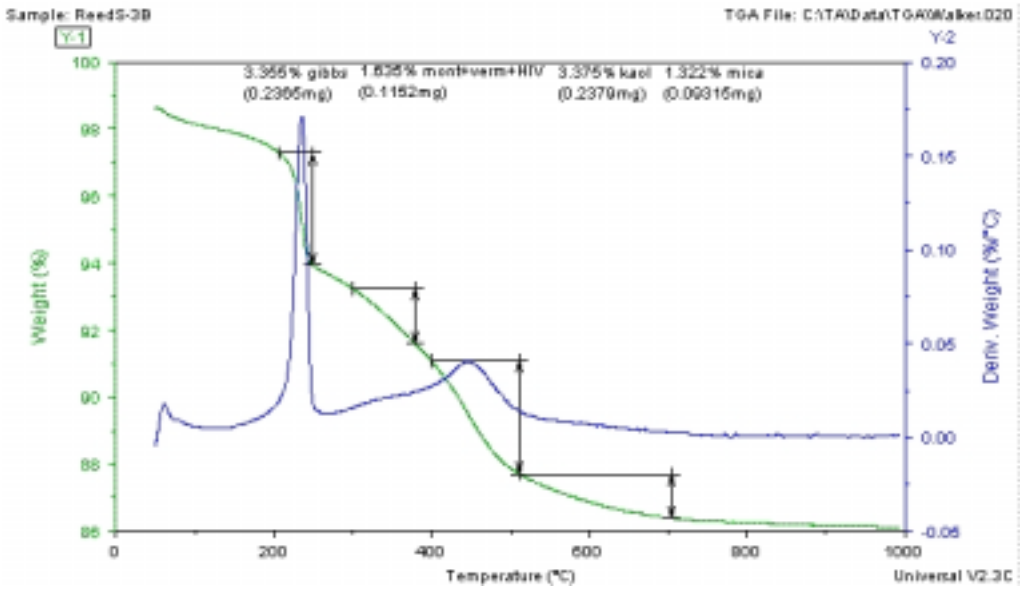

Figure A.19 TGA curve with derivative weight loss and approximated weight loss due to indicated minerals for the S-3B sample.

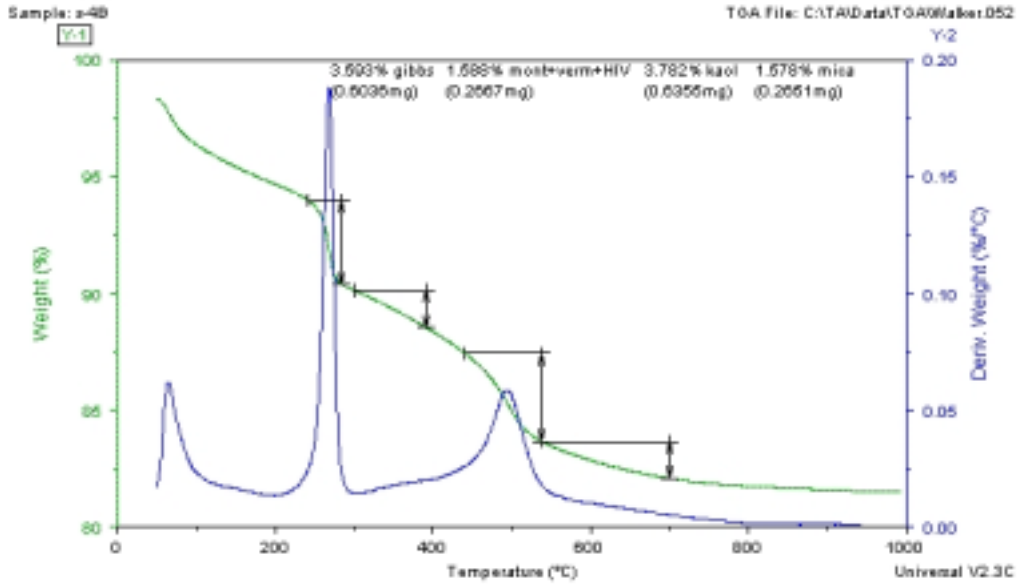

Figure A.20 TGA curve with derivative weight loss and approximated weight loss due to indicated minerals for the S-4B sample.

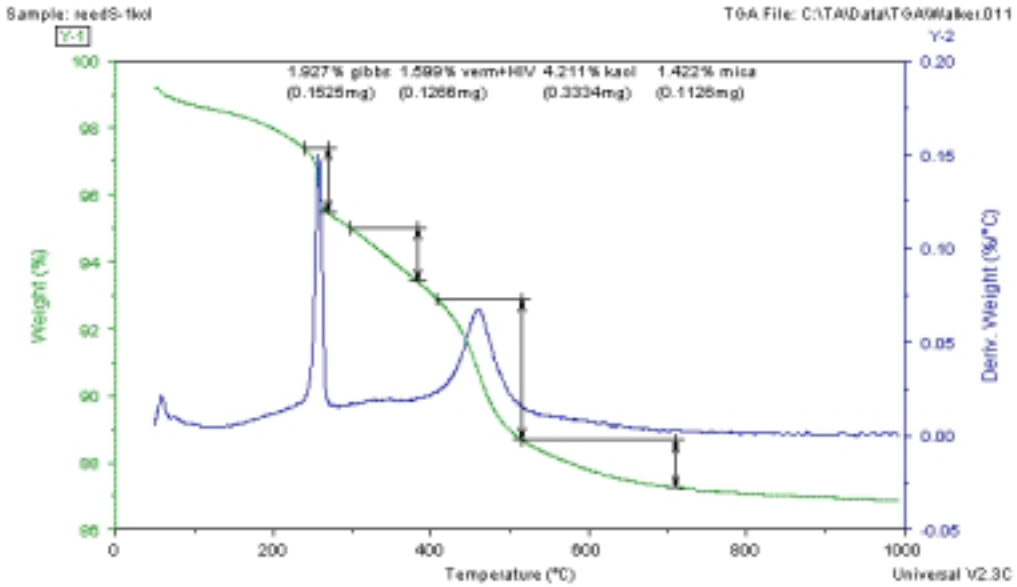

Figure A.21 TGA curve with derivative weight loss and approximated weight loss due to indicated minerals for the S-1C sample.

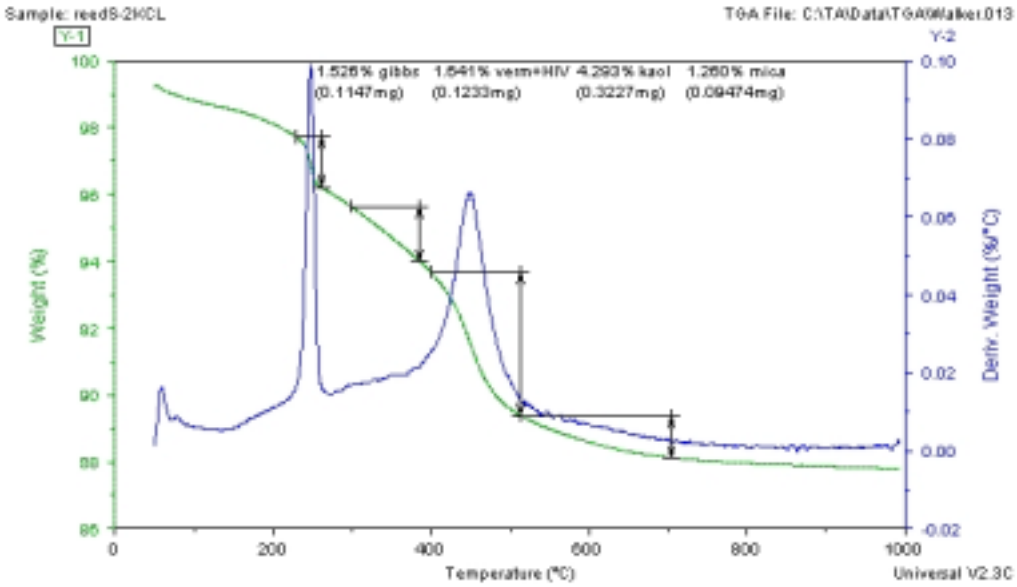

Figure A.22 TGA curve with derivative weight loss and approximated weight loss due to indicated minerals for the S-2C sample.

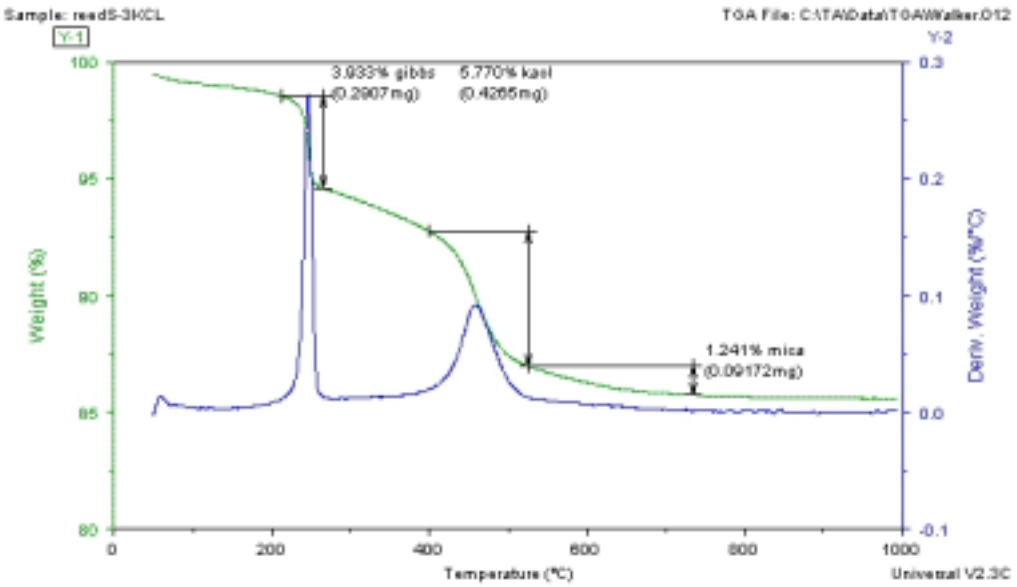

Figure A.23 TGA curve with derivative weight loss and approximated weight loss due to indicated minerals for the S-3C sample.

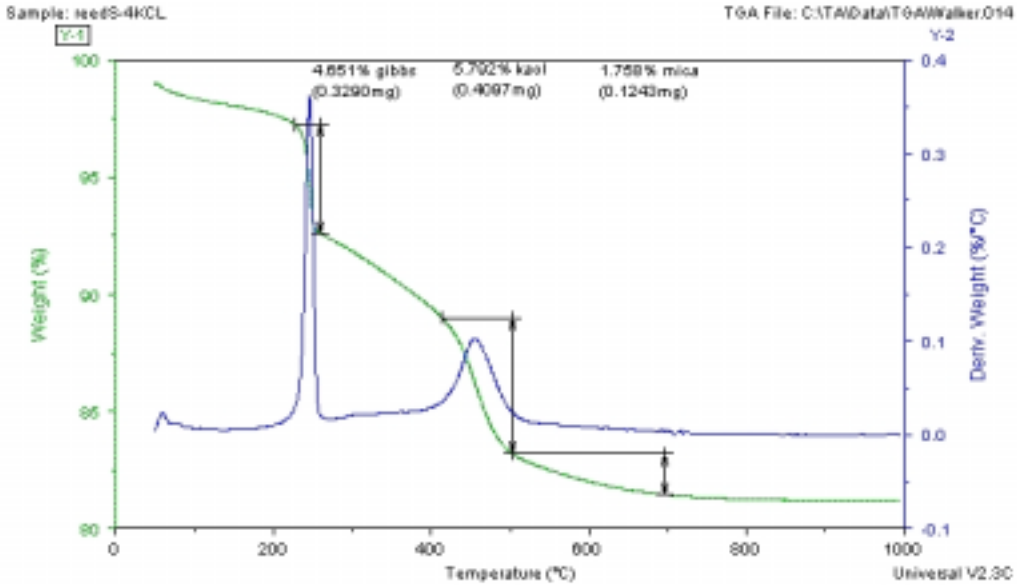

Figure A.24 TGA curve with derivative weight loss and approximated weight loss due to indicated minerals for the S-4C sample.

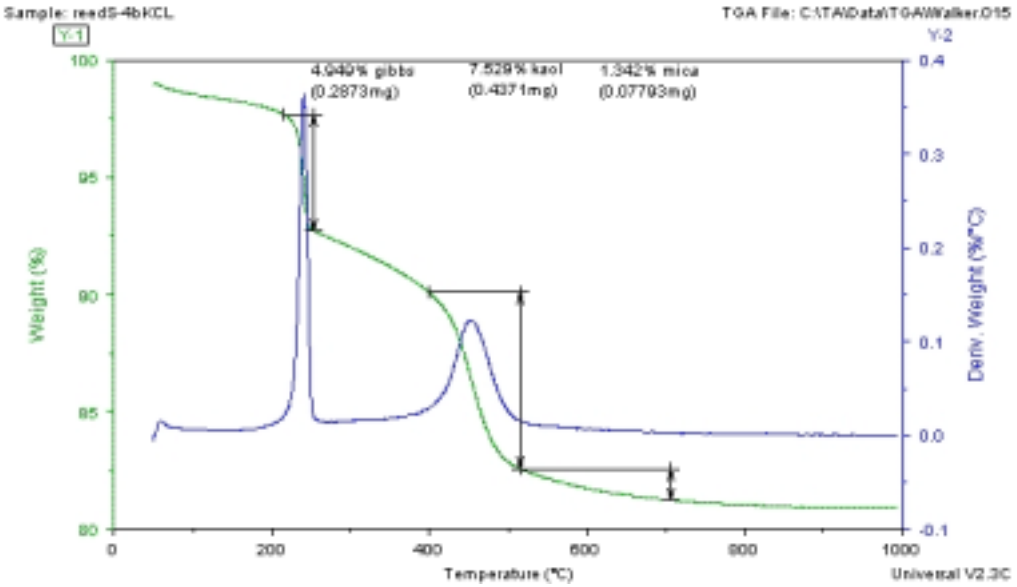

Figure A.25 TGA curve with derivative weight loss and approximated weight loss due to indicated minerals for the saprolite sample.

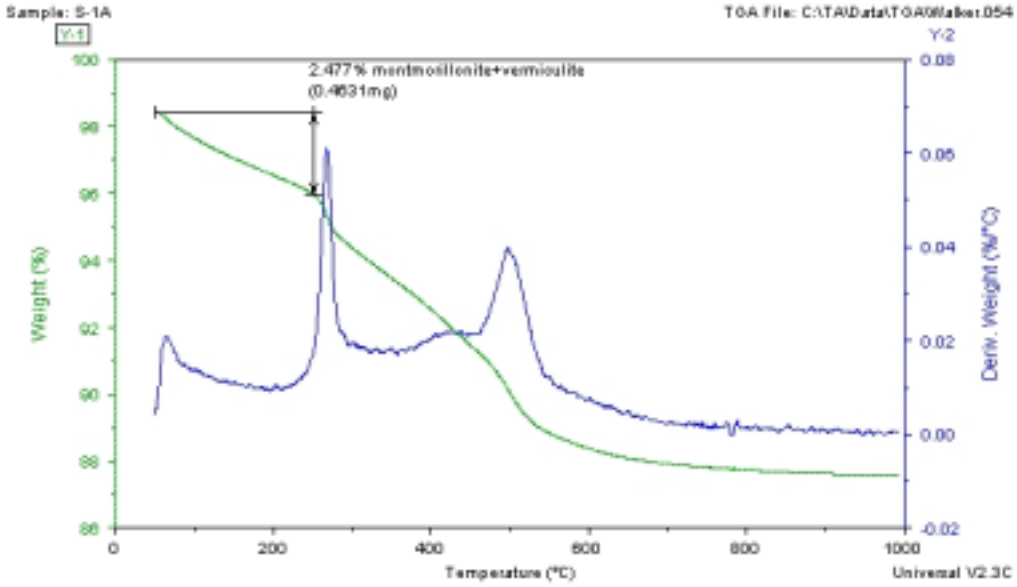

Figure A.26 TGA curve with derivative weight loss and approximated weight loss due to montmorillonite and vermiculite for the S-1A sample at a relative humidity of 56%.

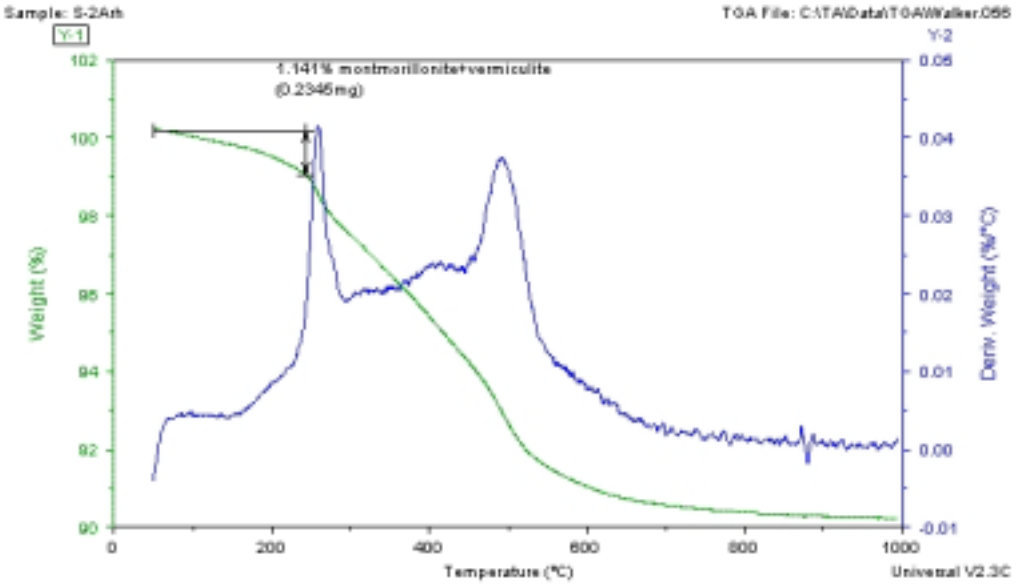

Figure A.27 TGA curve with derivative weight loss and approximated weight loss due to montmorillonite and vermiculite for the S-2A sample at a relative humidity of 56%.

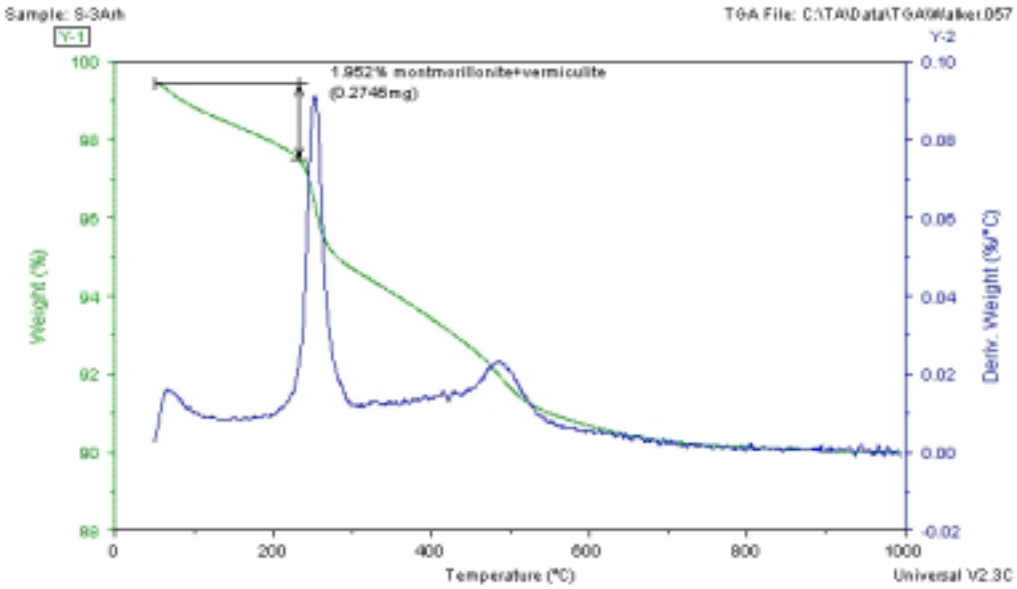

Figure A.28 TGA curve with derivative weight loss and approximated weight loss due to montmorillonite and vermiculite for the S-3A sample at a relative humidity of 56%.

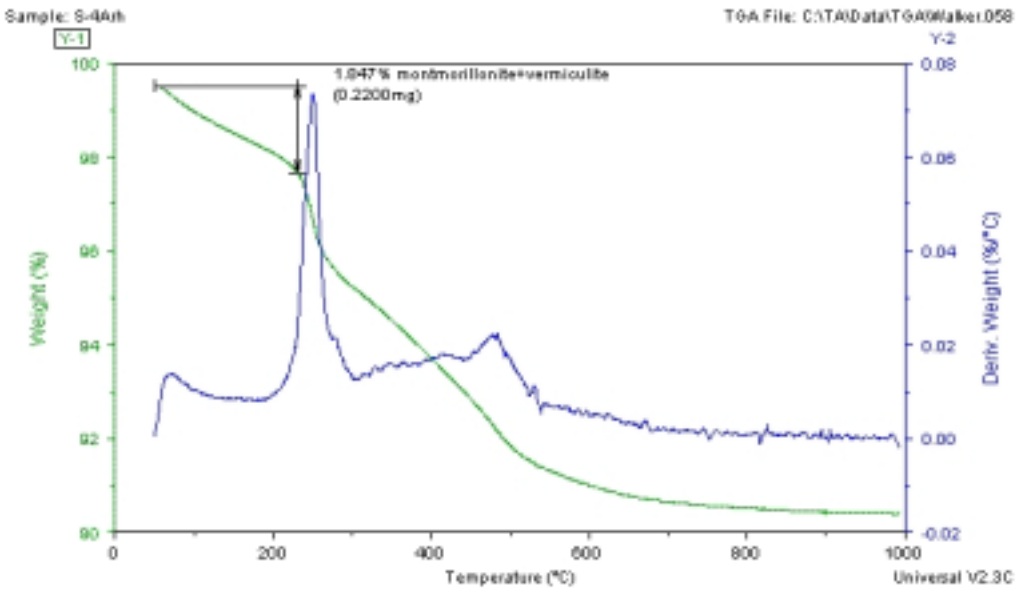

Figure A.29 TGA curve with derivative weight loss and approximated weight loss due to montmorillonite and vermiculite for the S-4A sample at a relative humidity of 56%.

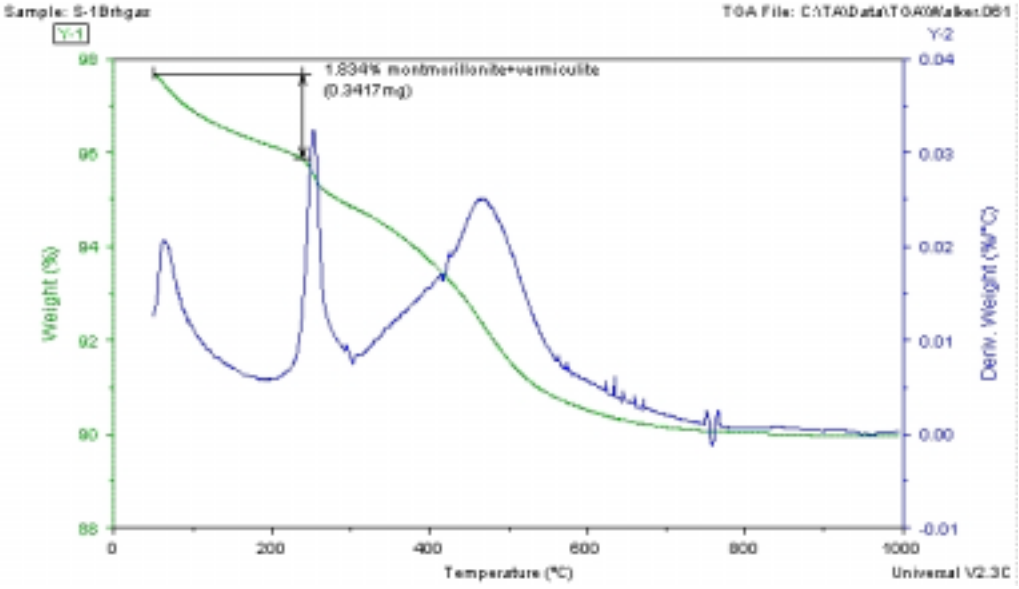

Figure A.30 TGA curve with derivative weight loss and approximated weight loss due to montmorillonite and vermiculite for the S-1B sample at a relative humidity of 56%.

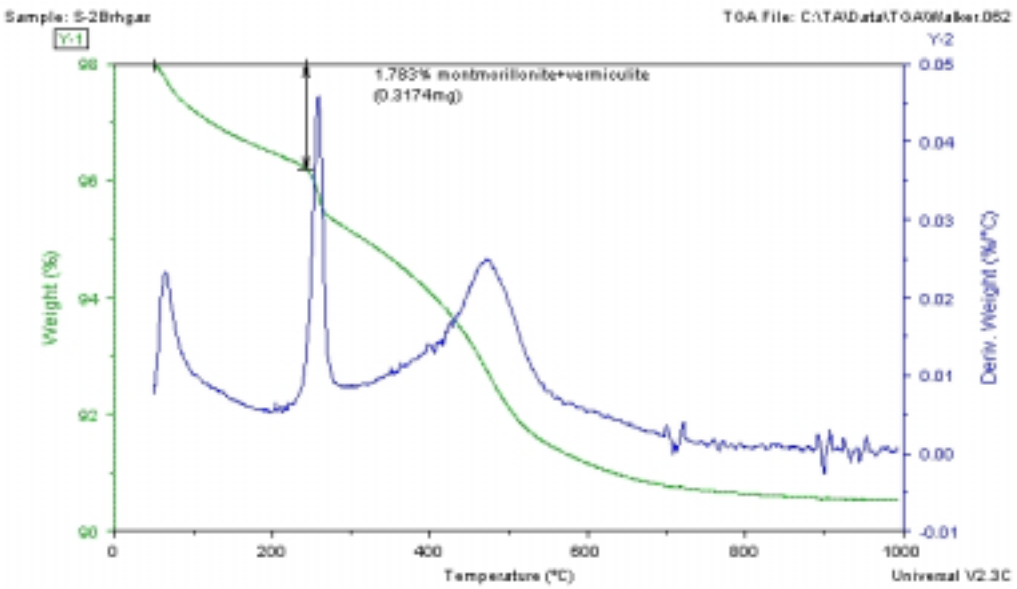

Figure A.31 TGA curve with derivative weight loss and approximated weight loss due to montmorillonite and vermiculite for the S-2B sample at a relative humidity of 56%.

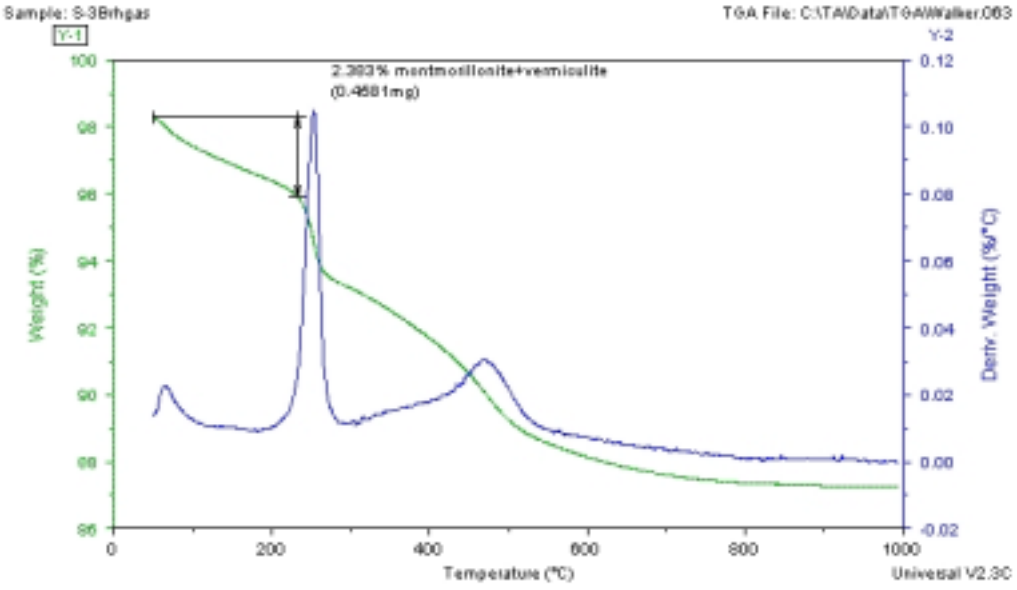

Figure A.32 TGA curve with derivative weight loss and approximated weight loss due to montmorillonite and vermiculite for the S-3B sample at a relative humidity of 56%.

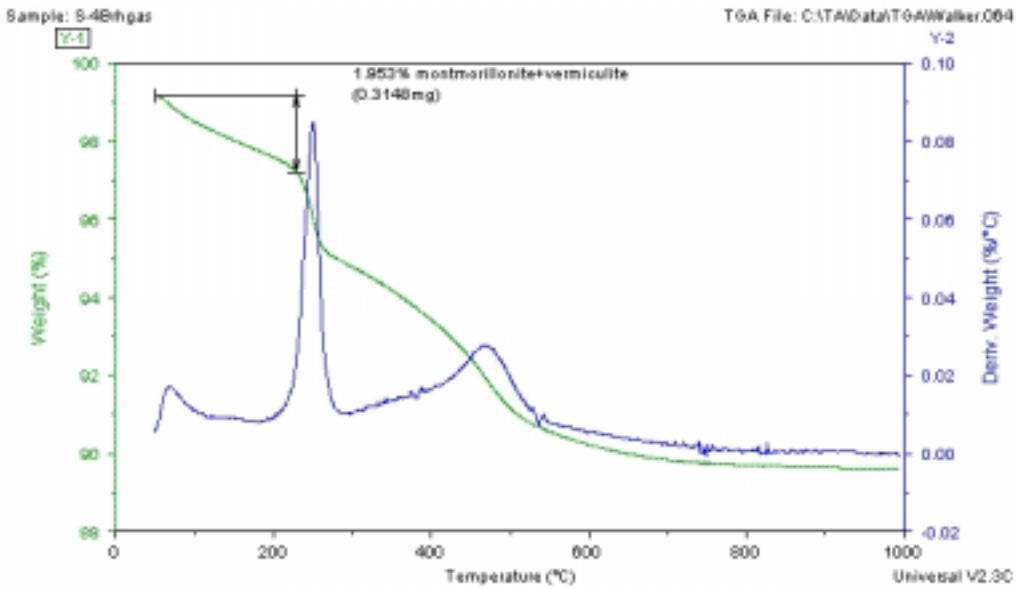

Figure A.33 TGA curve with derivative weight loss and approximated weight loss due to montmorillonite and vermiculite for the S-4B sample at a relative humidity of 56%.

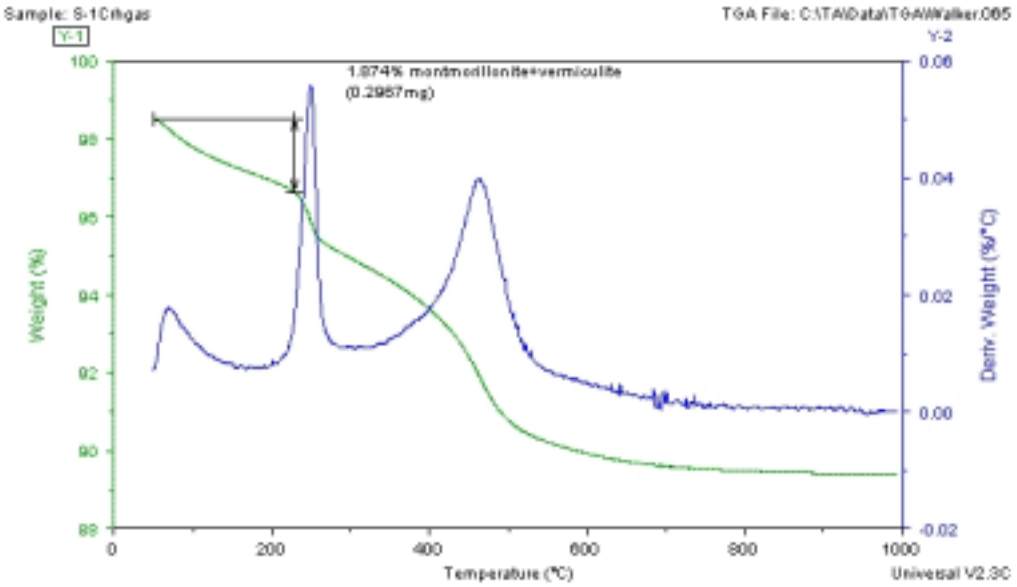

Figure A.34 TGA curve with derivative weight loss and approximated weight loss due to montmorillonite and vermiculite for the S-1C sample at a relative humidity of 56%.

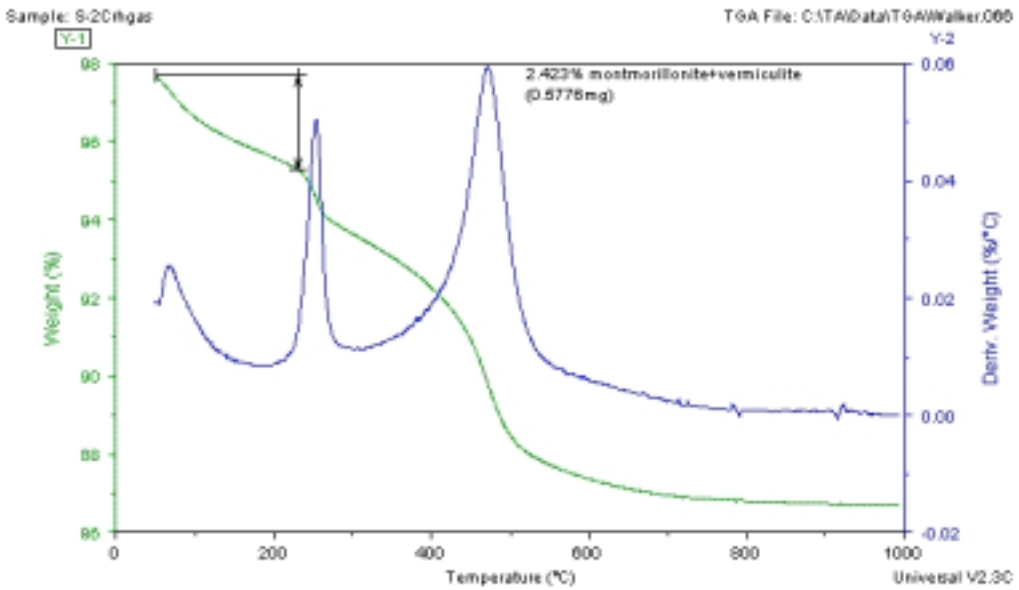

Figure A.35 TGA curve with derivative weight loss and approximated weight loss due to montmorillonite and vermiculite for the S-2C sample at a relative humidity of 56%.

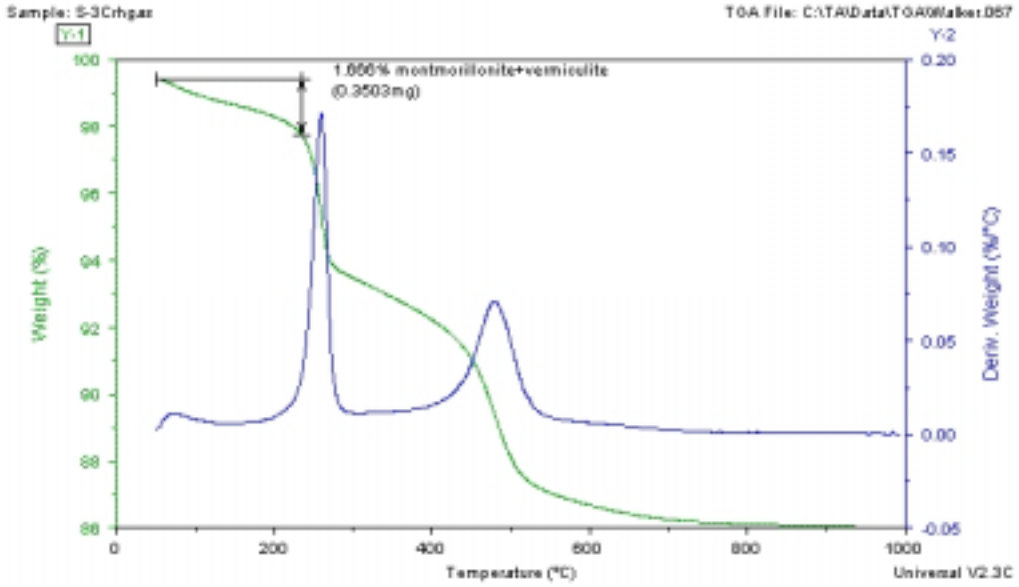

Figure A.36 TGA curve with derivative weight loss and approximated weight loss due to montmorillonite and vermiculite for the S-3C sample at a relative humidity of 56%.

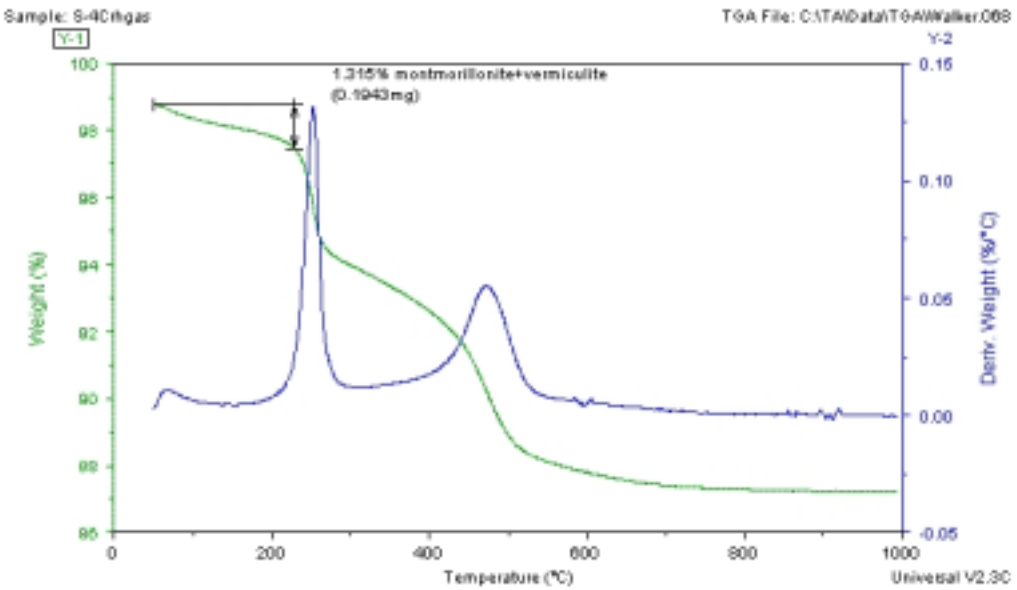

Figure A.37 TGA curve with derivative weight loss and approximated weight loss due to montmorillonite and vermiculite for the S-4C sample at a relative humidity of 56%.

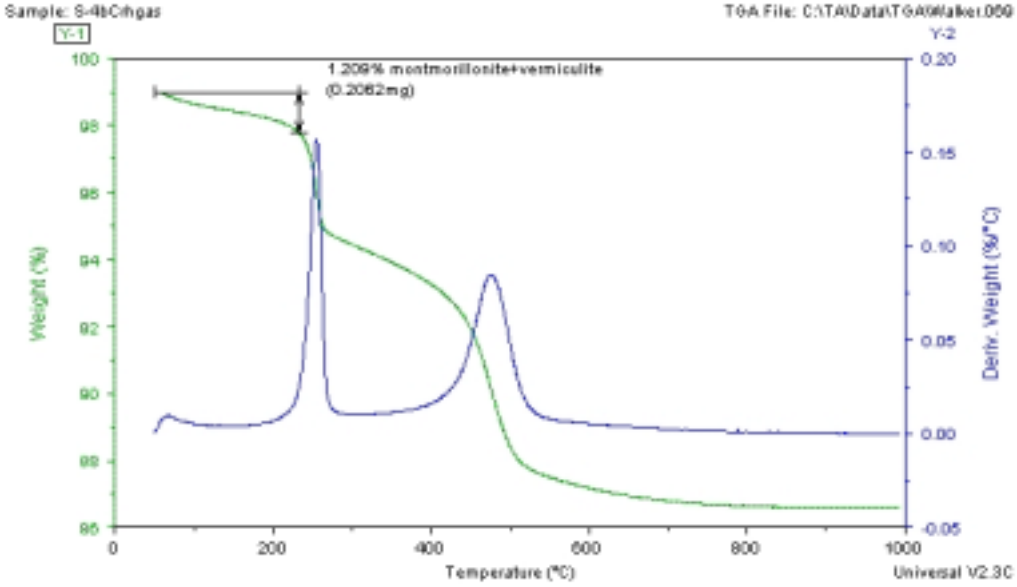

Figure A.38 TGA curve with derivative weight loss and approximated weight loss due to montmorillonite and vermiculite for the saprolite sample at a relative humidity of 56%.

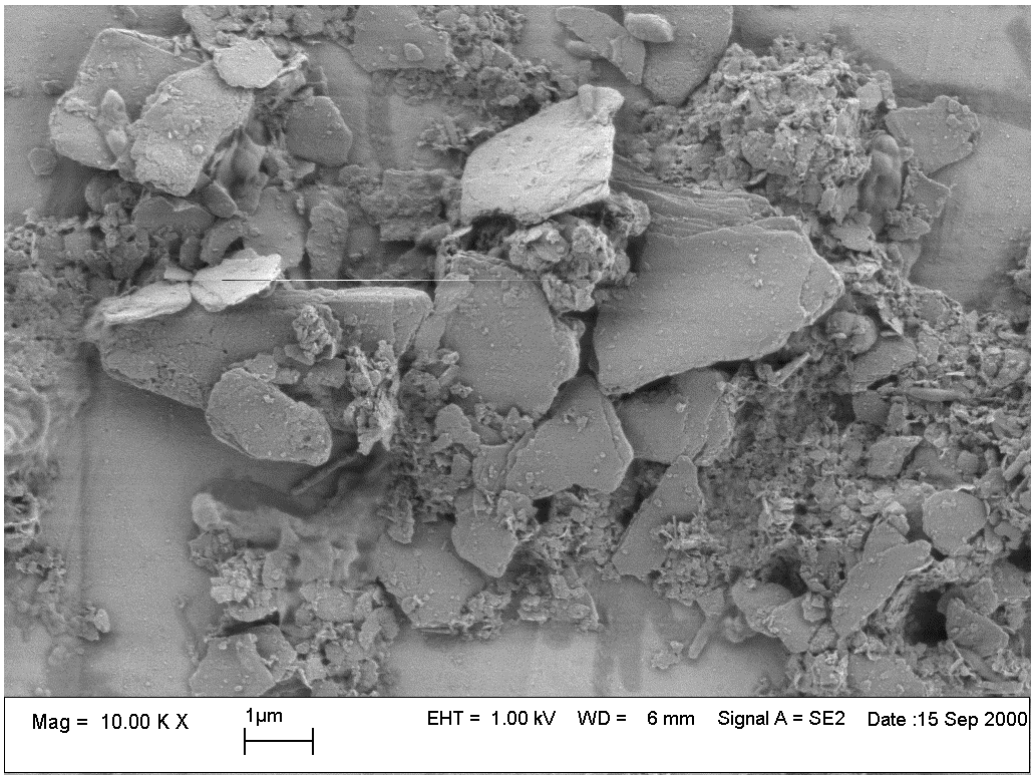

Figure A.39 Scanning electron micrograph of S-1A.

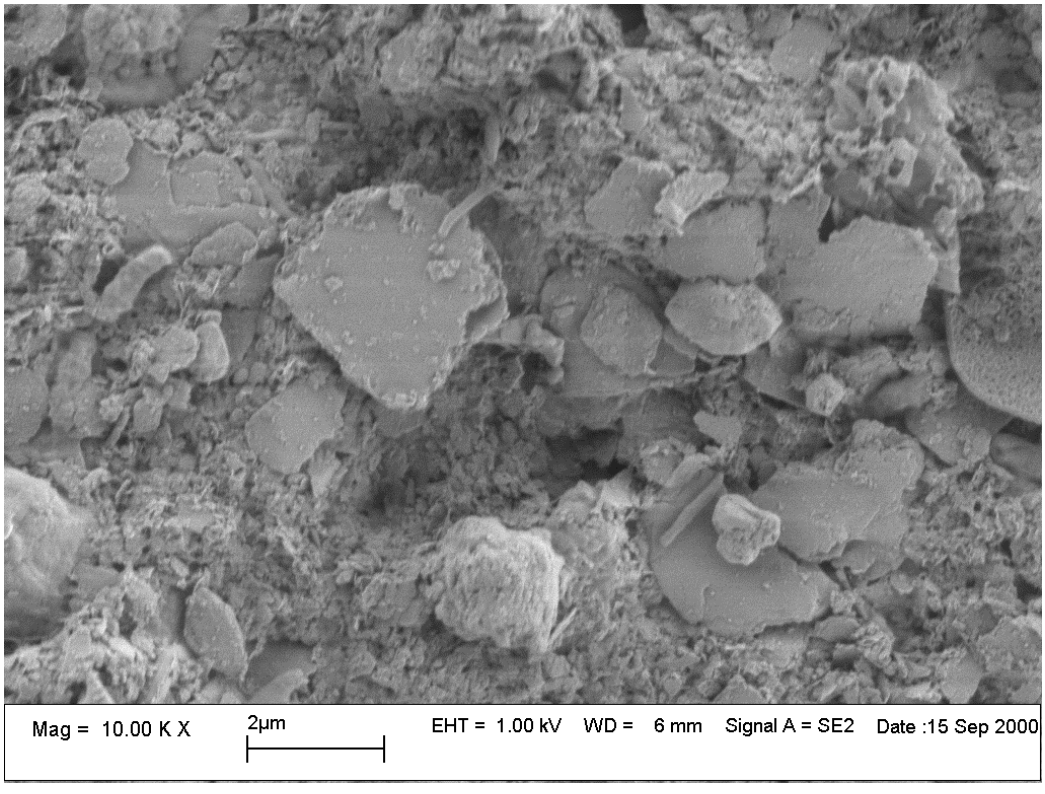

Figure A.40 Scanning electron micrograph of S-1A.

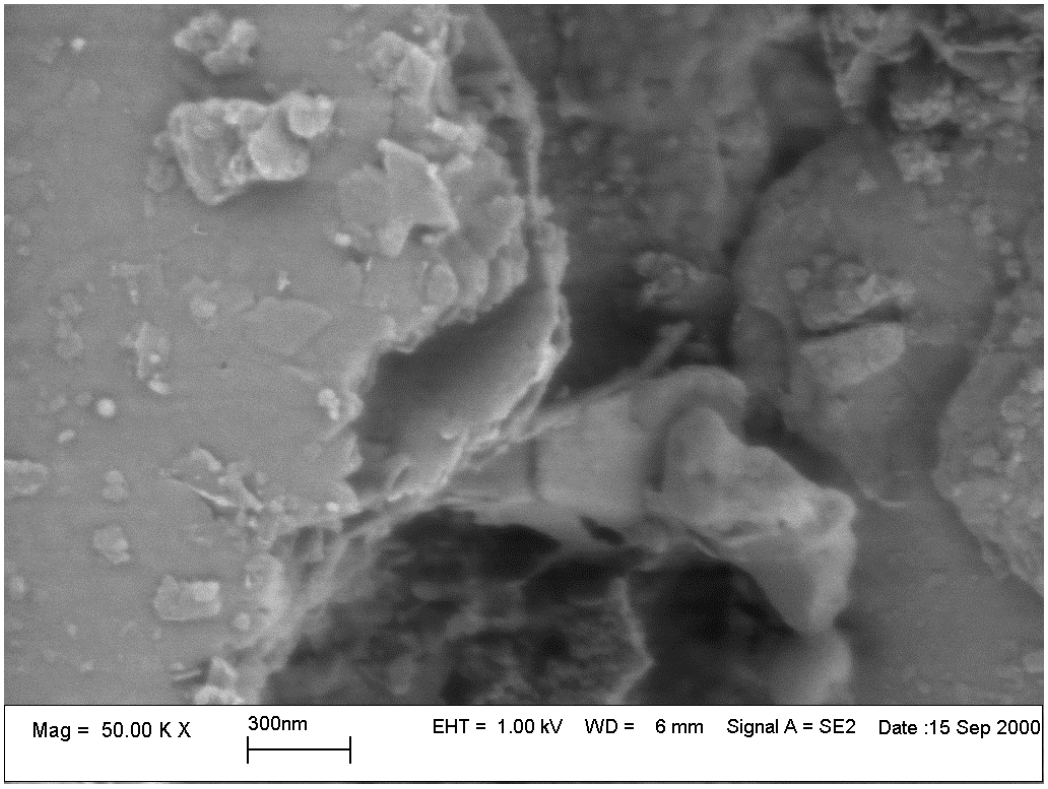

Figure A.41 Scanning electron micrograph of S-1A.

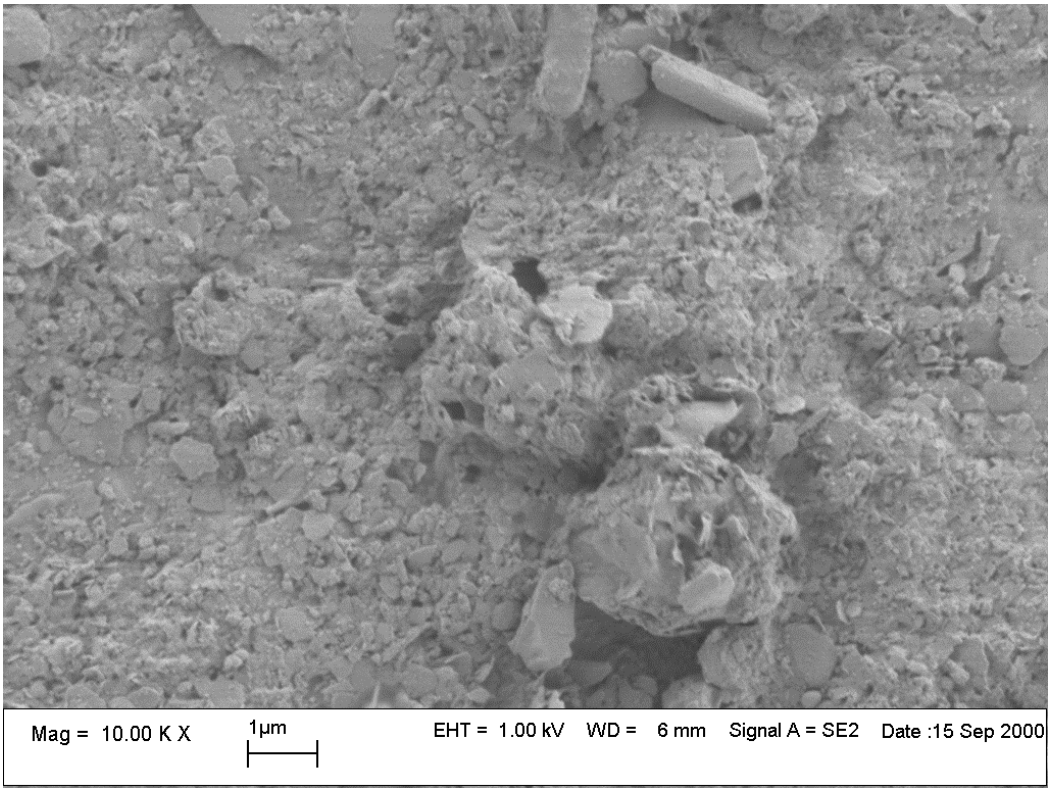

Figure A.42 Scanning electron micrograph of S-3A.

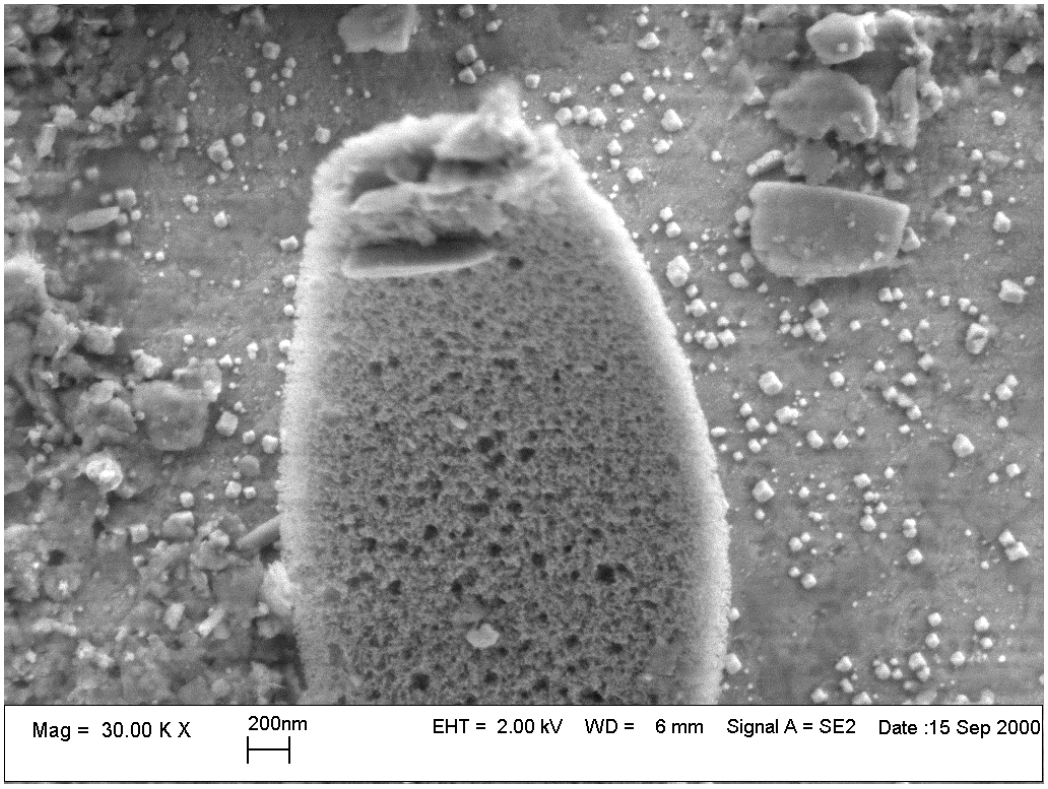

Figure A.43 Scanning electron micrograph of a montmorillonite aggregate in the S-3A.

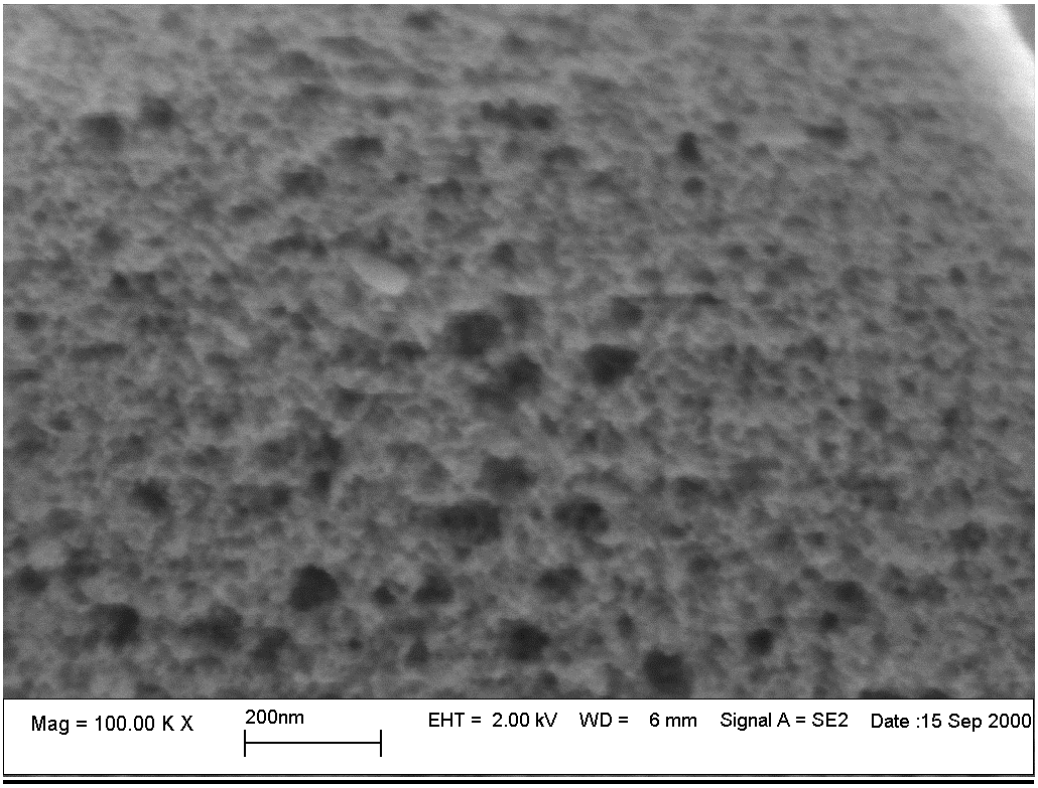

Figure A.44_Scanning electron micrograph of a montmorillonite aggregate in the S-3A.

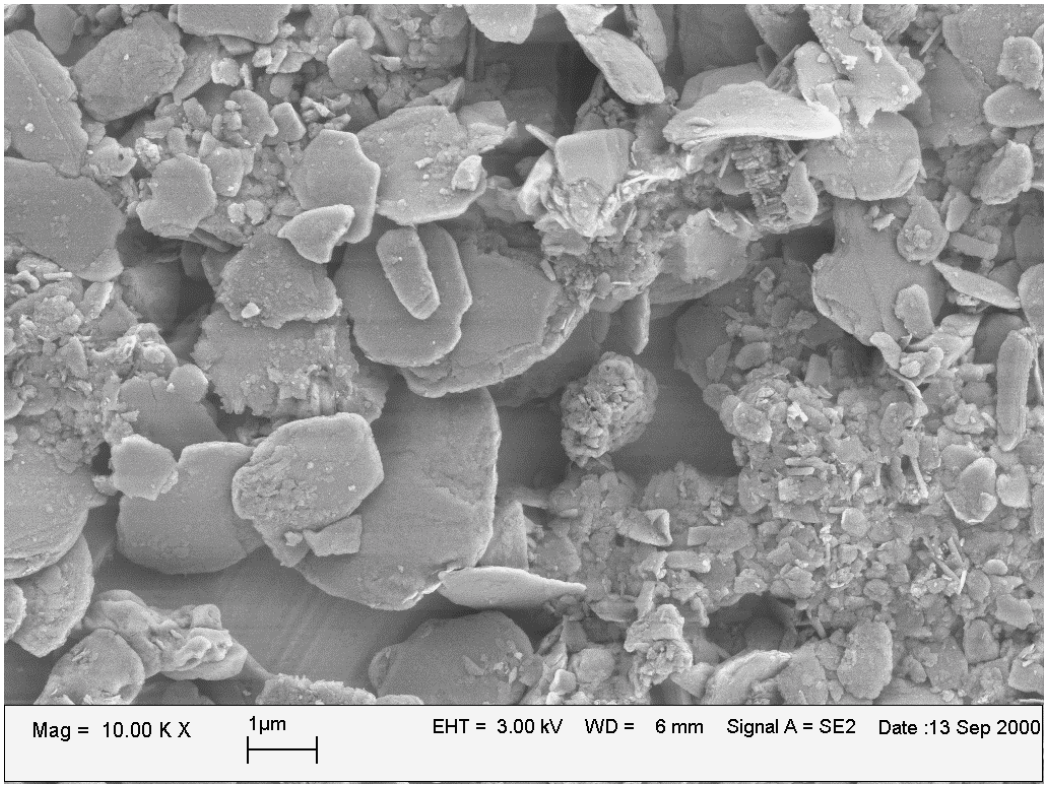

Figure A.45 Scanning electron micrograph of the S-1B.

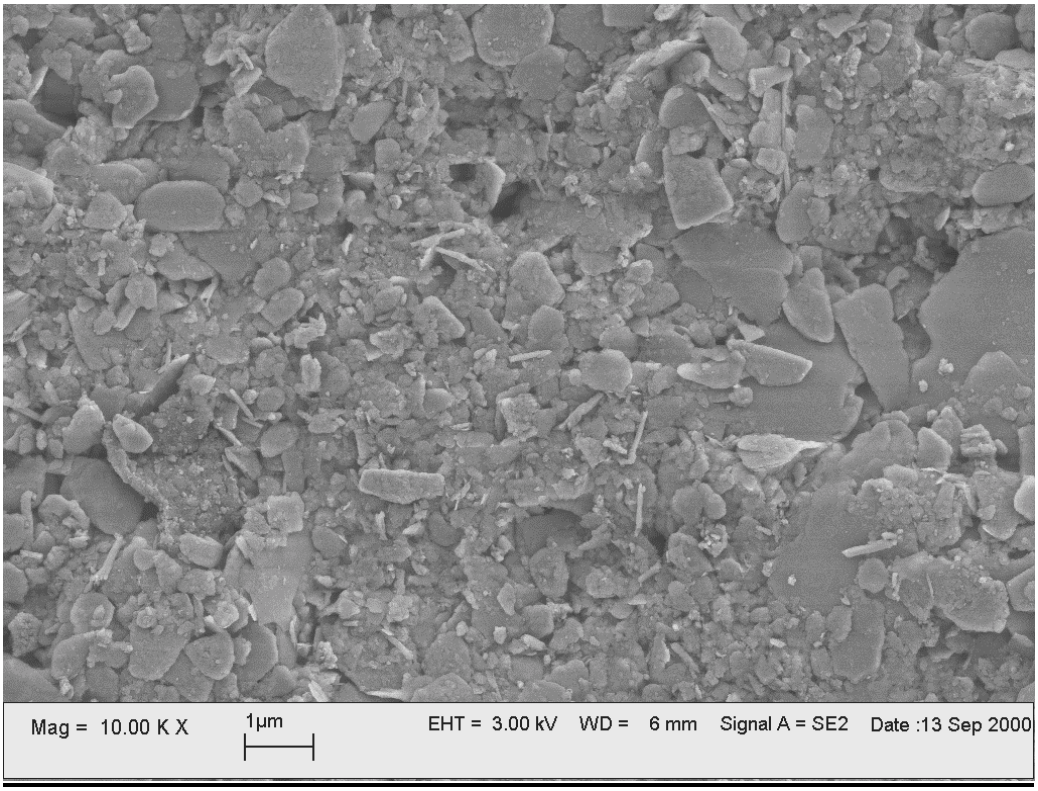

Figure A.46_Scanning electron micrograph of the S-1B.

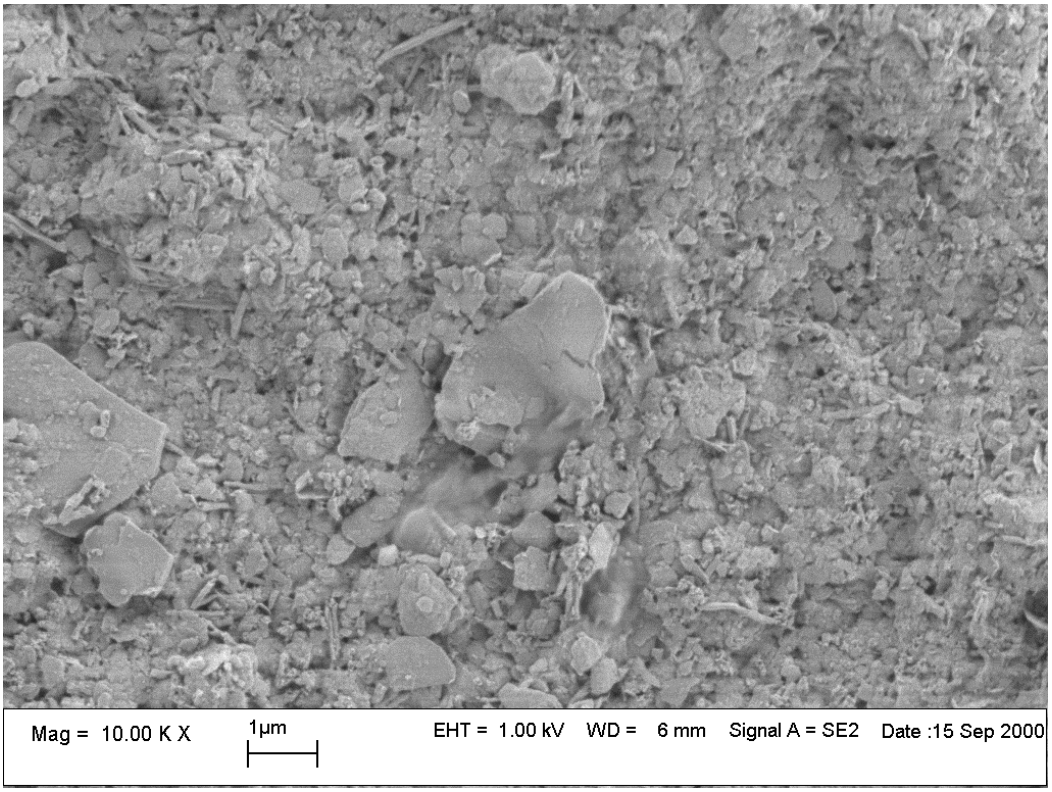

Figure A.47 Scanning electron micrograph of the S-3B.

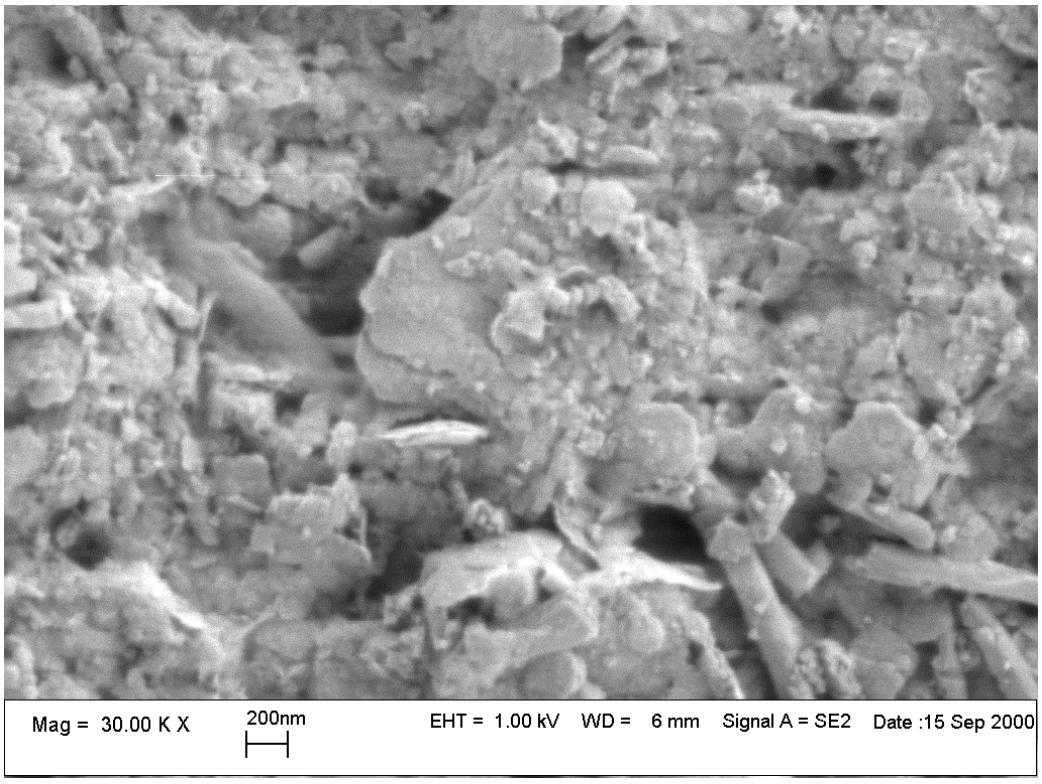

Figure A.48 Scanning electron micrograph of the S-3B.

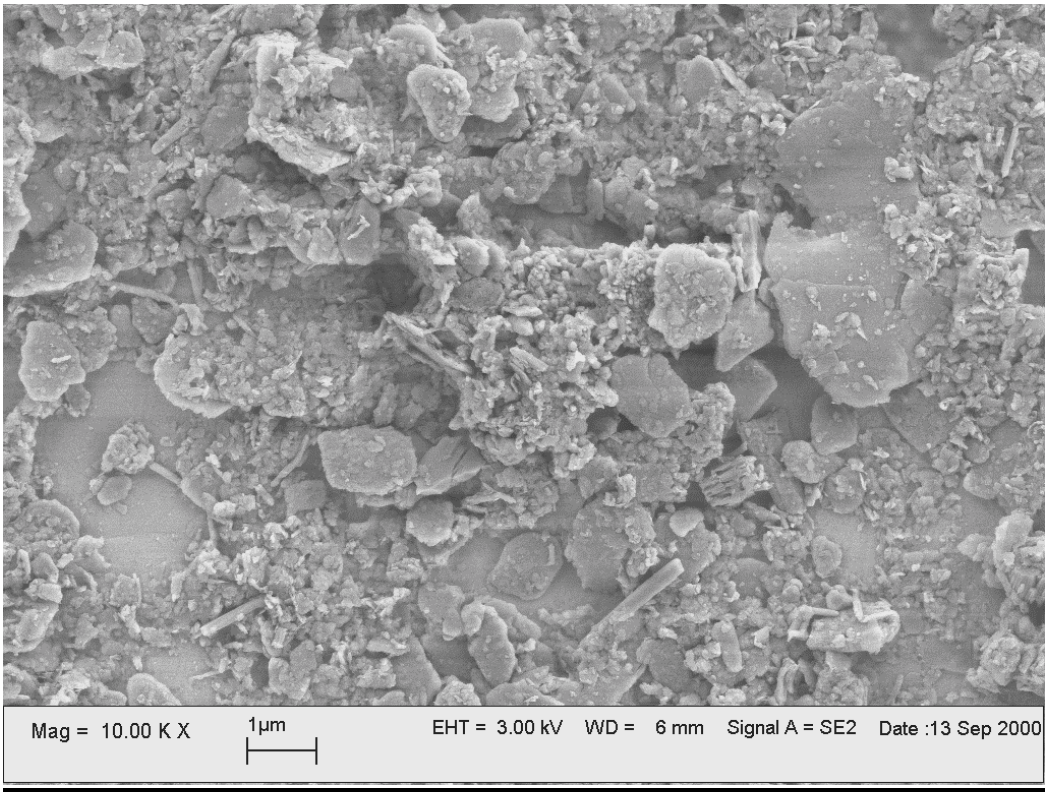

Figure A.49_Scanning electron micrograph of the S-1C.

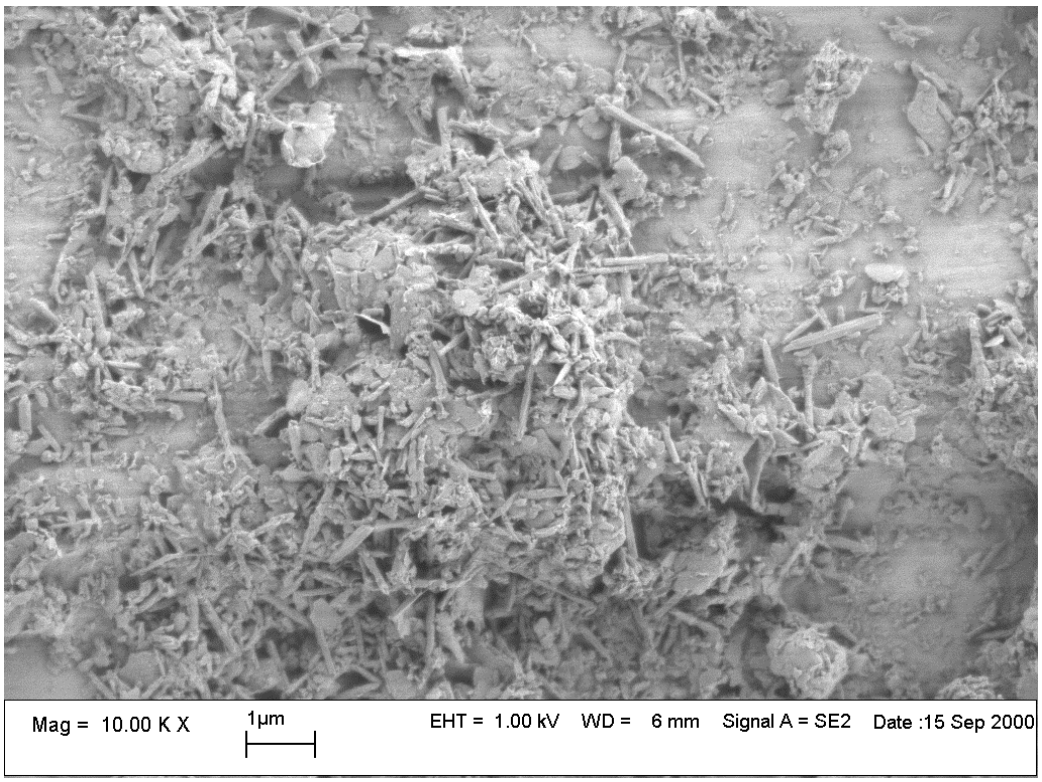

Figure A.50 Scanning electron micrograph of the S-3C.

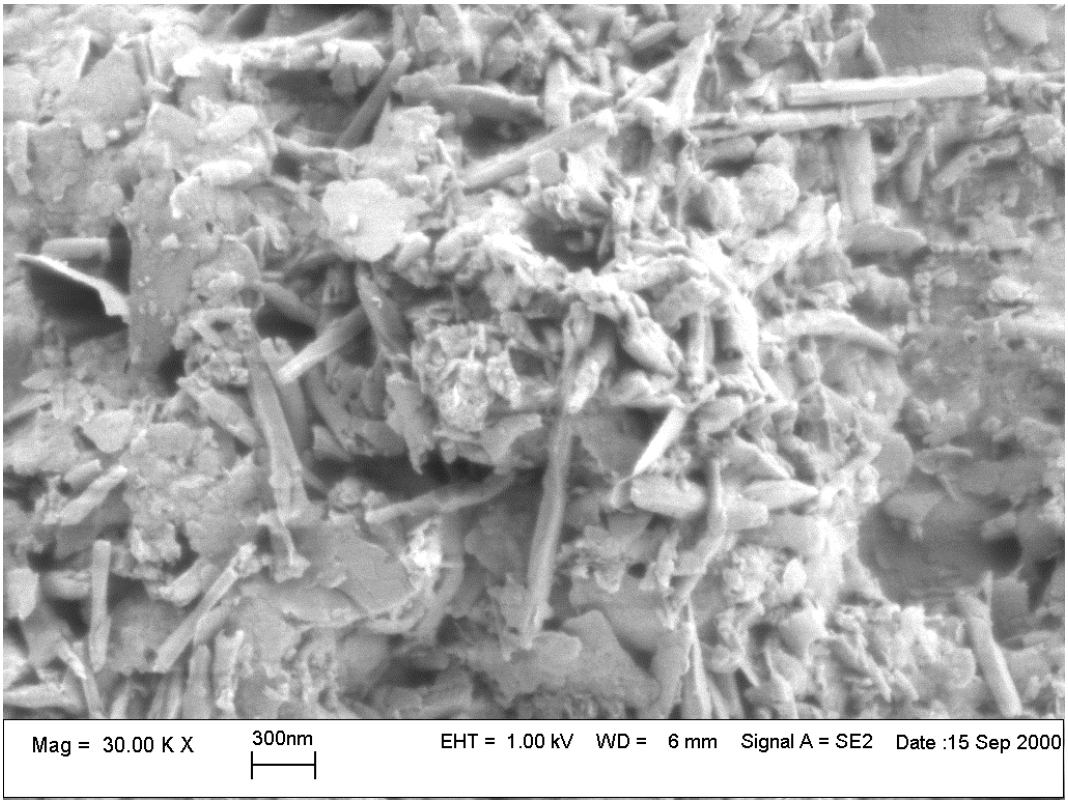

Figure A.51 Scanning electron micrograph of the S-3C.

APPENDIX B

Pictures of sampling location

Figure B.1_Low elevation, Sites 1 and 2, NE of Independence, VA.

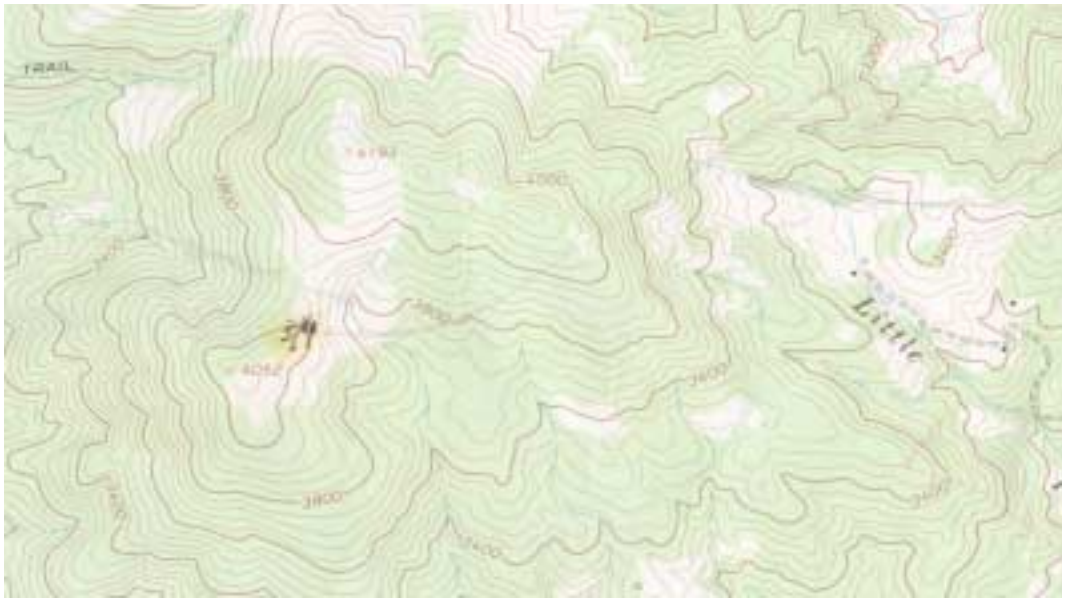

Figure B.2 High elevation, Sites 3 and 4, NW of Independence, VA.

Vita

Born June 3, 1976, in the Children's Hospital in Cheverly Maryland, I am proud to say I am a bicentennial baby. Before relocating to the much more rural, Western Maryland when I was 2, my mother would have arguments with the neighbors wife (he, the head coach of the Terps football team) as to whether I would become a football player or a concert pianist. As I developed a great appreciation for both interests, it became apparent as I grew, that I had another love; dirt.

Despite my aversion for studying, I loved to go to school, because that's where all the people were (especially the girls, I never thought they were icky). Alas, the painstaking efforts of my mother to temper my hyper-activity by denying me sugar and hotdogs (?) and the sweet-talking my teachers to be pardoned of my mischief paid off . . .in the Fall of 1994, I entered Virginia Tech. With lacrosse to keep me out of trouble, I managed to receive my B.S. degree in the Fall of 1998 in Environmental Science with a minor in Chemistry. The influence of Dr. Jim Baker, Dr. Matt Eick, and Dr. Pam Thomas caused me to switch gears, and through the persuasion of my parents and Dr. Dan Brann (my "Virginia Dad") I began a masters program in Soil Science at Virginia Tech. Dr. Lucian Zelazny has managed to curb my mischieviousness and restlessness over the past two years by keeping my sleep to a minimum as I pursue this degree. Maybe that was it Mom, you let me sleep too much!